Unusual Dual-Emissive Heteroleptic Iridium Complexes Incorporating TADF Cyclometalating Ligands

Helen Benjamin,[a] Yonghao Zheng,[a,b] Valery N. Kozhevnikov,[a,c] Jamie S. Siddle,[a] Luke J. O'Driscoll,[a] Mark A. Fox,[a] Andrei S. Batsanov,[a] Gareth C. Griffiths,[d] Fernando B. Dias,[d] Andrew P. Monkman,[d] and Martin R. Bryce*[,a]

[a] *Department of Chemistry, Durham University, Durham DH1 3LE, U.K. email: m.r.bryce@durham.ac.uk*

[b] *School of Optoelectronic Science and Engineering, University of Electronic Science and Technology of China (UESTC), Chengdu 610054, China*

[c] *Department of Applied Sciences, Northumbria University, Newcastle-Upon-Tyne, NE1 8ST, U.K.*

[d] *Department of Physics, Durham University, Durham DH1 3LE, U.K.*

Five new neutral heteroleptic iridium(III) complexes IrL_2(pic) (**2**-**6**) based on the archetypical blue emitter **FIrpic** have been synthesised. The cyclometallating ligands L are derived from 2-(2,6-F_2-3-pyridyl)-4-mesitylpyridine (**7**), 2-(3-cyano-2,6-F_2-phenyl)-4-mesitylpyridine (**8**), 2-(2,6-F_2-phenyl)-4-[2,7-$(HexO)_2$-9*H*-carbazol-9-yl]pyridine (**9**), 2-(2,6-F_2-3-pyridyl)-4-[2,7-$(HexO)_2$-9*H*-carbazol-9-yl]pyridine (**10**) and 2-(3-cyano-2,6-F_2-phenyl)-4-[2,7-$(HexO)_2$-9*H*-carbazol-9-yl]pyridine (**11**) for complexes **2**, **3**, **4**, **5** and **6**, respectively. The carbazole-functionalised ligands **9**-**11** show weak thermally activated delayed fluorescence (TADF) in solution. Complexes **5** and **6** reveal dual emission in polar solvents. A broad charge transfer (CT) band appears and increases in intensity relative to the higher energy emission band as solvent polarity is increased. The dual emission occurs when the energy of the ligand ^{3}CT state is comparable to that of the ^{3}MLCT state of the complex, resulting in fast interconversion between the two. Assignment of the ligand TADF and dual emission properties is supported by hybrid density functional theory (DFT) and time dependent DFT (TD-DFT) calculations. Phosphorescent organic light emitting devices (PhOLEDs) have been fabricated using these complexes as sky-blue emitters, and their performance is compared to devices using **FIrpic** and the previously reported complex IrL_2(pic) **1** (L from the 2-(2,6-F_2-phenyl)-4-mesitylpyridine ligand). For identical device structures, the device containing the carbazole complex **4** performs best out of the seven complexes. The dual emission observed in solution for complexes **5** and **6** is not observed in their devices.

INTRODUCTION

A vast number of luminescent transition metal complexes (LTMCs) have been studied because of their fundamentally interesting photophysical properties and for their versatile applications, notably bioimaging, photocatalysis, sensing, phosphorescent organic light emitting diodes (PhOLEDs) and solid-state lighting.[1–5] However, there are notably few reports of complexes that exhibit dual emission, a phenomenon where two distinct excited states of a molecule emit simultaneously. Dual emission can be facilitated by the strong spin-orbit coupling (SOC) associated with heavy metal atoms, and the multiple charge-transfer transitions that occur in LTMCs. Platinum[6,7] and iridium complexes[8] with extended π-conjugated ligands show both fluorescence from a peripheral organic substituent and phosphorescence

associated either with the metal and ligating unit, or purely from the ligand, sensitised by the strong SOC effect of the metal. Neutral[9] and cationic[10] iridium complexes that emit from different chromophoric ligands have been reported, and the relative intensities of the emission bands were modulated by the presence of certain metal ions. Cationic cyclometalated Ir complexes with pendant ligands that show dual emission from ligand-centred (LC) and interligand charge transfer (ILCT) states have been synthesised and shown to function as sensors for biomolecules.[11] An iridium complex containing a dibenzoylmethane ancillary ligand has been reported to exhibit different emission spectra from two distinct polymorphs, related to the difference in π-stacking interactions in the solid state.[12] Iridium complexes have also been incorporated into polymer chains containing other emissive materials of different colours.[13,14] Some iridium complexes with relatively simple structures that display dual emission include a neutral *mer*-homoleptic complex studied by Yeh *et al.*, which displayed two main emission features in solution, assigned to an ILCT/MLCT state and a localised ligand to ligand charge transfer (LLCT)/MLCT state, whose relative intensities varied with temperature.[15] Zysman-Colman *et al*. investigated a neutral heteroleptic complex that displayed strong solvatochromism in solution, with wavelength-dependent excited state lifetimes and oxygen quenching sensitivity.[16,17] Kumar *et al.* described a family of complexes with 8-sulfonamidoquinoline-based ancillary ligands that displayed two emission bands, both in solution (DMSO) and the frozen glass state, originating from different MLCT, LLCT and LC transitions.[18] Climent *et al.* reported a dual emissive complex containing a Schiff base ligand with a solvatochromic higher energy fluorescent band at 400-525 nm and a lower energy phosphorescent band at 525-700 nm which were assigned to ^{1}ILCT and ^{3}MLCT respectively.[19]

As highlighted above, reports of dual emissive complexes are sporadic, often limited to a single molecule or related to a single functional group, providing little guidance for future synthetic design. We previously reported that complex **1** (Chart 1), which differs from the ubiquitous blue emitter iridium(III) bis[4,6-(difluorophenyl)pyridinato-*N*,*C*2']picolinate (**FIrpic**)[20] only by the presence of the mesityl groups, is an efficient sky-blue emitter in PhOLEDs with a solution-processed emitting layer.[21] The mesityl groups increase solubility and reduce concentration quenching in devices, thus devices fabricated from **1** are more efficient than those from **FIrpic**.

The motivation for the present work was to explore **1** as a platform for the systematic development of complexes with dual emission properties where the expected blue emission is accompanied with a second lower energy emission. In a previous study by Wu *et. al.*, donor (diarylamine or phenoxy) and acceptor (phenylsulfone) units were attached to cyclometalating ligands within the same complex; however, dual emission was not observed.[22] Here, a family of related complexes **2**-**6**, were synthesised by introducing a strong acceptor (difluoropyridyl or difluorobenzonitrile) and/or a donor (carbazole) unit into the ligand structure. Dual emission in solutions was observed only from complexes **5** and **6** where *both* strong acceptor and donor units are present. PhOLEDs fabricated from these dual emitters along with the sky-blue emitters **FIrpic** and complexes **1**-**4** are also discussed. To the best of our knowledge, the devices fabricated using complexes **5** and **6** are the first PhOLEDs to be reported using dual emissive Ir complexes.

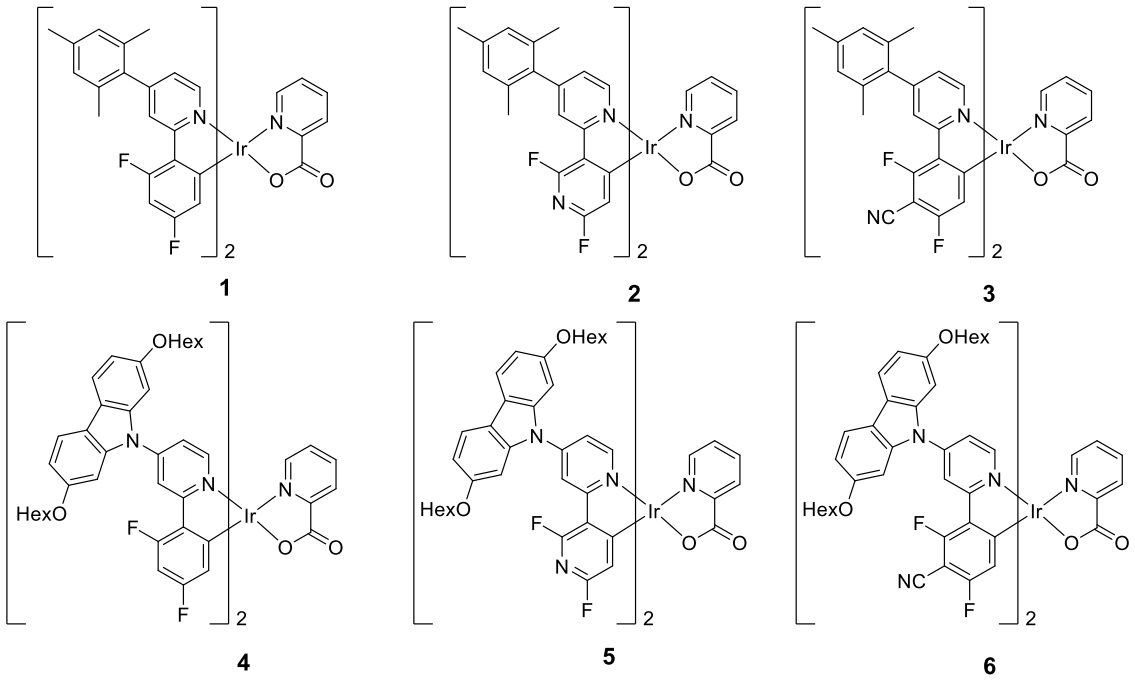

Chart 1: Complexes **1**-**6** studied in this work.

RESULTS AND DISCUSSION

Synthesis

The syntheses of the ligands **7**-**11** for the target complexes **2**-**6** are shown in Scheme 1 and Scheme 2. Ligands **7** and **8** were synthesised via Suzuki couplings between 2-chloro-4-(2,4,6-trimethylphenyl)pyridine[21] **12** and the desired boronate ester (**13** or **14**) in moderate yields (34-51%). For ligands containing the dialkoxy substituted carbazole moiety dimethoxycarbazole[23] **15** was first coupled with 2-chloro-4-iodopyridine in an Ullman-type reaction to give **16** (96% yield). The methoxy ethers were then deprotected with BBr_3 to give the dihydroxycarbazole derivative **17** (72%) and hexyl chains were added to improve the solubility of the resulting complexes, via a Williamson ether synthesis, to give the key intermediate **18** (79%).

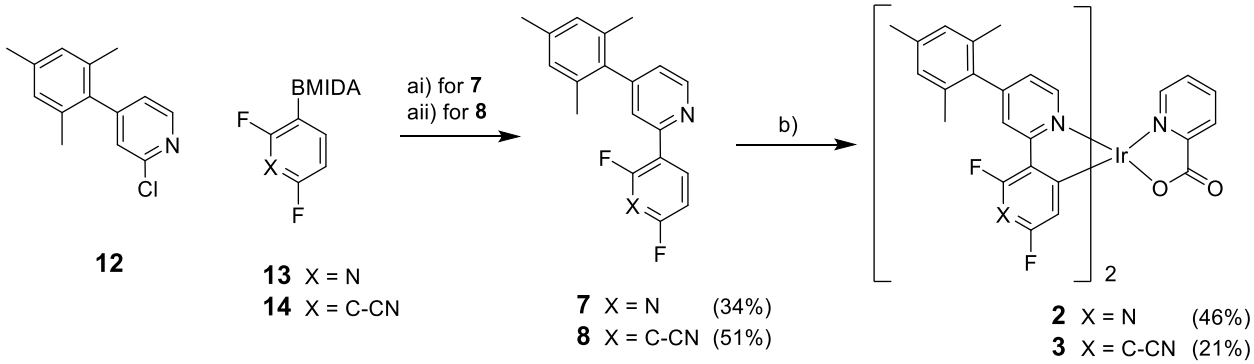

Scheme 1: Synthesis of mesityl-functionalised complexes **2** and **3**. Reagents and conditions: (ai) $Pd_2(dba)_3$, PCy_3, K_3PO_4, 1,4-dioxane/water, 60 °C; (aii) $Pd(OAc)_2$, SPhos, K_3PO_4,1,4-dioxane/water, 90 °C; (b) $IrCl_3 \bullet 3H_2O$, 2-ethoxyethanol/water, 110 °C followed by picolinic acid, 2-ethoxyethanol, 110 °C.

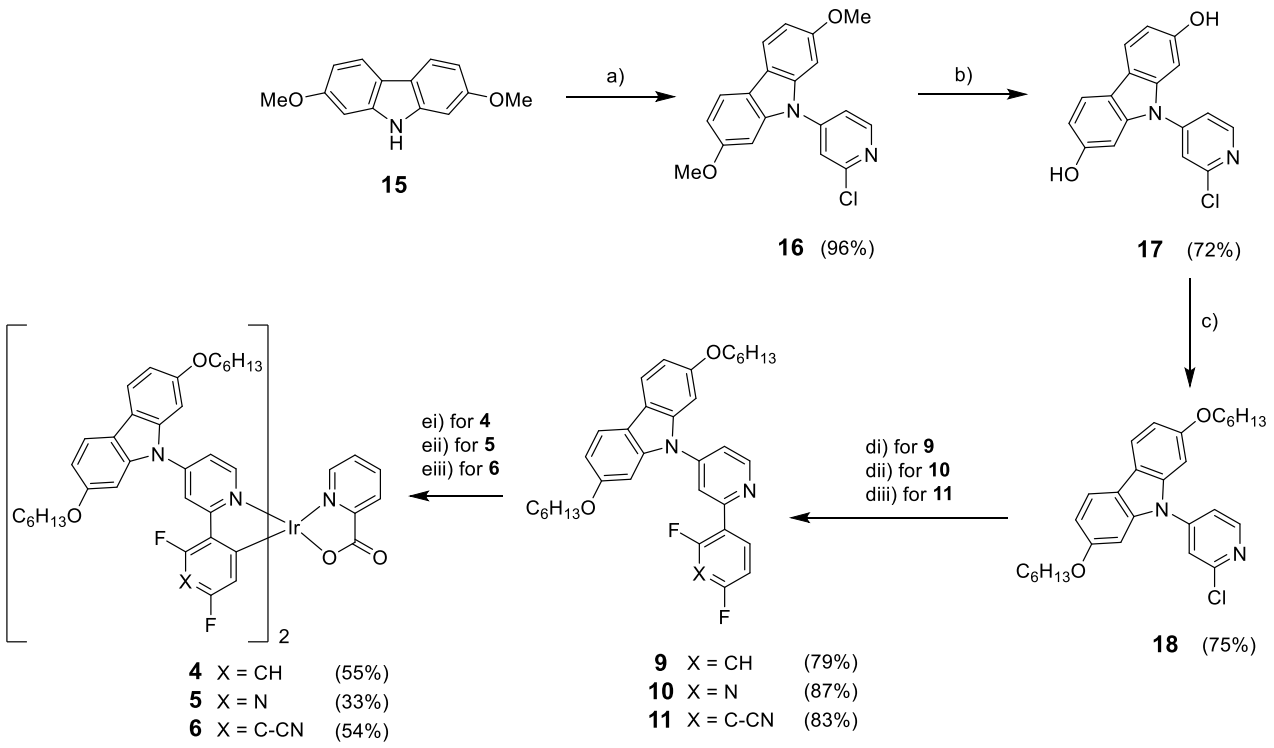

Scheme 2: Synthesis of carbazole-functionalised complexes **4**-**6**. Reagents and conditions: (a) 4-iodo-2-chloropyridine, CuI, 1,10-phenanthroline, K_2CO_3, DMF (dry), 120 °C; (b) BBr_3, CH_2Cl_2 (dry), 0 °C; (c) 1-bromohexane, K_2CO_3, DMSO; (di) 2,4-difluorophenylboronic acid, $Pd(PPh_3)_4$, K_2CO_3,1,4-dioxane/water, 90 °C; (dii) **13**, SPhos, $Pd(OAc)_2$, K_3PO_4, 1,4-dioxane/water, 60 °C; (diii) **14**, SPhos, $Pd(OAc)_2$, K_3PO_4, 1,4-dioxane/water, 60 °C; (ei) $IrCl_3$•$3H_2O$, 2-ethoxyethanol/water, 120 °C followed by picolinic acid, Na_2CO_3, 2-ethoxyethanol, 120 °C; (eii) $IrCl_3$•$3H_2O$, diglyme, 130 °C followed by picolinic acid, 130 °C; (eiii) $IrCl_3$•$3H_2O$, 2-ethoxyethanol/water, 110 °C followed by picolinic acid, Na_2CO_3, 2-ethoxyethanol, 110 °C.

The next step was to perform Suzuki coupling reactions with 2,4-difluorophenylboronic acid or *N*-methyliminodiacetic acid (MIDA) boronate derivatives **13** or **14**. The synthesis of the MIDA derivatives followed literature procedures with experimental details described in the Supporting Information (Scheme S1). The MIDA esters were used due to the instability of the parent boronic acids under the reaction conditions. Longer reaction times, as required for coupling reactions with the less active 2-chloropyridine derivatives, suffer from competing deborylation, particularly for highly electron-deficient boronic acids.[24,25] The Suzuki couplings between boronic esters **13** and **14** and chloride **18** followed the protocol described by Burke *et al*,[25] and the products were isolated in good yields (87% for **10** and 83% for **11**).

The target heteroleptic picolinate iridium complexes **2**-**6** were then synthesised (Scheme 1, Scheme 2) via the standard method.[26,27] Reaction of the ligands (**7**-**11**) with $IrCl_3$•$3H_2O$ gave yellow precipitates presumed to be the intermediate μ-dichloro-bridged dimers. Picolinic acid was added and the solution heated to 110-130 °C. The desired complexes **2**-**6** were isolated in 21-55% yields. For **5** and **6**, if the reaction temperature was increased to 130 °C a large number of products was observed, identified by mass spectrometry as the products of sequential replacements of fluorine substituents with 2-ethoxyethoxy groups, presumably via an SN_{Ar} reaction (Figure S1). The instability of the 2,4-difluoro-2',3-bipyridine ligand under the standard reaction conditions has been observed previously, wherein the methoxyethanol solvent attacks the ligands and the tetra-alkoxylated heteroleptic complex was isolated as the major product in good yield.[28] Single crystal X-ray structures obtained for complexes **2** and **3** are depicted in Figure 1 with the

crystal data summarised in Table S1. As expected for complexes synthesised from the μ-dichloro-bridged dimers the N atoms of the two C^N ligands are *trans* to each other and ca. 0.08 Å shorter than the Ir-N(picolinato) bond, which is affected by the *trans*-influence of an Ir-C bond. Both Ir-C bonds in **2** are slightly shorter than in the isoelectronic complex **1** (2.001(2) and 1.988(2) Å, Table S2).[29] In both **2** and **3**, the dihedral angles between each pyridine ring and its attached mesityl ring are such as to preclude π-conjugation, viz. 63.4° and 78.0° in **2**, 69.1° and 63.4° (or 70.2° for an alternative position of the disordered mesityl) in **3**, cf. 67.0° and 78.7° in **1**. Interestingly, the Mes-Py-Ir-Py-Mes rod is substantially non-linear, bending by 16.5° in **2** or 21° in **3**, as in other analogous complexes (cf. 39.6° in **1**).[29] The packing of both **2** and **3** shows no π-π stacking and is dominated by edge-to-face or arene-solvent interactions. In both complexes, the Ir atom has a distorted octahedral coordination, with metal-ligand bond lengths similar to the reported crystal structures for **FIrpic**. [30-34]

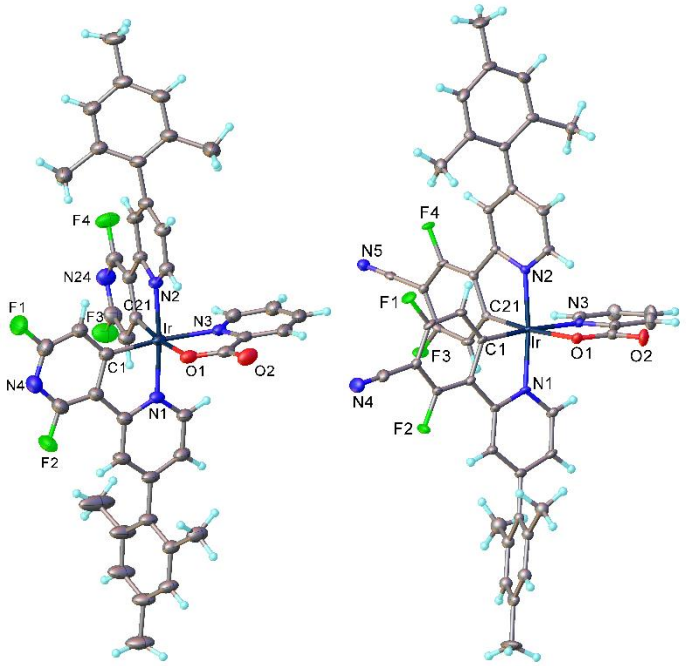

Figure 1: X-ray molecular structures of **2** (left) and **3** (right). Minor disorder components and solvent of crystallisation are omitted, thermal ellipsoids are drawn at the 50% probability level.

PHOTOPHYSICAL AND ELECTROCHEMICAL PROPERTIES

Electrochemistry

The electrochemical properties of complexes **1**-**6** and the carbazole ligands **9**-**11** were investigated by cyclic voltammetry with the data summarised in Table 1 and their cyclic voltammograms shown in Figure 2. The oxidation potentials of complexes **1**-**3** are assigned to the Ir^{3+}/Ir^{4+} couple and are similar to those reported for their mesityl-free analogues.[35] The potentials required to oxidise the iridium centre increase in accordance with the increased electron withdrawing properties of the ligand L (difluorophenyl < difluorocyanophenyl < difluoropyridyl). By contrast, the first oxidation potentials of the complexes **4**-**6** containing the 2,7-dialkoxycarbazole moiety are similar (anodic potentials at 0.63-0.66

V). This observation, and comparison with the voltammograms of ligands **9**-**11**, suggests that, for these complexes, the first oxidation originates from the carbazole moiety. The voltammograms of complexes **4**-**6** and ligands **9**-**11** also show a change in profile on increasing the number of cycles (Figures S3-8). It is known that oxidation of carbazole derivatives results in the formation of a radical cation on the carbazole subunit, and that these radical cations can dimerise at the 3-(6-) positions.[25] The additional peaks observed in the subsequent scans are assigned to the oxidation of dimeric/polymeric species formed via carbazole dimerisations.

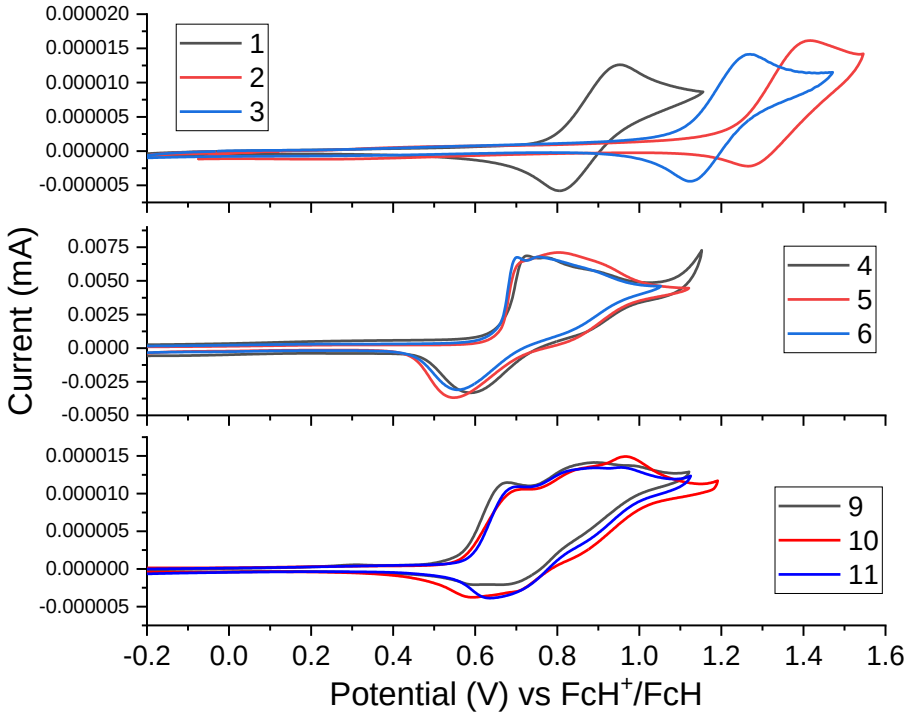

Figure 2: Cyclic voltammograms of complexes **1**-**6** and ligands **9**-**11**.

Table 1: Electrochemical data and energy levels for complexes **1**-**6** and ligands **9**-**11**

Complex	E_a / V[a]	HOMO[b] / eV	LUMO[c] / eV	Optical Gap (eV)[d]
FIrpic	0.95	-5.69	-2.96	2.73
1	0.94	-5.68	-3.06	2.62
2	1.26	-6.00	-3.24	2.76
3	1.40	-6.14	-3.46	2.68
4	0.66	-5.40	-2.82	2.58
5	0.63	-5.37	-2.69	2.68
6	0.65	-5.39	-2.77	2.62
9	0.64	-5.38	-1.83	3.55
10	0.65	-5.39	-1.91	3.48
11	0.67	-5.41	-1.98	3.43

[a] All values reported vs FcH/FcH$^+$ = 0.00 V; measured in 0.1 M ^{n}Bu$_4$NPF$_6$ in CH_2Cl_2 at 298 K with scan rate of 100 mV/s. [b] E(HOMO) = −4.74 – E_a eV with respect to the FcH/FcH$^+$ couple at 4.80 V. [c] LUMO energies estimated from the HOMO level + the optical gap determined from Figure 3/Figure S9. [d] Optical gap determined from the onset of absorption in Figure 3/Figure S9.

Absorption and emission

The absorption spectra of complexes **1**-**6** and ligands **9-11** in toluene are shown in Figure 3 and Figure S9, respectively, with data listed in Table 2. The complexes possessing carbazole units (**4**-**6**) show larger extinction coefficients than the other complexes (**1**-**3**). The strong bands between 290-325 nm are assigned to π-π* transitions on the ligand based on the absorption spectra of ligands **9**-**11** (Figure S9). The intense bands at 350-425 nm are assigned to the ^{1}MLCT bands, as they are not present in the ligand spectrum, while the significantly weaker (0.8-1.8 x 10^3 dm^3/mol cm) ^{3}MLCT bands can be seen at 425-475 nm based on the calculations of Hay.[36] The influence of solvent polarity on the absorption spectra of complexes **4**-**6** and corresponding ligands **9**-**11** was investigated (Figure S10), and negligible solvatochromic behaviour was observed.

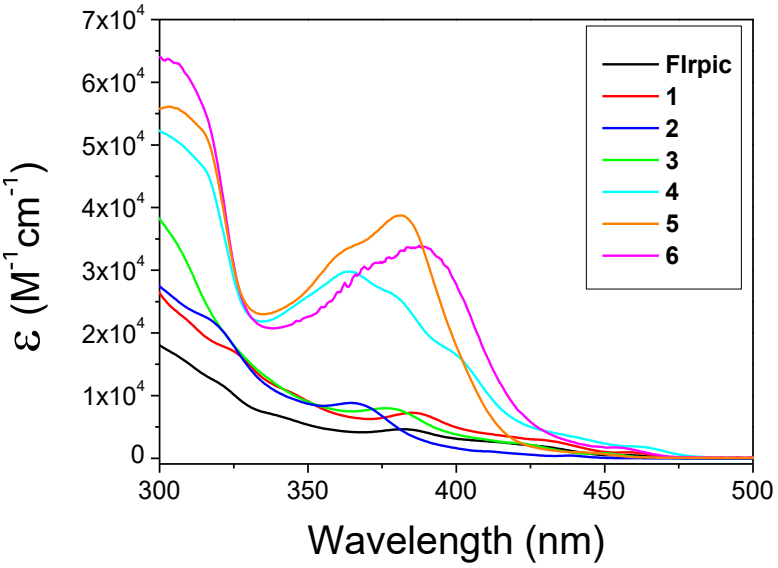

Figure 3: UV-Vis absorption spectra of the complexes in toluene [10^{-5} M].

The emission spectra of the complexes **1**-**6** in various solvents are shown in Figure 4. In the non-polar solvent methylcyclohexane (MCH), all the complexes display structured emissions in the 450-500 nm region, typical of emission from a mixed LC/MLCT state. On increasing the solvent polarity (to chlorobenzene, then chloroform) little change can be seen in the emission profiles for complexes **1**-**4**. However, complexes **5** and **6** exhibit a broadening of emission, with the appearance of a featureless band at 510-560 nm that increases in intensity relative to the higher energy LC/MLCT emission band on increasing solvent polarity. Compared to **5**, the effect of solvent polarity on the emission of **6** is weaker.

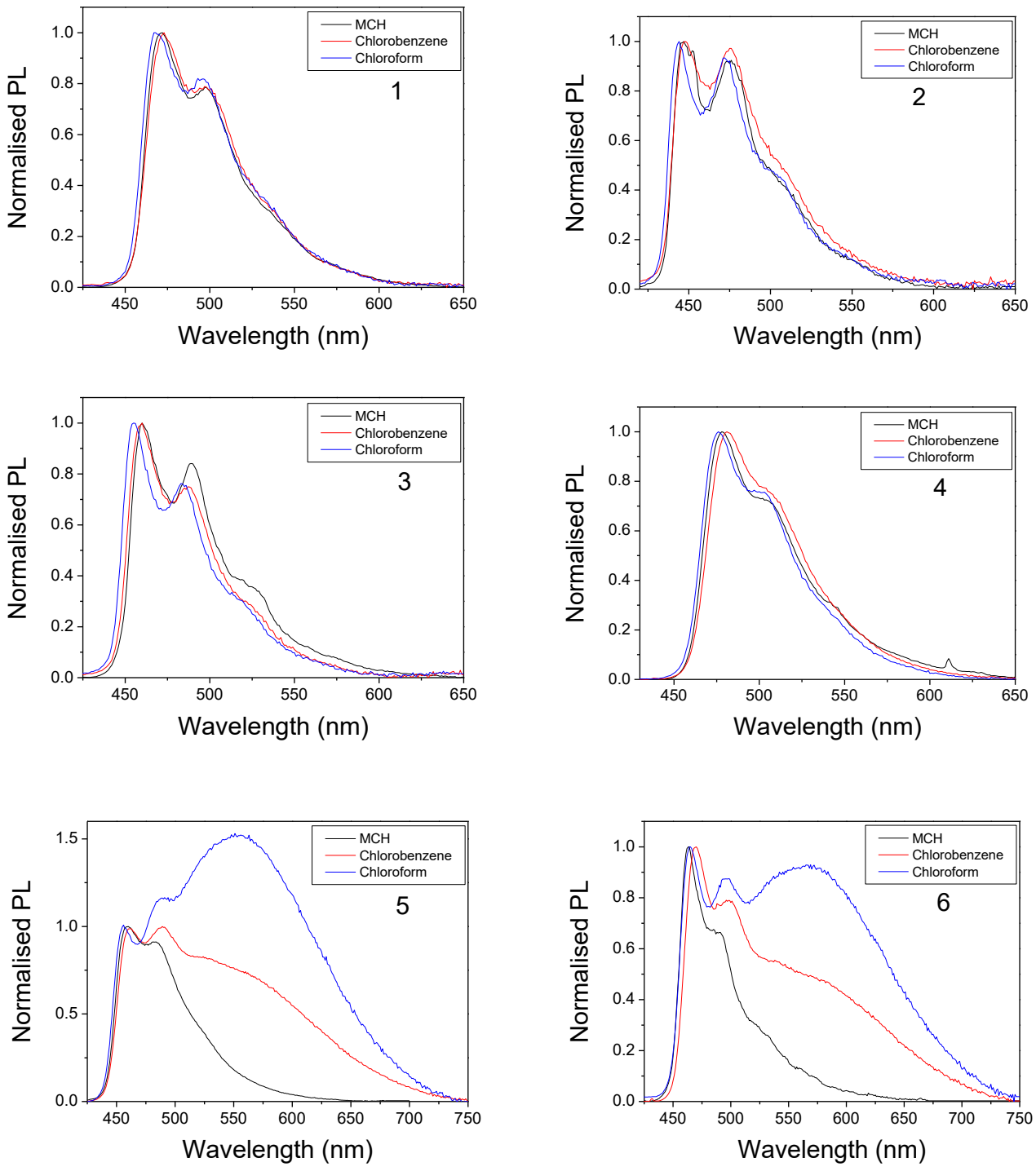

Figure 4: Emission spectra of complexes **1**-**6** in different solvents [10^{-5} M]. MCH = methylcyclohexane

The PLQYs and lifetimes of complexes **1**-**6** in solution (chlorobenzene) are listed in Table 2. For complexes **5** and **6**, the lifetimes of the two emission bands were measured, and the values for the two features are the same within experimental error. This is highlighted by the decay profile of complex **5** (Figure S11), which shows no significant change in spectral features during the decay, suggesting that the emission bands come from two states where interconversion is fast.

Table 2: Photophysical data for selected compounds.

Compound	λ_{max}^{abs} (ε) / nm (x10^3 M^{-1} cm^{-1})[a]	λ_{max}^{em} / nm[b]		PLQY / Φ_{PL}[c]	τ_P / µs[d]
1	290 (32.7), 323 (17.6), 345 (10.2), 385 (7.3), 430 (2.9), 459 (0.9)	MCH	470, 497	-	-
		CBZ	472, 498	0.44	1.72
		$CHCl_3$	467, 496	-	-
2	290 (31.5), 317 (22.3), 365 (8.8), 411 (1.1), 438 (0.4),	MCH	446, 475	-	-
		CBZ	447, 474	0.37	1.76
		$CHCl_3$	444, 472	-	-
3	293 (40.8), 306 (34.2), 377 (8.0), 422 (2.4), 450 (0.8),	MCH	460, 489	-	-
		CBZ	459, 486	0.30	1.61
		$CHCl_3$	454, 484	-	-
4	296 (52.4), 315 (46.6), 364 (29.8), 379 (26.2), 400 (16.7), 436 (3.8), 463 (1.8)	MCH	477, 508	-	-
		CBZ	480, 510	0.41	1.90
		$CHCl_3$	475, 506	-	-
5	306 (55.9), 313 (53.0), 365 (33.8), 382 (38.7), 445 (0.9)	MCH	460, 484	-	-
		CBZ	461, 489, 565	0.30	0.83 (460) 0.79 (550)
		$CHCl_3$	456, 488, 564	-	-
		Zeonex	459, 486	0.08	1.69
6	296 (64.5), 308 (62.3), 372 (31.0), 389 (33.8), 454 (1.7)	MCH	463, 490	-	-
		CBZ	469, 499, 583	0.13	0.52 (470) 0.49 (550)
		$CHCl_3$	464, 496, 581	-	-
9	306 (24.6)	MCH	406	-	-
		CBZ	469	0.09 [0.02]	0.039,[e] 0.768[e] [0.030]
		$CHCl_3$	479	-	-
10	302 (24.1), 314 (sh, 23.6)	MCH	427	-	-
		CBZ	504	0.10 [0.01]	0.099,[e] 0.946[e] [0.029]
		$CHCl_3$	521	-	-
11	302 (26.5), 315 (sh, 24.1)	MCH	451	-	-
		CBZ	512	0.09 [0.02]	0.094,[e] 0.574[e] [0.023]
		$CHCl_3$	534	-	-

[a] Data obtained in toluene solution at 20 °C, sh = shoulder. [b] Data obtained in degassed solvent, with λ_{ex} = 365 nm for **1**-**6**, λ_{ex} = 340 nm for **9-11**. MCH = methylcyclohexane, CBZ = chlorobenzene, Zeonex = a cyclic olefin polymer.[37] [c] For **1**-**6**, measured in degassed solvent, relative to quinine sulfate (Φ_{PL} = 0.546 in 0.5 M H_2SO_4) at 20 °C; for **9**-**11**, measured using an integrating sphere**,** [ ] refers to the PLQY in aerated solvent; estimated error ±5%. [d] Estimated error ±5%, measured in deaerated solvent. The number within ( ) refers to the wavelength corresponding to the lifetime. [ ] refers to a lifetime in aerated solvent. [e] Lifetimes for prompt and delayed fluorescence respectively.

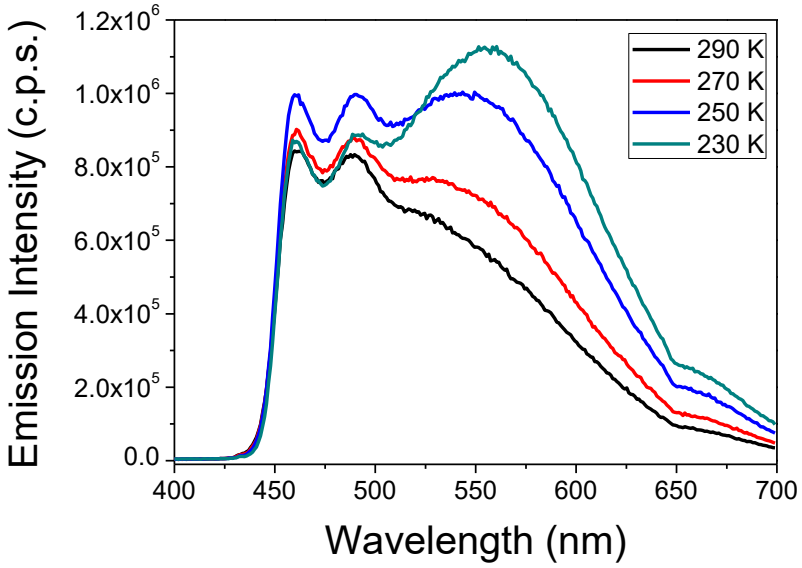

Figure 5: The temperature dependence of the emission profile of **5** in chlorobenzene [10^{-5} M].

In order to better understand the source of the broadened emission in complexes **5** and **6**, more photophysical measurements were conducted on complex **5**. The effect of temperature on the emission spectrum of complex **5** in chlorobenzene (Figure 5) showed that on decreasing the temperature from room temperature to 230 K the ratio between emission bands changed, with an increase in the intensity of the lower energy feature relative to the higher energy feature. The possibility of the second feature corresponding to emission from an excimer was dismissed as emission spectra of **5** recorded in both concentrated and dilute chlorobenzene solution had comparable spectral profiles (Figure S12). Additionally, there was no change in spectral profile on exposure to oxygen (Figure S13); the emission intensity decreased as expected for a state with triplet character. These findings are consistent with the lifetime measurements, which indicated that the emission bands originate from states that are able to quickly interconvert. The possibility of the dual emission being due to a degradation product of **5** in polar solvents was also ruled out. The emission spectrum of a sample of **5** dissolved in $CHCl_3$ was measured and showed the dual emission feature, the solvent was then removed *in vacuo* and the residue redissolved in MCH. The emission spectrum was then measured again and the second emission feature was not observed (Figure S14).

The emission measurements of **5** were also investigated in the solid state, in the form of spin-coated zeonex (a cyclic olefin polymer)[37] films (1-5% w/w), and are summarised in Table 2. The emission profile (Figure S15) resembles that of the emission in non-polar MCH solution. The emission of the film was also investigated at low temperatures (to 230 K), but no change in emission profile was observed (Figure S15). The lack of a broadened emission in these films compared to chlorobenzene solutions could be due to the low polarity of host material, the lack of free molecular motions in the solid state, or both.

As the appearance of the second emission feature was observed only for complexes **5** and **6** it is clear that the carbazole moiety plays a significant role in the emissions. In order to understand this, the emissions of ligands **9**-**11** were investigated (Figure 6), with lifetime and PLQY data listed in Table 2. All three ligands exhibit broad, featureless emissions with large Stokes shifts. The emission maximum in each ligand shifs significantly on increasing solvent polarity, consistent with a charge transfer (CT) state. Notably, the emission of **9** is significantly blue-shifted in all solvents compared to the emission of **10** and **11**; this can be attributed to the significantly weaker acceptor strength of the difluorophenyl group compared to the difluorocyanophenyl or difluoropyridyl groups. The emission of the ligands was quenched by oxygen (Figures S16-18), and the ratio (Φ_{DF}/Φ_{PF}) between the prompt emission (PF) and the delayed emission (DF), calculated from the steady-state emission spectra, ranged from 1.02 (for **9**) to 3.07 (for **11**). Lifetime measurements (Figures S19-21) indicated the presence of two decays, one on the order of 40-100 ns, and the other on the order of 500-1000 ns. Based on these observations, and the donor-acceptor structure of the ligands, the emissions from **9**-**11** are attributed to TADF processes.[38]

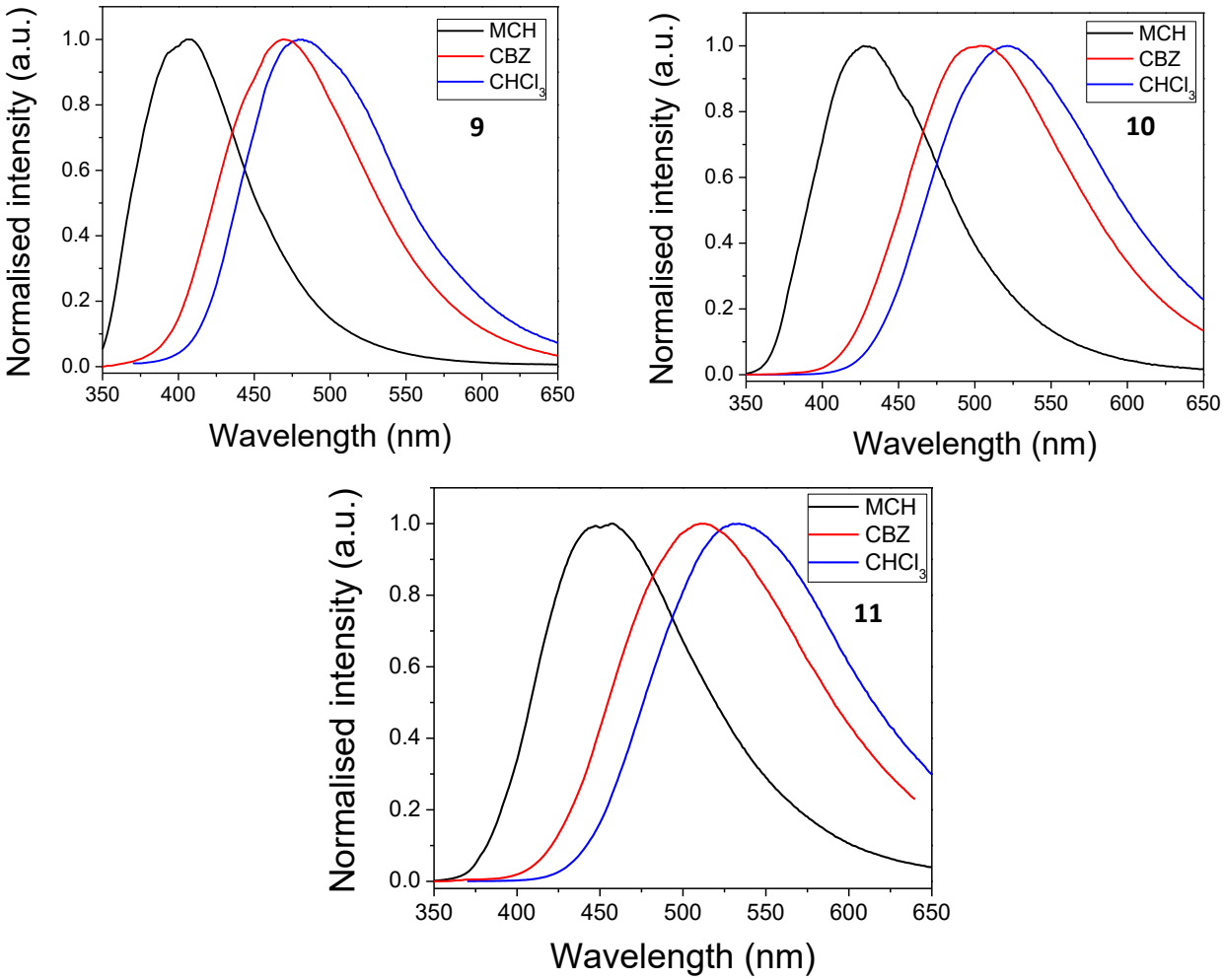

Figure 6: Emission spectra of ligands **9-11** in solvents of differing polarities**.** MCH = methylcyclohexane, CBZ = chlorobenzene.

With the knowledge that ligands **9**-**11** possess low-lying emissive states, the emission behaviour of complexes **4**-**6** can now be interpreted. In Figure 7, the energies of the ligand ^{1}CT states, estimated from the onset of the emission of **9**-**11**, were compared to the energies of the LC/MLCT states of the complexes, which were determined from the onset of their characteristic emission feature. This comparison clearly highlights the difference between complex **4**, where the ligand has a weaker acceptor, and complexes **5** and **6**, where the ligands have stronger acceptors. In the case of **4**, the energy of the emissive state of the ligand was always significantly greater (>0.3 eV) than that of the MLCT state of the complex irrespective of solvent polarity. However, for **5** and **6** while the gap is wide (>0.3 eV) in MCH it decreased dramatically on increasing solvent polarity, dropping to only 0.05 eV in chloroform. Based on this observation, we propose that the emissive behaviour of **5** and **6** is due to the formation of a mixed CT-MLCT state, which arises when the ^{1}CT state on the ligand lies close in energy to that of the ^{3}MLCT state of the complex. As TADF was observed for ligands **9**-**11**, the energy of the ^{3}CT state is expected to be similar to that of the ^{1}CT state. The lack of change in the emission decay profile of **5** in chlorobenzene, and the fact that the profile emission is unchanged on exposure to oxygen, indicates that a fast equilibrium exists between the ^{3}CT and ^{3}MLCT states. Changing solvent, or changing the temperature, perturbs this equilibrium and shifts the emission to favour either the ^{3}CT or ^{3}MLCT state. Under conditions where the gap between the ^{3}CT and ^{3}MLCT is large (>0.3 eV), such as for complex **4** in all solvents, and complexes **5** and **6** in MCH, there is no state mixing and emission occurs purely from the MLCT state. It is noted here that the broad CT feature in the emission of complexes **5** and **6** is lower in energy than in the spectra of the free ligands; this can be explained by coordination to the metal centre shifting the energy of the ^{3}CT state.

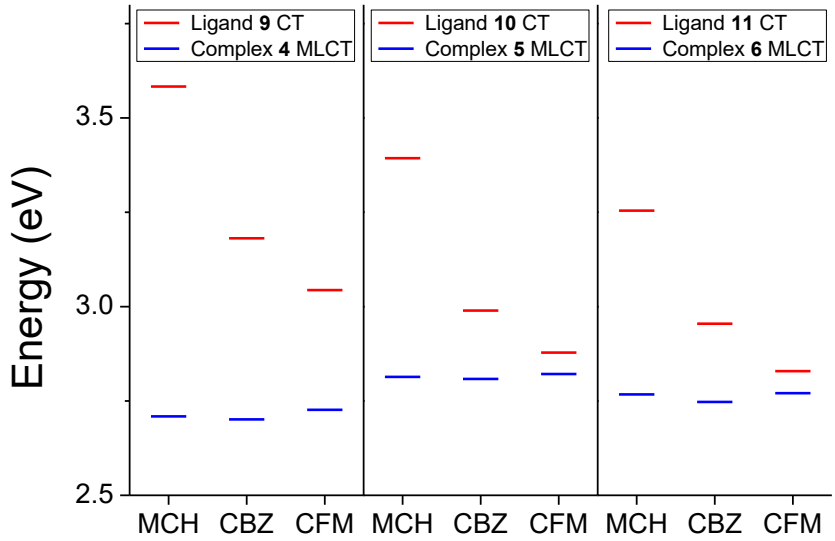

Figure 7: Energy levels of the free ligand CT state in ligands **9**-**11**, measured from the onset of the emission, compared to the energy level of the LC/MLCT state in complexes **4**-**6**, measured from the onset of the emission. MCH = methylcyclohexane, CBZ = chlorobenzene, CFM = chloroform.

DFT Calculations.

Electronic structure calculations were carried out on complexes **2**-**6** and ligands **7**-**11** to explore their frontier orbitals and understand the nature of the transitions involved in the emissions. In the case of complexes with carbazole moieties

(**4**-**6**) four minima were located with approximately equal energies, differing only by orientation of the carbazole groups (Figures S22-24). The orbital contributions were comparable for all four conformers so only one conformer is discussed here for convenience.

The frontier orbitals for representative Ir complexes **2**, **4** and **5** are shown in Figure 8, with the orbitals for complexes **3** and **6** presented in the SI (Figure S25). The percentage contributions of groups to the MOs are listed in Tables S3-S16. A clear difference can be seen between the complexes that contain carbazole moieties (**4**-**6**) and those that do not (**2**, **3**). For complexes **2** and **3** the HOMO has a considerable contribution from the Ir centre (40-55%), while for complexes **4**-**6** the HOMO and HOMO-1 are located on the two carbazole fragments, with the Ir contributing to occupied orbitals at lower energies (HOMO-2 and below, see Tables S5 - S16). This is consistent with the cyclic voltammetry measurements which indicated that the first oxidation takes place at the carbazole units in complexes **4**-**6**.

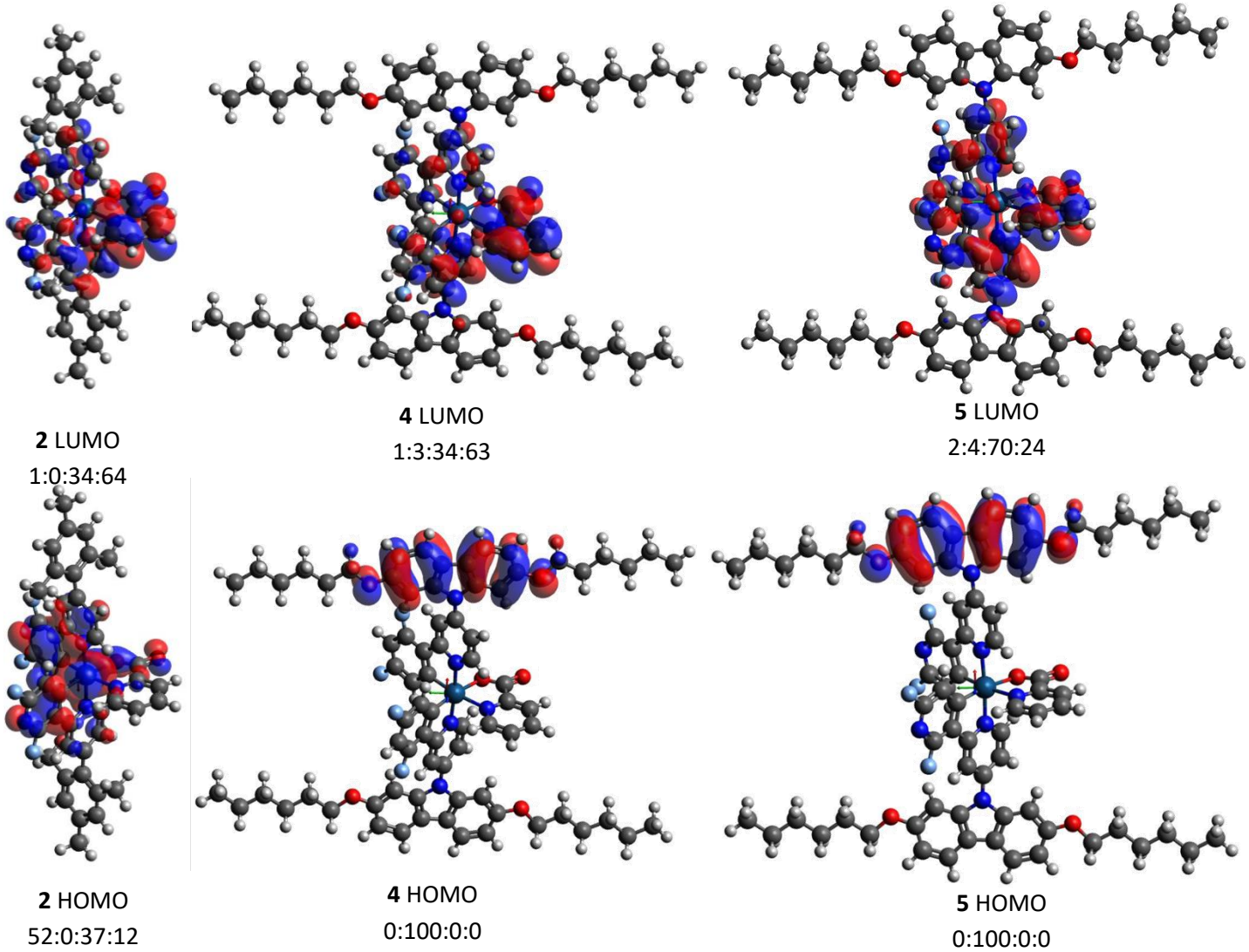

Figure 8: Frontier molecular orbitals for **2**, **4**, and **5**. Isocontours set to ±0.02 e/bohr^3. The % orbital contribution ratio is listed for each orbital in the order Ir:mesityl/carbazolyl:phenylpyridyl:picolyl .

There is also a noticeable difference in the molecular orbitals between the carbazole complexes **5** and **6,** which display dual emissions, and the carbazole complex **4**, which does not. In **5** and **6**, the orbitals possessing significant Ir contribution are much lower in energy (HOMO-4, HOMO-5, see Tables S5 to S16) than those of **4**. This lack of metal contribution in the frontier occupied orbitals could explain the relatively low quantum yields of these complexes compared to the mesityl analogues. The complexes that show dual emission also have a different LUMO makeup to the other complexes. The LUMOs of complexes **2**-**4** all possess large contributions (30-60%) from the picolinate ligand, while its contribution to the LUMOs of **5** and **6** is below 25% (see Tables S2 to S15).

TD-DFT calculations were performed on the S_0 optimised geometries of **2**-**6** to give insight into their emission behaviour; the results are summarised in Tables S17-S30. For complexes **2** and **3** the character of all the lowest energy triplet transitions is similar and can be described as MLCT/LLCT in nature, with electron density transferring from the Ir (with 35-50% change in character) and the phenyl groups to the pyridine rings and picolinate ligand. The corresponding transitions for complex **4** still show a large amount of MLCT character across all geometries, with changes of 26-40% in the Ir electron density, despite the fact the HOMO and HOMO-1 are carbazole based. The carbazole moiety contributes to some of the transitions, with contributions ranging from 2 to 40%, with greater contributions to states higher in energy. Electron density is mostly transferred to the picolinate ligands and the pyridine moiety.

In the case of complexes **5** and **6**, there exist four states within 0.06 eV in energy that differ quite significantly in their composition. Two of the four states involve electron density transfer from one of the carbazole units (95-100%) to the pyridine, difluoropyridyl/difluorocyanophenyl and picolinate moieties, indicating a state of strong CT character. The other two states can be described as mixed MLCT/LLCT states, with electron density being transferred predominantly from Ir (13-16% change) and carbazole (47-62% change) to the pyridine, difluoropyridyl/difluorocyanophenyl and picolinate moieties. Compared to complexes **2**-**4** the metal centre is clearly less involved in the transitions for **5** and **6**. These two different transition characters correspond to the ^{3}CT and ^{3}MLCT emissions observed for **5** and **6**.

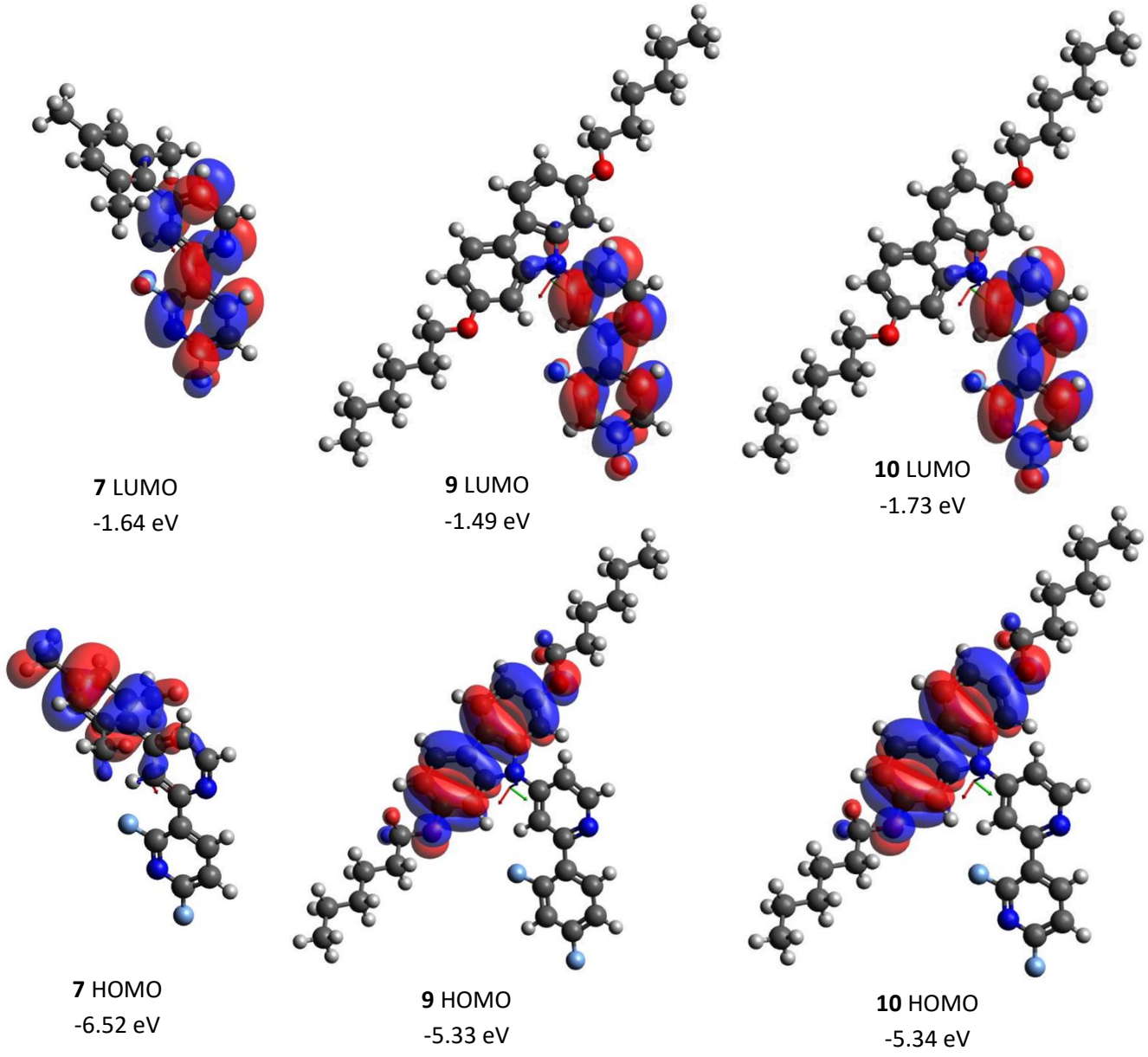

Figure 9: Frontier molecular orbitals for **7**, **9**, and **10**. Isocontours set to ±0.02 e/bohr^3.

The frontier orbitals of ligands **7**, **9** and **10** are shown in Figure 9, with the orbitals for ligands **8** and **11** visualised in the SI (Figure S26). For ligands **7** and **8**, the HOMOs are located over the mesityl groups, while for ligands **9**-**11** the HOMOs are exclusively located on the carbazole moieties. In all ligands, the LUMOs are spread over the 2-phenylpyridine framework. The HOMO-LUMO gaps for ligands **9**-**11** are notably smaller (3.47-3.84 eV) than those of **7**-**8** (4.70-4.90 eV), a result of the introduction of the electron-rich carbazole moiety.

Small singlet-triplet energy gaps ($\Delta E_{S\text{-}T}$) in donor-acceptor molecules usually promote TADF so $\Delta E_{S\text{-}T}$ energies for ligands **7**-**11** were calculated from the vertical excitation energies determined from TD-DFT and listed in Table 3. At the optimised S_0 geometries, $\Delta E_{S\text{-}T}$ is relatively small for ligands **9**-**11** (<0.30 eV) while the values are much larger for ligands

7-**8** (1.02 eV), which is consistent with the assignment of TADF emissions from ligands **9**-**11**. When the dihedral angle between the carbazole donor and the pyridyl acceptor is restricted to 90° ('Perpendicular' Geometry in Table 3) the ΔE_{S-T} drops to ca. 0.12 eV for **9** and < 0.005 eV for **10** and **11**, thus TADF would increase. This dependence on conformation may be a factor in the differences between solution and solid state emissions for complexes **5** and **6**.

Table 3: ΔE_{S-T} for ligands **7**-**11** from TD-DFT computations.

Ligand	Optimised Geometry			'Perpendicular' Geometry		
	E_{S1} (eV)	E_{T1} (eV)	ΔE_{S-T} (eV)	E_{S1} (eV)	E_{T1} (eV)	ΔE_{S-T} (eV)
7	4.290	3.267	1.023	-	-	-
8	4.195	3.179	1.016	-	-	-
9	3.369	3.080	0.289	3.216	3.094	0.122
10	3.162	3.067	0.095	3.012	3.008	0.004
11	3.056	3.022	0.034	2.914	2.911	0.003

The lack of solvatochromic effects in the absorption spectra for **9**-**11** (Figure S10) can be explained as their S0 -> S1 CT transitions have low oscillator strengths (Tables S31-33) due to the almost total lack of overlap between the HOMO and the LUMO in each case. The solvatochromic low energy bands predicted at 3.1-3.4 eV (Table 3) for **9**-**11** were not observed above the noise levels in the absorption spectra (Figure S10). The TD-DFT results for ligands **9**-**11** indeed predict that the oscillator strengths for these transitions are very weak.

DEVICE DATA

To our knowledge, no OLED devices have been reported that use complexes that display dual emissive properties in solution as the emissive material. Complexes containing ligands with donor and acceptor groups, both on the same ligand,[28] and on different ligands,[36] that do not show dual emission properties in solution have been used in OLED devices, and display favourable performances due to their enhanced charge transport properties. OLEDs using complexes **1**-**6** as the emitters were fabricated and compared to a reference device containing **FIrpic**. The hole transporting layer and emissive layer were deposited by solution processing techniques, and the electron transporting, electron injection layers and the cathode were then fabricated by vacuum deposition. The device structure is as follows: ITO/ poly(3,4-ethylenedioxythiophene):poly(styrenesulfonate) (PEDOT:PSS, 50 nm)/ poly(vinylcarbazole) (PVK) : 1,3-bis[(4-*tert*-butylphenyl)-1,3,4-oxadiazolyl]phenylene (OXD-7):Ir complex [100:50:8] (75 nm)/ 2,2',2"-(1,3,5-benzinetriyl)-tris(1-phenyl-1*H*-benzimidazole) (TPBi, 25 nm)/LiF (1 nm)/Al. The efficiency and luminance data of the devices are summarised in Table 4.

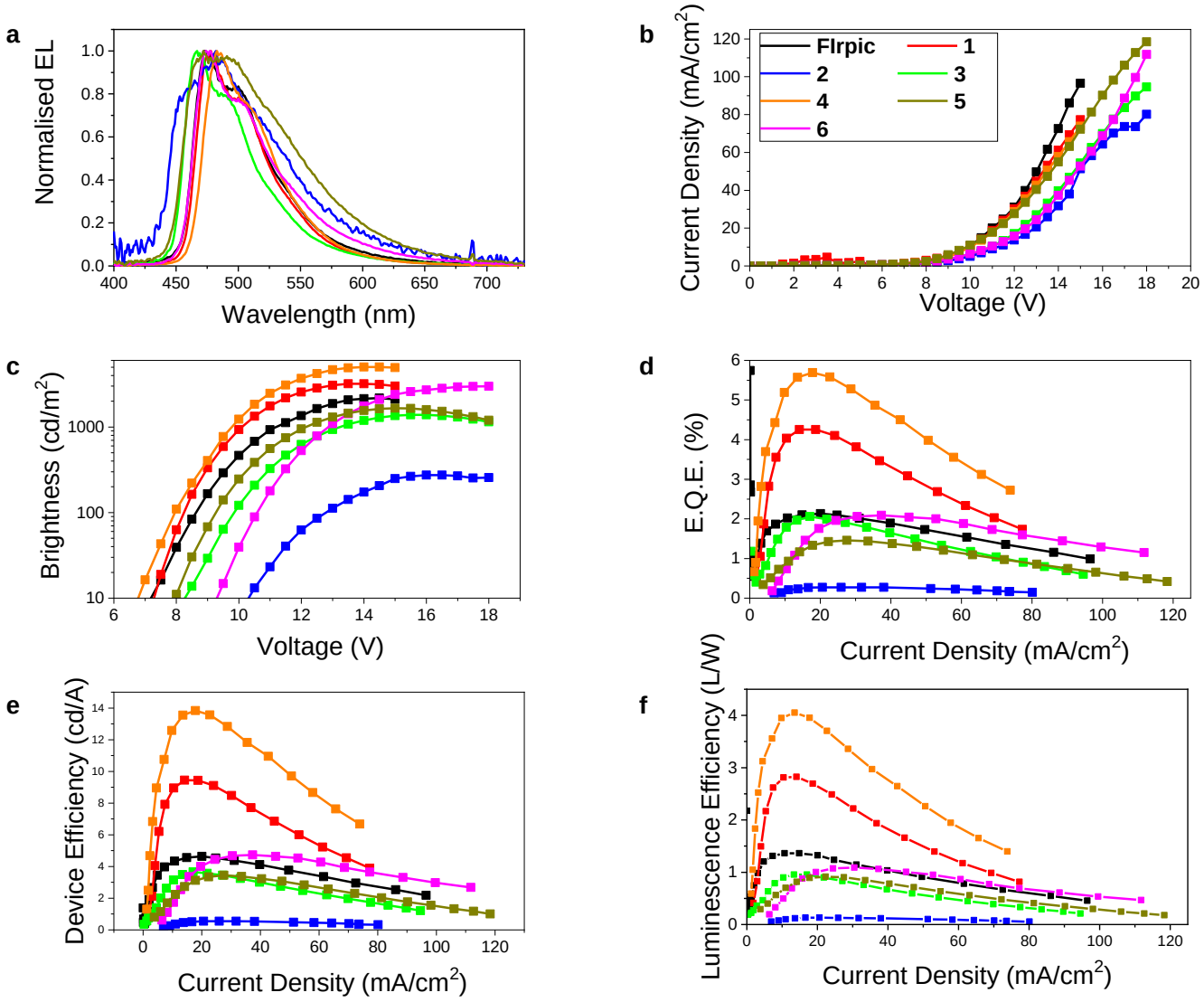

Figure 10: Device data for complexes **1**-**6**. The device structure is as follows: ITO/PEDOT:PSS (50 nm)/PVK:OXD:Ir complex [100:50:8] (75 nm)/TPBi (25 nm)/LiF (1 nm)/Al.

The electroluminescence (EL) spectra from the devices are shown in Figure 10a. For complexes **1**, **3** and **4**, the EL spectra are comparable to the solution-state PL spectra while the EL spectrum for **6** displays no sign of the dual emission present in the PL spectra of **6** in polar solvents. The EL spectra for the devices containing **2** and **5** are significantly broadened compared to the solution PL spectra, suggesting that the bipyridyl ligands in these systems are responsible for the broadening. However, the broadening of the EL band for **5** is not in accord with the dual emission bands present in the PL spectra of **5** in polar solvents. The absence of dual emission may relate to reduced rotational freedom of the complexes in the emissive layer, in agreement with the observations in the thin film studies above.

The device of complex **4** performed the best, outperforming those of **FIrpic** and complex **1** in terms of EQE and brightness; however the device emission was less blue (λ_{ELmax} 484 nm for **4** vs 473 nm for **FIrpic** and 477 nm for **1**). This

improved performance may be explained by the steric bulkiness and solubility enhancement afforded by the carbazole units, which reduce concentration quenching as explained elsewhere for the mesityl groups in **1** compared to **FIrpic**.[21] The devices of the carbazole complexes **5** and **6** also showed improved performances compared to the devices based on the related mesityl complexes **2** and **3**, with superior maximum brightnesses (Figure 10c), current efficiencies (Figure 10e) and turn-on voltages; however, the emission of devices based on carbazole-containing complexes was again less blue than their mesityl analogues (Table 4). The device from the carbazole complex **6** showed very similar performance and emission colour to the **FIrpic** device.

Table 4: Summary of device data.

Complex	λ_{ELmax} / nm	Max Brightness / cd/m^2	Turn-on voltage / V [a]	Max EQE / %	Current efficiency / cd/A	Power efficiency / lm/W	CIE coordinates / (x,y) [b]
FIrpic	473	2179	7.2	2.14	4.63	1.36	(0.17, 0.37)
1	477	3195	7.3	4.26	9.44	2.83	(0.17, 0.39)
2	450-500	274.4	10.3	0.27	0.55	0.13	(0.22, 0.33)
3	468	1383	8.2	2.06	3.57	0.96	(0.16, 0.29)
4	484	5013	6.8	5.69	13.84	4.05	(0.17, 0.46)
5	472-491	1657	9.3	1.46	3.44	0.91	(0.22, 0.38)
6	476	2988	8.0	2.09	4.73	1.09	(0.19, 0.38)

[a] Measured at a brightness of 10 cd/m^2. [b] Measured at 12 V.

Conclusions

A series of iridium complexes (**2**-**6**) were synthesised containing ligands with donor and acceptor groups of varying strengths to establish design rules for dual-emitting complexes. Ligands containing the carbazole group (**9**-**11**) showed weak TADF emissions due to their strong donor-acceptor systems, with small $\Delta E_{S\text{-}T}$ gaps as determined by TD-DFT computations compared to ligands with a mesityl group (**7**, **8**) which have large $\Delta E_{S\text{-}T}$ gaps. Complexes **5** and **6**, derived from TADF ligands **10** and **11** respectively, showed dual emissions in polar solvents with a broad CT band that increases in relative intensity compared to the MLCT emission with increasing solvent polarity. Photophysical investigations revealed that dual emission occurs when the energy of the ligand ^{3}CT state, which is highly susceptible to the solvent environment, approaches the energy of the ^{3}MLCT state, which experiences little change on increasing solvent polarity. The nature of these states was confirmed by DFT calculations. Dual emission is observed from both states simultaneously and with the same lifetime, indicating a fast equilibrium between the ^{3}LC and ^{3}MLCT states. This equilibrium can be perturbed to favour one state over the other by changes in temperature and solvent polarity. Devices of the iridium complexes were fabricated with identical structures and their performances compared with an equivalent **FIrpic** device. The device containing the carbazole complex **4** showed superior performance compared to the **FIrpic** device. To the best of our knowledge, the devices containing complexes **5** and **6** are the first devices based on dual-

emissive iridium complexes but they did not display dual emissions under operation. The device containing **6** performed similarly to that containing **FIrpic**. There remains considerable scope for harnessing dual-emissive complexes in PhOLEDs.

EXPERIMENTAL SECTION

Materials, Synthesis, and Characterization

General procedures

All commercially available chemicals were used without further purification unless stated otherwise. Reactions requiring an inert atmosphere were performed under a blanket of argon gas, which was dried over a phosphorus pentoxide column. Anhydrous solvents were dried through an HPLC column on an Innovative Technology Inc. solvent purification system. Column chromatography was performed using 40-60 μm mesh silica gel. Analytical TLC was performed on plates pre-coated with silica gel (Merck, silica gel $60F_{254}$) and visualised using UV light (254, 315, 365 nm). NMR spectra were recorded on Bruker Avance 400 MHz, Varian Mercury 200, and 400 MHz, Varian Inova 500 MHz or Varian VNMRS 600 and 700 MHz spectrometers. ^{1}H and ^{13}C chemical shifts are referenced to tetramethylsilane [TMS, $Si(CH_3)_4$] at 0.00 ppm, ^{19}F chemical shifts are referenced externally to $BF_3.Et_2O$ at 0.0 ppm. Melting points were determined in open ended capillaries using a Stuart Scientific SMP3 melting point apparatus at a ramping rate of 1 °C/min. They are reported to the nearest 0.1 °C. ESI and MALDI mass spectra were recorded on a Thermo-Finnigan LTQ FT (7.0 T magnet) spectrometer. ASAP mass spectra were recorded on a Waters Xevo QTOF spectrometer. GCMS spectra were recorded on a Thermo-Finnigan Trace GCMS (EI and CI ion sources). Elemental analyses were obtained on an Exeter Analytical Inc. CE-440 elemental analyser. Where solvent mixtures are mentioned any percentage/ratio is by volume.

Electrochemistry

Cyclic voltammetry (CV) measurements were recorded at a scan rate of 100 mV s^{-1} at room temperature using an air-tight single-compartment three-electrode cell equipped with a Pt working electrode (1.2 mm surface diameter), Pt wire counter electrode and Pt wire pseudo-reference electrode. The cell was connected to a computer-controlled Autolab PG-STAT 30 potentiostat using GPES software. The solutions contained the compound (1 mg/mL) and *n*-Bu_4NPF_6 (0.1 M) as the supporting electrolyte in dichloromethane (CH_2Cl_2). All potentials were determined with the ferrocene/ferrocenium couple (FcH/FcH^+) as an internal reference at $E_{1/2}$ = 0.0 V.

Solution photophysics

Solution state photophysical data of the complexes **1**-**6** were obtained using freshly prepared solutions in the solvent specified. UV-vis absorption measurements were measured using a UV-3600 double beam spectrophotometer (Shimadzu). Baseline correction was achieved by reference to pure solvent in the same cuvette. Absorption measurements were obtained using quartz cuvettes with a path length of 1 cm.

Emission and lifetime measurements were taken using thoroughly degassed solutions achieved by three freeze−pump−thaw cycles, and obtained using a quartz cuvette with a path length of 1 cm. The solutions had absorbance below 0.10 to minimise inner filter effects. Emission spectra of complexes **1**-**6** were recorded on a Horiba Jobin Yvon SpexFluoromax 3 Spectrometer or a Horiba Jobin Yvon SPEX Fluorolog 3-22 spectrofluorometer. Solution PLQYs were recorded in degassed solvent, and determined using the relative method using quinine sulfate (Φ_{PL} = 0.546 in 0.5 M H_2SO_4) as the reference. The PLQYs are computed according to the following equation:

$$\Phi_x = \Phi_{ref} \frac{Grad_x}{Grad_{ref}} \cdot \left(\frac{\eta_x}{\eta_{ref}}\right)^2$$

where subscripts 'x' and 'ref' denote the material being measured and the reference, respectively. Φ represents the PLQY, Grad is the gradient from the plot of integrated fluorescence intensity vs absorbance, and η is the refractive index of the solvent.

Solutions of the complexes in degassed solvent [< 10^{-5} M] were used for decay measurements. The sample was excited by the output of a pulse laser diode which produced a 1 kHz train of pulses of 20 ns duration at 405 nm. The luminescence was collected at 90° and focused onto the entrance slit of a monochromator (Bethan TM 300V). The emission was detected by a photon counting PMT and the arrival times of photons at the detector were determined using a multichannel scaler. Time-resolved phosphorescence spectra and decay curves were recorded using nanosecond gated luminescence and lifetime measurements (from 1 ns to 1 s) using either third harmonics of a high energy pulsed Nd:YAG laser emitting at 355 nm (EKSPLA) or a N_2 laser emitting at 337 nm. Emission was focused onto a spectrograph and detected on a sensitive gated iCCD camera (Stanford Computer Optics) having sub-nanosecond resolution.

All optical analyses for **9**-**11** were carried out in quartz cuvettes with a path length of 1 cm. Absorbance spectra were measured on a Cary 5000 UV-Vis-NIR spectrometer with Cary WinUV Scan software. Emission spectra were recorded on a Jobin Yvon Fluorolog-3 luminescence spectrometer with a CCD detector using FluorEssence software. Photoluminescence quantum yields (PLQYs) were measured using a calibrated Quanta-ϕ integrating sphere coupled with a Jobin Yvon FluoroLog-3 spectrometer and PMT detector (0.5 s integration time) and analysed using FluorEssence software. Time-resolved measurements (TCSPC, time-correlated single-photon counting) were performed on a Horiba Deltaflex system with EzTime software.

Thin films and devices

Details of thin film and device fabrication are included in the Supporting Information.

Computational studies

All calculations were run using the Gaussian09 software package.[39] Analysis of the molecular orbital contributions was conducted with GaussSum.[40] Calculations on complexes **2**-**6** and ligands **7**-**11** were carried out using the B3LYP[41,42]

functional with the LanL2DZ[43–46] pseudopotential for Ir and the 3-21G* basis set for N, C, O, F and H.[47,48] The solvent effect (solvent = chloroform) was applied within the self-consistent reaction field (SCRF) theory using the solvation model density (SMD) keyword that performs a polarised continuum model (PCM)[49,50] calculation with the use of the solvation model of Truhlar and co-workers.[51] All S_0 optimised geometries of the most stable conformers were true minima based on no imaginary frequencies being found. Electronic structure and TD-DFT calculations were generated from the optimised geometries at B3LYP/LANL2DZ:3-21G*.

Synthesis

2-(2,6-difluoro-3-pyridyl)-4-(2,4,6-trimethylphenyl)pyridine 7

2-Chloro-4-(2,4,6-trimethylphenyl)pyridine, **12** (1.50 g, 6.47 mmol), 2,6-difluoropyridyl-3-MIDA boronate, **13** (2.10 g , 7.77 mmol), $Pd_2(dba)_3$ (0.089 g, 0.097 mmol) and PCy_3 (0.065 g, 0.233 mmol) were placed under an argon atmosphere. Degassed aqueous 1.27 M K_3PO_4 (16.2 ml, 48.6 mmol) and 1,4-dioxane (80 ml) were added with stirring to the reaction mixture. The reaction mixture was stirred at 60 °C for 60 h and monitored by TLC. After cooling to room temperature the 1,4-dioxane was removed *in vacuo*. Ethyl acetate (150 ml) was added, and the mixture was transferred to a separating funnel and washed with brine (3 x 100 ml). The organic layer was then dried over $MgSO_4$, filtered and the solvent removed *in vacuo*. The residue was purified by column chromatography (4:1 hexane/ethyl acetate) followed by recrystallisation from methanol, to give **7** as a white solid (0.69 g, 34%); 74.5 – 75.9 °C; Anal. Calcd. for $C_{19}H_{16}F_2N_2$: C, 73.53; H, 5.20; N, 9.03. Found: C, 73.70; H, 5.09; N, 9.12; δ_H (400 MHz; $CDCl_3$; Me_4Si) 8.96 – 8.65 (2H, m), 7.71 (1H, d, *J* 1.5), 7.18 (1H, dd, *J* 5.0, 1.5), 7.03 (1H, dd, *J* 8.2, 3.0), 7.00 (2H, s), 2.37 (3H, s), 2.06 (6H, s); δ_C (125 MHz; $CDCl_3$; Me_4Si) 164.8 (dd, *J* 244.0, 13.6), 163.5 (dd, *J* 246.3, 14.7), 151.9, 151.0, 148.5, 145.0 (d, *J* 4.4), 138.9, 138.0, 137.2, 128.1, 120.8 (dd, *J* 26.2, 5.7), 118.7, 114.3, 107.7 (dd, *J* 35.5, 5.2), 24.7, 18.1; m/z (ES+) 311.3 $(M+H)^+$.

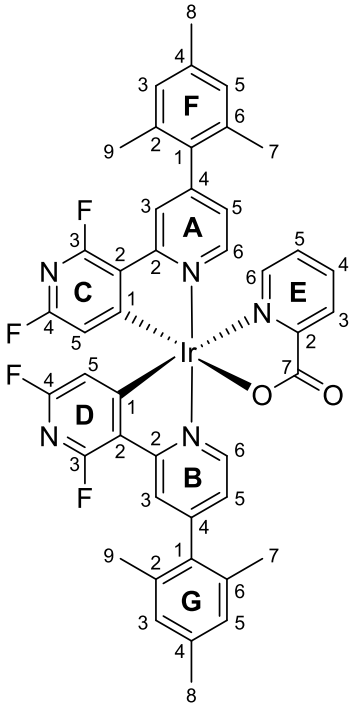

Iridium complex 2

A mixture of 2-(2,6-difluoro-3-pyridyl)-4-(2,4,6-trimethylphenyl)pyridine **7** (1.20 g, 3.88 mmol), $IrCl_3•3H_2O$ (0.58 g, 1.65 mmol), 2-ethoxyethanol (32 ml) and water (12 ml) was heated to 110 °C overnight under an argon atmosphere. The resulting yellow precipitate was collected by filtration and washed sequentially with water (100 ml) and a mixture of ethanol and acetone (1:1 v/v 80 ml). Picolinic acid (0.95 g, 7.73 mmol) and 2-ethoxyethanol (20 ml) were added to the precipitate, and the mixture was heated to 110 °C for 16 h. The solution was cooled and water was added. The precipitate was collected, dried and purified by column chromatography (hexane:EtOAc 2:1, then a second column, CH_2Cl_2:EtOAc 5:1), to give **2** as a pale yellow solid (0.708 g, 46%); Anal. Calcd. for **2**•0.2(CH_2Cl_2) Anal. Calcd. for $C_{44.2}H_{34.4}Cl_{0.4}F_4IrN_5O_2$: C, 55.88; H, 3.65; N, 7.37. Found: C, 55.63; H, 3.66; N, 7.28; δ_H (400 MHz; $CDCl_3$; Me_4Si) 8.83 (1H, d, *J* 5.8 H_{A6}), 8.42 (1H, d, *J*

7.7, H_{E3}), 8.12 (m, H_{B3}), 8.07 (1H, m, H_{A3}) 8.07 (1H, m, H_{E4}), 7.89 (1H, dd, *J* 5.4, 0.5 H_{E6}), 7.58 (1H, ddd, *J* 7.2, 5.4, 1.5, H_{E5}), 7.49 (1H, d, *J* 5.8 H_{B6}), 7.18 (1H, dd, *J* 5.8, 1.6, H_{A5}), 7.04 (1H, s, $H_{F3/5}$), 7.01 (2H, s, $H_{F3/5}$+$H_{G3/5}$), 6.98 (1H, s, $C_{G3/5}$), 6.95 (1H, dd, *J* 5.9, 1.8 Hz, H_{B5}), 5.81 (1H, t, *J* 1.7, H_{C5}), 5.55 (1H, t, *J* 1.7, H_{D5}), 2.34 (6H, s, H_{G8}+H_{F8}), 2.13 (3H, s, $H_{F7/9}$), 2.10 (3H, s, $H_{G7/9}$), 2.08 (3H, s, $H_{G7/9}$), 1.95 (3H, s, $H_{F7/9}$); δ_F (376 MHz; $CDCl_3$; Me_4Si) -67.73 (1F, d, *J* 9.3), -68.26 (1F, d, *J* 9.4 Hz), -69.30 (1F, d, *J* 9.3), -70.01 (1F, d, *J* 9.4); δ_C (125 MHz, $CDCl_3$; Me_4Si) 172.38 (C_{E1}), 170.38 (d, *J* 6.0, C_{D1}), 169.86 (d, *J* 6.0, C_{C1}), 163.59 (d, *J* 10.1, C_{B2}), 162.17 (d, *J* 10.1, C_{A2}), 161.13 (dd, *J* 253.4, 15.5, $C_{C3/4}$), 160.58 (dd, *J* 252.5, 15.5, $C_{D3/4}$), 157.66 (dd, *J* 254.2, 16.7, $C_{C3/4}$), 157.43 (dd, *J* 254.2, 16.2, $C_{D3/4}$), 153.49 (C_{A4}), 153.55 (C_{B4}), 151.26 (C_{E2}), 148.67 (C_{A6}), 148.31 (C_{E6}), 147.97 (C_{B6}), 139.21 (C_{E4}), 138.66 ($C_{F/G4}$), 138.61 ($C_{F/G4}$), 135.23 ($C_{G2/6}$), 134.99 ($C_{F2/6}$), 134.71 ($C_{G2/6}$), 134.55 (C_{G1}+$C_{F2/6}$), 134.52 (C_{F1}), 129.02 (C_{E3}), 128.92 (C_{E5}), 128.88($C_{F3/5}$), 128.79 ($C_{G3/5}$), 128.63 ($C_{F3/5}$+$C_{G3/5}$), 125.00 (C_{A5}), 124.99 (C_D+C_{C2}), 124.96 (d, *J* 16.9, C_{B3}), 124.76 (C_{B5}), 124.43 (d, *J* 16.9, C_{A3}) 109.57 (dd, *J* 29.6, 4.3, C_{C5}) 109.26 (dd, *J* 30.2, 4.0, C_{D5}), 21.3 (C_{F8}+C_{G8}), 20.83 ($C_{G7/9}$), 20.56 ($C_{G7/9}$+C_{F7}+C_{F9}); MS (MALDI+): *m/z* = 933.2 (M+, 100%). Single crystals of **2**·1.5C_6H_{14} for X-ray analysis were grown by slow evaporation of solvent from a solution of **2** in CH_2Cl_2-hexane.

2-(3-Cyano-2,4-difluorophenyl)-4-(2,4,6-trimethylphenyl)pyridine 8

2-Chloro-4-(2,4,6-trimethylphenyl)pyridine, **12** (1.50 g, 6.47 mmol), 3-cyano-2,4-difluorophenyl MIDA boronate, **14** (2.17 g, 7.78 mmol), palladium(II) acetate (0.073 g, 0.33 mmol) and SPhos (0.266 g, 0.65 mmol) were placed under an argon atmosphere. Degassed aqueous 3 M K_3PO_4 (16.2 ml, 48.6 mmol) and 1,4-dioxane (80 ml) were added with stirring to the reaction mixture. The reaction mixture was stirred at 90 °C for 60 h and monitored by TLC. After this time, more **14** (0.181 g, 0.65 mmol) was added and the reaction stirred at 90 °C for a further 6 h. After cooling to room temperature the 1,4-dioxane was removed by rotary evaporation. Ethyl acetate (150 ml) was added before transferring the mixture to a separating funnel and washing with brine (3 x 100 ml). The organic layer was then dried over $MgSO_4$, filtered and the solvent removed *in vacuo*. The residue was purified by column chromatography (silica, 4:1 hexane / ethyl acetate), and the product-containing fractions were combined and dried *in vacuo*. The crude product was recrystallised from methanol (5 ml) giving **8** as an off-white powder (1.10 g, 51%); m.p. 117 – 118 °C (from MeOH); Anal. Calc. For $C_{21}H_{16}F_2N_2$; C, 75.43; H, 4.82; N, 8.38; Found: C, 75.13; H, 4.90; N, 8.39.; δ_H (400 MHz; $CDCl_3$; Me_4Si) 8.80 (1H, d, *J* 5.6), 8.45 (1H, dt, *J* 8.8, 6.4), 7.63 (1H, s), 7.21 - 7.25 (1H, m), 7.19 (1H, dd, *J* 4.8, 1.6), 7.00 (2H, s), 2.37 (3H, s), 2.06 (6H, s); δ_F (376 MHz; $CDCl_3$) -103.0 - -102.9 (1F, m), -107.2 - -107.1 (1F, m); δ_C (100 MHz; $CDCl_3$; Me_4Si) 164.5 – 164.6 (wk m), 161.8 – 162.1 (wk m), 159.3 – 159.5 (wk m), 150.7, 150.5 (d, *J* 2.3), 150.2, 137.9, 137.1 (dd, *J* 5.1 and 9.8), 135.7, 135.1, 128.5 , 125.4 (d, *J* 9.5), 124.7 – 124.9 (m), 124.6, 112.6 (dd, *J* 9.1, 3.9), 109.2, 21.1, 20.6; MS (ES^+): *m/z* = 335.3 ($M+H^+$, 100 %).

Iridium complex 3

A mixture of 2-(3-cyano-2,4-difluorophenyl)-4-(2,4,6-trimethylphenyl)pyridine **8** (1.277 g, 3.81 mmol), $IrCl_3$•$3H_2O$ (0.58 g, 1.63 mmol), 2-ethoxyethanol (32 ml) and water (12 ml) was heated to 110 °C overnight under an argon atmosphere. The resulting yellow precipitate was collected by filtration and washed sequentially with water (100 ml) and a mixture of

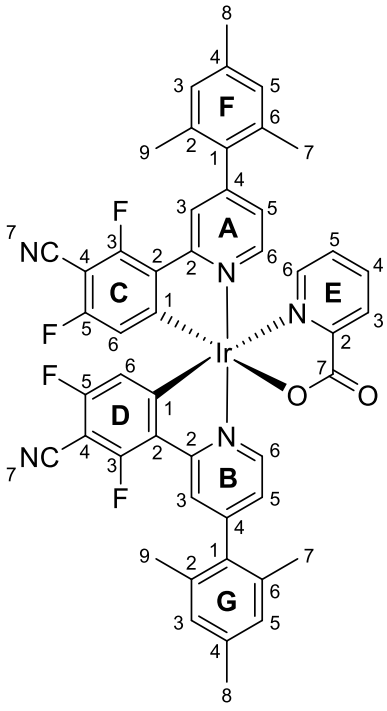

water/methanol (1:1 v/v). Picolinic acid (0.94 g, 7.64 mmol) and 2-ethoxyethanol (20 ml) were added to the precipitate, and the mixture was heated to 120 °C for 18 h. The solution was cooled and water was added. The precipitate was collected, dried and purified by column chromatography (firstly CH_2Cl_2:EtOAc 4:1, then another column using 1:1 CH_2Cl_2:EtOAc) followed by recrystallisation to give **3** as a pale yellow powder (384 mg, 21%); Anal. Calcd. for **3**•0.2(CH_2Cl_2) Anal. Calcd. for $C_{48.2}H_{34.4}Cl_{0.4}F_4IrN_5O_2$ C, 58.01; H, 3.47; N, 7.02. Found: C, 58.26; H, 3.67; N, 6.85; δ_H (500 MHz; $CDCl_3$; Me_4Si) 8.83 (1H, d, *J* 5.5, H_{A6}), 8.46 (1H, d, *J* 7.8, H_{E3}), 8.16 (1H, m, H_{B3}), 8.11 (1H, t, *J* 7.7, H_{A3}), 8.09 (1H,dd, *J* H_{E4}), 7.87 (1H, d, *J* 4.5, H_{E6}), 7.61 (1H, t, *J* 6.5, H_{E5}), 7.49 (1H, d, *J* 6.0, H_{B6}), 7.23 (1H, dd, *J* 6.0, 2.0, H_{A5}), 7.04 (1H, br s, $H_{F3/5}$), 7.01 (2H, s, $H_{F3/5}$+$H_{G3/5}$), 6.99 (1H, dd, *J*, H_{B5}), 6.99 (1H, s, $H_{G3/5}$) , 6.00 (1H, d, *J* 8.5, H_{C6}), 5.72 (1H, d, *J* 8.5, H_{D6}), 2.38 (6H, s, H_{F8}+H_{G8}), 2.16 (3H, s, $H_{F7/9}$), 2.11 (3H, s, $H_{G7/9}$), 2.09 (3H, s, $H_{G7/9}$), 1.99 (3H, s, $H_{F7/9}$); δ_F (376 MHz; $CDCl_3$; Me_4Si) -102.41 (1F, d, *J* 3.9), -103.19 (1F, d, *J* 3.5), -105.21 (1F, d, *J* 4.0), -105.85 (1F, d, *J* 3.7); δ_C (151 MHz; $CDCl_3$; Me_4Si) 172.48 (C_{E7}), 163.80 (d, *J* 6.9, C_{B2}), 162.64 (dd, *J* 268.3, 4.2, $C_{C3/5}$), 162.39 (d, *J* 6.7, C_{A2}), 162.27 (dd, *J* 268.3, 4.2, $C_{D3/5}$), 161.55 (d, *J* 7.2, C_{D1}) , 160.90 (d, *J* 7.2, C_{C1}), 160.17 (dd, *J*, $C_{C3/5}$), 160.07 (dd, *J* 271.1, 4.5, $C_{D3/5}$), 153.99 (C_{A4}), 153.94 (C_{B4}), 151.30 (C_{E2}), 148.68 (C_{A6}), 148.43 (C_{E6}), 148.09 (C_{B6}), 139.52 (C_{E4}), 138.94 ($C_{F/G4}$), 138.89 ($C_{F/G4}$), 135.28 ($C_{G2/6}$), 135.00 ($C_{F2/6}$), 134.75 ($C_{G2/6}$), 134.63 ($C_{F2/6}$), 134.47 ($C_{F/G1}$), 134.45 ($C_{F/G1}$), 129.58 ($C_{C/D2}$), 129.56 ($C_{C/D2}$), 129.25 (C_{E3}), 129.18 (C_{E5}), 129.06 ($C_{F3/5}$), 128.99 (7.01 $C_{G3/5}$), 128.85 ($C_{F3/5}$+$C_{G3/5}$), 125.77 (C_{A5}), 125.63 (C_{B5}), 125.56 (d, *J* C_{B3}), 125.10 (d, *J*, C_{A3}), 115.53 (d, *J* 15.4, C_{C6}), 115.17 (d, *J* 15.9, C_{D6}), 110.47 ($C_{C/D7}$), 110.44 ($C_{C/D7}$), 86.20 (t, *J* 20.1, C_{D4}), 85.85 (t, *J* 20.9, C_{C4}), 21.17 (C_{F8}+C_{G8}), 20.92 ($C_{G7/9}$), 20.66 (C_{F7}+C_{F9}+$C_{G7/9}$); MS (MALDI+): *m/z* = 981.9 ($M+H^+$, 100 %), 980.9 (84.0), 979.9 (49.6), 982.9 (37.3), 978.9 (29.5), 983.9 (5.7). Single crystals of **3**·4$CDCl_3$ for X-ray analysis were grown by slow evaporation of solvent from an NMR sample of **3** in $CDCl_3$.

9-(2-Chloropyridin-4-yl)-2,7-dimethoxy-9*H*-carbazole 16

2,7-Dimethoxycarbazole **15** (3.16 g, 13.90 mmol) and 4-iodo-2-chloropyridine (3.61 g, 13.91 mmol) were dissolved in 10 ml of dry DMF. The reaction mixture was degassed by bubbling argon for 15 min, followed by addition of CuI (0.77 g, 4.04 mmol), 1,10-phenanthroline (1.43 g, 7.93 mmol) and K_2CO_3 (3.84 g, 27.83 mmol). The reaction mixture was heated at 120 °C for 3 days. The solution was cooled and water was added. The precipitate was collected, dried and purified by column chromatography (CH_2Cl_2) to give **16** (4.51 g, 96%) as a white solid; m.p. 109.3 – 110.9 °C; δ_H (400 MHz; $CDCl_3$; Me_4Si) 8.62 (1H, dd, *J* 5.4, 0.6), 7.88 (2H, dd, *J* 8.6, 0.5), 7.63 (1H, dd, *J* 1.9, 0.6), 7.52 (1H, dd, *J* 5.4, 1.9), 6.98 (2H, d, *J* 2.2), 6.93 (2H, dd, *J* 8.5, 2.2), 3.87 (6H, s); δ_C (101 MHz; DMSO-d_6; Me_4Si) 158.65, 158.00, 152.43, 152.28, 147.51, 140.59, 121.04, 120.45, 117.89, 110.03, 95.23, 55.97; MS (ASAP+): *m/z* 338.1 (M+, 100%).

9-(2-Chloropyridin-4-yl)-9*H*-carbazole-2,7-diol 17

9-(2-Chloropyridin-4-yl)-2,7-dimethoxy-9*H*-carbazole **16** (4.51 g, 13.31 mmol) was dissolved in dry CH_2Cl_2 (150 ml) and the solution was cooled to 0 °C under an argon atmosphere. BBr_3 (20.01 g, 79.87 mmol) was slowly added over 10 mins. After 1 h, the reaction was stopped by addition of water (40 ml). The precipitate was collected, dried and recrystallised from ethanol to give **17** as a white solid (3.00 g, 72%); m.p. 289.0 – 290.5 °C; δ_H (400 MHz; DMSO-d_6; Me_4Si) 9.53 (2H, br s), 8.65 (1H, d, *J* 5.4), 7.85 (1H, d, *J* 1.7), 7.83 (2H, d, *J* 8.4), 7.74 (1H, dd, *J* 5.4, 1.9), 6.89 (2H, d, *J* 2.0), 6.73 (2H, dd, *J* 8.4, 2.1); δ_C (151 MHz; DMSO-d_6; Me_4Si) 156.33, 152.23, 152.11, 147.81, 140.42, 120.65, 120.61, 120.06, 117.03, 110.80, 96.48; MS (ASAP+): *m/z* 310.1 (M+, 100%).

9-(2-Chloropyridin-4-yl)-2,7-bis(hexyloxy)-9*H*-carbazole 18

9-(2-Chloropyridin-4-yl)-9*H*-carbazole-2,7-diol **17** (2.46 g, 7.9 mmol) and K_2CO_3 (3.28 g, 23.7 mmol) were dissolved in DMSO (80 ml) and the solution was stirred at RT for 2 h. 1-bromohexane (3.32 ml, 23.7 mmol) was slowly added over 10 mins. The reaction mixture was stirred at RT overnight. The reaction was stopped by an addition of water (50 ml). The precipitate was collected, dried and purified by column chromatography (CH_2Cl_2) to give **18** (2.83 g, 75%) as a white solid; m.p. 176.1 – 177.5 °C; δ_H (400 MHz; $CDCl_3$; Me_4Si) 8.61 (1H, dd, *J* 5.4, 0.6), 7.86 (2H, d, *J* 8.5), 7.61 (1H, dd, *J* 1.9, 0.6), 7.51 (1H, dd, *J* 5.4, 1.8), 6.87-7.00 (4H, m), 4.00 (4H, t, *J* 6.5), 1.81 (4H, dq, *J* 8.0, 6.6), 1.55 (3H, s), 1.28-1.42 (9H, m), 0.91 (6H, m); δ_C (176 MHz; $CDCl_3$; Me_4Si) 158.08, 153.18, 151.27, 147.86, 140.56, 120.73, 120.32, 119.22, 118.19, 109.64, 95.59, 68.66, 31.59, 29.30, 25.74, 22.57, 14.00; MS (ASAP+): *m/z* 478.2 (M+, 100%).

3-(4-(2,7-Bis(hexyloxy)-9*H*-carbazol-9-yl)pyridin-2-yl)-2,6-difluorobenzene 9

(2-Chloropyridin-4-yl)-2,7-bis(hexyloxy)-9*H*-carbazole **18** (1.20 g, 2.51 mmol) and 2,4-difluorophenylboronic acid **19** (0.66 g, 4.18 mmol) were dissolved in 1,4-dioxane (20 ml), and the reaction mixture was degassed by bubbling argon for 15 mins. $Pd(PPh_3)_4$ (0.05 g, 0.04 mmol) and degassed aqueous 2 M K_2CO_3 (5.2 ml, 10.4 mmol) were added, and the reaction mixture was heated at 90 °C for 18 h. The solution was cooled and water was added. The precipitate was collected, dried and purified by column chromatography (CH_2Cl_2) to give **9** (1.10 g, 79%) as a white solid; Anal. Calc. for $C_{35}H_{38}N_2F_2O_2$; C, 75.51; H, 6.88; N, 5.03; Found: C, 75.50; H, 6.89; N, 4.91; δ_H (700 MHz; $CDCl_3$; Me_4Si) 8.92 (1H, d, *J* 5.2), 8.14 (1H, dd, *J* 15.6, 8.5), 8.05 (1H, t, *J* 2.1), 7.87 (2H, d, *J* 8.5), 7.55 (1H, dd, *J* 5.4, 1.9), 7.12 – 7.03 (3H, m), 7.00-6.88 (3H, m), 4.01 (4H, t, *J* 6.6), 1.88 – 1.76 (4H, m), 1.48 (4H, dd, *J* 14.5, 7.0), 1.39 – 1.31 (8H, m), 0.92 (6H, t, *J* 6.6); δ_F (658 MHz; $CDCl_3$; Me_4Si) -108.15, -113.3; δ_C (176 MHz; $CDCl_3$; Me_4Si) 163.73 (dd, *J* 252.0, 12.2), 160.89 (dd, *J* 252.4, 12.0), 158.18, 154.58 (d, *J* 1.96), 151.66, 146.15, 140.90 , 132.40 (dd, *J* 9.7, 4.2), 123.41 (dd, *J* 11.3, 3.7), 121.13 (d, *J* 9.3), 120.40, 119.04, 118.19, 112.46 (dd, *J* 21.2, 3.5), 109.98, 104.06 (dd, *J* 26.67, 25.60), 95.44, 68.68, 31.74, 29.47, 25.90, 22.76, 14.18; MS (ASAP+): *m/z* 556.3 (M+, 100%).

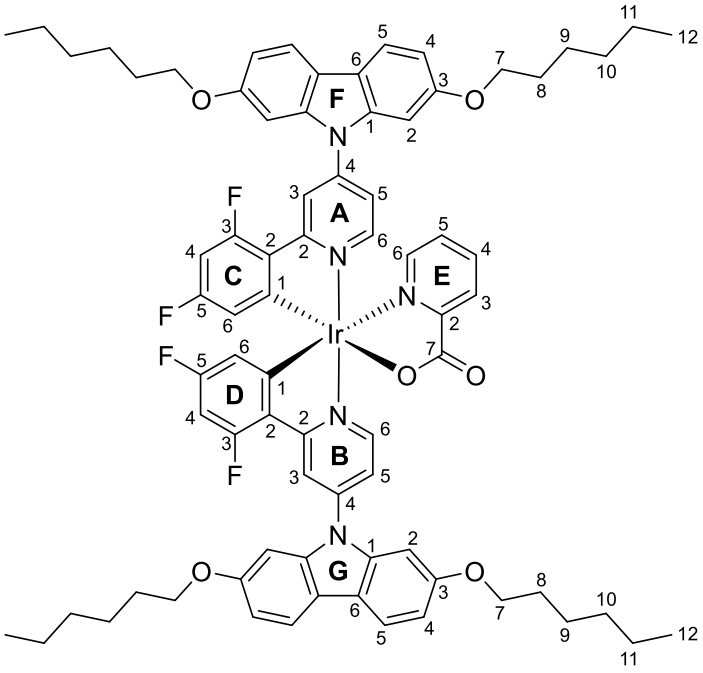

Iridium complex 4

A mixture of 3-(4-(2,7-bis(hexyloxy)-9*H*-carbazol-9-yl)pyridin-2-yl)-2,6-difluorobenzene **9** (0.36 g, 0.66 mmol), $IrCl_3 \bullet 3H_2O$ (0.11 mg, 0.31 mmol) and 2-ethoxyethanol (10 ml) was heated to 120 °C overnight. Picolinic acid (0.10 g, 0.81 mmol) and sodium carbonate (0.1 mg, 0.01 mmol) were added and the mixture was heated to 120 °C for 2 h. The solution was cooled and water was added. The precipitate was collected, dried and purified by column chromatography (CH_2Cl_2/EtOAc 20:1) to give **4** (0.23 g, 55%) as a yellow solid; Anal. Calc. For $C_{76}H_{78}F_4N_5O_6Ir$; C, 64.03; H, 5.51; N, 4.91; Found: C, 64.04; H, 5.45; N, 4.77; δ_H (400 MHz; $CDCl_3$; Me_4Si) 8.94 (1H, d, *J* 6.4, H_{A6}), 8.64 (1H, m, H_{B3}), 8.57 (1H, m, H_{A3}), 8.47 (1H, d, *J* 7.8, H_{E3}), 8.07 (1H, t, *J* 7.5 H_{E4}), 7.98 (1H, d, *J* 5.0, H_{E6}), 7.89 (2H, d, *J* 8.5, $H_{F5/G5}$) 7.87 (2H, d, *J* 8.5, $H_{F5/G5}$), 7.62–7.52 (3H, m, H_{B6}+H_{A5}+H_{E5}), 7.31 (1H, d, *J* 5.9, H_{B5}), 7.17 (2H, d, *J*, 2.1, H_{G2}) 7.13 (2H, d, *J*, 2.1, H_{F2}), 6.95 (4H, dd, *J* 8.6, 2.1, H_{F4}+H_{G4}), 6.55 (1H, dd, *J* 12.0, 9.0, H_{C4}), 6.46 (1H, dd, *J* 12.0, 9.0, H_{D4}), 6.08 (1H, dd, *J* 8.4, 2.3 H_{C6}), 5.82 (1H, dd, *J* 8.6, 2.3 H_{D6}), 4.04 (8H, q, *J* 6.2, H_{F7}+H_{G7}), 1.83 (8H, p, *J* 6.6, H_{F8}+H_{G8}), 1.49 (8H, m, H_{F9}+H_{G9}), 1.35 (16H, m, H_{F10}+H_{G10}+H_{F11}+H_{G11}), 0.94 – 0.86 (12H, m, H_{F12}+H_{G12}); δ_F (564 MHz; $CDCl_3$; Me_4Si) -105.41 – -105.66 (1F, m), -106.23 – -106.51 (1F, m), -109.52 – -109.78 (1F, m), -110.29 – -110.57 (1F, m); δ_C (151 MHz; $CDCl_3$; Me_4Si) 172.98 (C_{E7}), 167.57 (d, *J* 6.8, C_{B2}), 166.05 (d, *J* 6.8, C_{A2}), 164.00 (dd, 257.72, 12.5, C_{C5}), 163.68 (dd, *J* 256.3, 12.5, C_{D5}), 161.77 (dd, *J* 259.1, 12.6, $C_{C/D3}$), 161.72 (dd, *J* 259.4, 12.6, $C_{C/D3}$), 158.35 ($C_{F/G3}$), 158.32 ($C_{F/G3}$), 153.12 (d, *J* 6.9, $C_{C/D1}$), 151.87 (C_{E2}), 151.68 (d, *J* 6.9, $C_{C/D1}$), 150.08 (C_{A6}), 149.24 (C_{B6}), 148.72 (C_{E6}), 147.85 ($C_{A/B4}$), 147.81 ($C_{A/B4}$), 140.49 ($C_{F/G1}$), 140.48 ($C_{F/G1}$), 138.81 (C_{E4}), 129.05 (C_{E3}), 128.93 (C_{E5}), 128.27 (C_{D2}), 128.07 (C_{C2}), 120.56 ($C_{F/G5}$), 120.48, ($C_{F/G5}$), 119.17 (d, *J* 20.5, C_{B3}), 118.72 ($C_{F/G6}$), 118.63 ($C_{F/G6}$), 118.49 (C_{A5}), 118.43 (d, *J* 20.5, C_{A3}) 118.34 (C_{A5}), 115.17 (d, *J* 16.9, C_{C6}), 114.91 (d, *J* 16.9, C_{D6}), 110.50 ($C_{F/G4}$), 110.21 ($C_{F/G4}$), 98.58 (t, *J* 26.8, C_{D4}), 98.22 (t, *J* 26.8, C_{C4}), 96.17 (C_{F2}), 96.03 (C_{G2}), 68.93($C_{F/G7}$), 68.89 ($C_{F/G7}$), 31.74 (C_{F7}+C_{G7}), 31.72 (C_{F10}+C_{G10}/C_{F11}+C_{G11}), 29.46 (C_{F8}+C_{G8}), 25.90 (C_{F9}+C_{G9}), 22.73 (C_{F12}+C_{G12}); MS (MALDI+): *m/z* = 1425.4 (M+, 100%).

9-(2',6'-Difluoro-[2,3'-bipyridin]-4-yl)-2,7-bis(hexyloxy)-9*H*-carbazole 10

9-(2-Chloropyridin-4-yl)-2,7-bis(hexyloxy)-9H-carbazole **18** (0.80 g, 1.67 mmol), MIDA ester **13** (0.68 g, 2.50 mmol) and SPhos (0.11 g, 0.13 mmol) were dissolved 1,4-dioxane (20 ml) and the reaction mixture was degassed by bubbling argon for 15 mins, before $Pd(OAc)_2$ (30 mg, 0.13 mmol) was added. Degassed aqueous 1.5 M K_3PO_4 (4 ml, 6.0 mmol) was added and the reaction mixture was heated to 60 °C for 18h. The solution was cooled and the solvent was removed *in vacuo*. The crude material was dissolved in CH_2Cl_2, which was washed with water before the solvent was removed. The crude material was purified by column chromatography (CH_2Cl_2) to give

9-(2',6'-difluoro-[2,3'-bipyridin]-4-yl)-2,7-bis(hexyloxy)-9*H*-carbazole **10** (0.81 g, 87%) as a white solid; Anal. Calc. for $C_{34}H_{37}N_3F_2O_2$; C, 73.23; H, 6.69; N, 7.53; Found: C, 72.96; H, 6.64; N, 7.46; δ_H (400 MHz; $CDCl_3$; Me_4Si) 8.92 (1H, dd, *J* 5.2, 0.7), 8.78 (1H, dt, *J* 9.7, 8.1), 8.10-8.16 (1H, m), 7.88 (2H, d, *J* 8.6), 7.60 (1H, dd, *J* 5.3, 2.0), 7.08 (2H, d, *J* 2.2), 7.05 (1H, dd, *J* 8.2, 3.0, 0.8), 6.92 (2H, dd, *J* 8.6, 2.2), 4.01 (4H, t, *J* 6.5), 1.81 (4H, dt, *J* 14.3, 6.7), 1.42-1.54 (4H, m), 1.22-1.40 (8H, m), 0.86-0.94 (6H, m); δ_F (376 MHz; $CDCl_3$; Me_4Si) -66.83 (ddd, *J* 10.5, 7.6, 3.0), -69.87 (1F, t, *J* 10.0); δ_C (151 MHz; $CDCl_3$; Me_4Si) 161.65 (dd, *J* 250.2, 14.6), 158.72 (dd, *J* 250.2, 14.2), 158.23, 152.81, 151.67, 146.45, 146.14, 140.65, 120.65 (d, *J* 10.3), 120.30, 119.46, 118.73 (d, *J* 23.8), 118.12, 109.94, 107.20 (d, *J* 34.3), 95.41 , 68.70 , 31.75 , 29.49 , 25.92 , 22.75 , 14.17; MS (ASAP+): *m/z* 557.3 (M+, 100%).

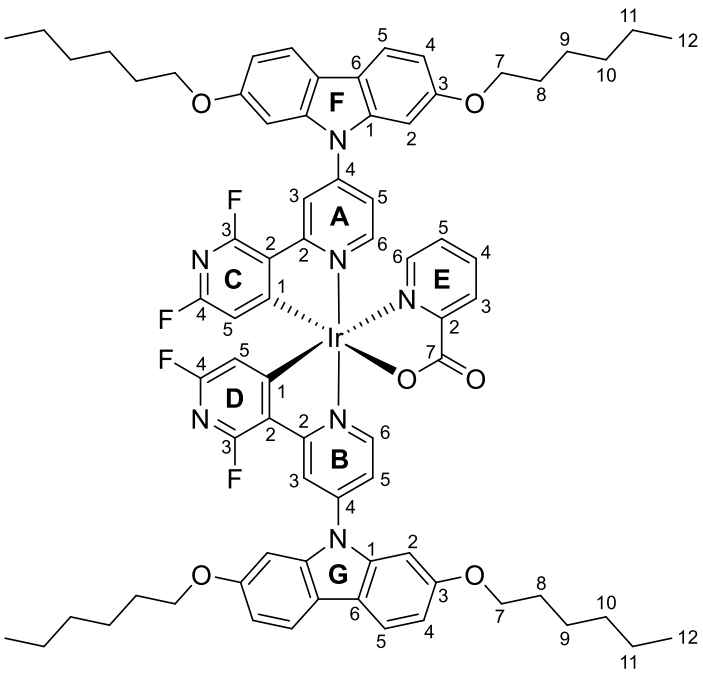

Ir complex 5

A mixture of **10** (270 mg, 0.48 mmol) and $IrCl_3 \bullet 3H_2O$ (81 mg, 0.23 mmol) in diglyme (10 ml) was heated to 130 °C overnight under argon. Picolinic acid (57 mg, 0.46 mmol) was added and the mixture was heated to 130 °C for 8 h. The reaction was cooled, the solvent removed *in vacuo* and the residue was purified by column chromatography (4% EtOAc in CH_2Cl_2) to leave **5** as a yellow solid (110 mg, 33%); Anal. Calc. for $C_{74}H_{76}F_4N_7O_6Ir$; C, 62.26; H, 5.37; N, 6.87; Found: C, 62.17; H, 5.33; N, 6.88; δ_H (600 MHz; $CDCl_3$; Me_4Si) 8.95 (1H, d, *J* 6.3, H_{A6}), 8.68 (1H, t, *J* 2.6, H_{B3}), 8.62 (1H, t, *J* 2.3, H_{A3}), 8.50 (1H, dd, *J* 7.6, 1.5, H_{E3}), 8.14 (1H, td, *J* 7.8, 1.6, H_{E4}), 7.99 (1H, dd, *J* 5.5 , 1.5, H_{E6}), 7.88 (2H, d, *J* 8.5, $H_{F5/G5}$), 7.87 (2H, d, *J* 8.5, $H_{F5/G5}$), 7.69 – 7.65 (2H, m, H_{A5}+H_{E5}), 7.57 (1H, d, *J* 6.3, H_{B6}), 7.45 (1H, dd, *J* 6.3, 2.5, H_{B5}), 7.18 (2H, d, *J* 2.1, H_{G2}), 7.15 (2H, d, *J* 2.1, H_{F2}), 6.96 (4H, dd, *J* 8.6, 2.0, H_{F5}+H_{G5}), 6.11 (t, *J* 1.8, H_{C5}), 5.84 (d, *J* 1.9, H_{D5}), 4.04 (8H, q, *J* 6.6, H_{F7}+H_{G7}), 1.86 – 1.78 (8H, m, H_{F8}+H_{G8}), 1.53 – 1.46 (8H, m, H_{F9}+H_{G9}), 1.39 – 1.30 (16H, m, H_{F10}+H_{G10}+H_{F11}+H_{G11}), 0.90 (12H, td, *J* 6.4, 5.8, 2.5, H_{F12}+H_{G12}); δ_F (376 MHz; $CDCl_3$; Me_4Si) -67.83 (1F, dt, *J* 9.1, 2.1), -68.29 (1F, dd, *J* 9.1, 2.4), -68.63 (1F, dt, *J* 9.2, 2.3), -68.96 (1F, dd, *J* 9.1, 2.4); δ_C (151 MHz; $CDCl_3$; Me_4Si) 172.60 (C_{E7}), 170.62 (d, *J* 5.9, C_{D1}), 170.18 (d, *J* 6.0, C_{C1}), 165.30 (d, J 10.1, C_{B2}), 163.87 (d, J 10.0, C_{A2}), 161.67 (dd, J 253.7, 15.9, $C_{C3/4}$), 161.05 (dd, J 253.63, 15.4, $C_{D3/4}$), 158.45 ($C_{F/G3}$), 158.42 ($C_{F/G3}$), 158.24 (dd, J 253.6, 16.5, $C_{C3/4}$), 157.81 (dd, J 250.1, 16.9, $C_{D3/4}$), 151.29 (C_{E2}), 150.20 (C_{A6}), 149.47 (C_{B6}), 148.79 (C_{A4}), 148.70 (C_{B4}), 148.55 (C_{E6}), 140.22 ($C_{F/G1}$), 140.20 ($C_{F/G1}$), 139.63 (C_{E4}), 129.43 ($C_{E3/5}$), 129.41 ($C_{E3/5}$), 125.06 (dd, *J* 15.8, 3.7, C_{D2}), 124.96 (dd, *J* 16.2, 3.7, C_{C2}), 120.69 ($C_{F/G5}$), 120.62 ($C_{F/G5}$), 119.20 (d, *J* 18.5, C_{B3}), 119.05 (C_{A5}), 118.96 (C_{B5}), 118.96 (C_{F6}) 118.87 (C_{G6}), 118.59 (d, *J* 17.3, C_{A3}), 110.64 ($C_{F/G4}$), 110.33 ($C_{F/G4}$), 110.30 (dd, *J* 28.8, 3.9, C_{C5}), 110.00 (dd, *J* 29.5, 3.9, C_{D5}), 96.40 (C_{F2}), 96.20 (C_{G2}), 68.98 ($C_{F7/G7}$), 68.94 ($C_{F7/G7}$), 31.74 ($C_{F10/G10/F11/G11}$), 31.73 ($C_{F10/G10/F11/G11}$), 29.48 ($C_{F8/G8}$), 29.45 ($C_{F8/G8}$), 25.92 ($C_{F9/G9}$), 22.73 ($C_{F10/G10/F11/G11}$), 22.72 ($C_{F10/G10/F11/G11}$), 14.16 (C_{F12}+C_{G12}); HRMS (FTMS+ESI): calcd for [$C_{74}H_{76}F_4{}^{191}IrN_7O_6$+H]: 1426.5477. Found: 1426.5470.

3-(4-(2,7-Bis(hexyloxy)-9*H*-carbazol-9-yl)pyridin-2-yl)-2,6-difluorobenzonitrile 11

9-(2-Chloropyridin-4-yl)-2,7-bis(hexyloxy)-9*H*-carbazole **18** (1.00 g, 2.09 mmol), MIDA ester **14** (0.92 g, 3.13 mmol) and SPhos (137 mg, 0.33 mmol) were dissolved 1,4-dioxane (20 ml) and the reaction mixture was degassed by bubbling argon for 15 mins, before $Pd(OAc)_2$ (37 mg, 0.16 mmol) was added. Degassed aqueous 2.1 M K_3PO_4 (4 ml, 8.4 mmol) was added and the reaction mixture was heated to 60 °C for 72 h. The solution was cooled and the solvent was removed *in vacuo*. The crude material was dissolved in CH_2Cl_2, which was washed with water before the solvent was removed. The crude material was purified by column chromatography (CH_2Cl_2) to give **11** (1.01 g, 83%) as a white solid; m.p. 126.1 – 127.9 °C; Anal. Calc. For $C_{36}H_{37}N_3F_2O_2$; C, 74.33; H, 6.41; N, 7.22; Found: C, 73.71; H, 6.34; N, 7.07; δ_H (400 MHz; $CDCl_3$; Me_4Si) 8.93 (1H, dd, *J* 5.3, 0.7), 8.45 (1H, td, *J* 8.9, 6.4), 8.03-8.07 (1H, m), 7.88 (2H, d, *J* 8.5), 7.63 (1H, dd, *J* 5.3, 2.0), 7.25 (1H, ddd, *J* 9.0, 7.7, 1.2), 7.07 (2H, d, *J* 2.1), 6.93 (2H, dd, *J* 8.5, 2.2), 4.02 (4H, t, *J* 6.6), 1.82 (4H, dq, *J* 8.7, 6.6), 1.42-1.58 (4H, m), 1.27-1.42 (8H, m), 0.84-0.99 (6H, m); δ_F (376 MHz; $CDCl_3$; Me_4Si) -101.89 (1F, ddd, *J* 8.0, 6.4, 1.8), -108.04 (1F, dq, *J* 8.7, 1.9); δ_C (178 MHz; $CDCl_3$; Me_4Si) 163.51 (dd, *J* 265.0, 3.8), 160.7 (dd, *J* 263.8, 4.2), 158.27, 152.39 (d, *J* 1.8), 152.05, 146.65, 140.80, 137.21 (dd, *J* 9.9, 4.8), 124.44 (dd , *J* 10.0, 3.9), 121.16 (d, *J* 9.2), 120.53, 119.94, 118.34, 113.05 (dd, *J* 19.1, 4.0), 110.02, 109.06, 95.51, 93.30 (dd, *J* 20.5, 19.5), 68.78, 31.76, 29.50, 25.91, 22.75, 14.19; HRMS (FTMS+ESI): calcd for $[C_{36}H_{37}N_3F_2O_2+H]^+$: 582.2932. Found: 582.2931.

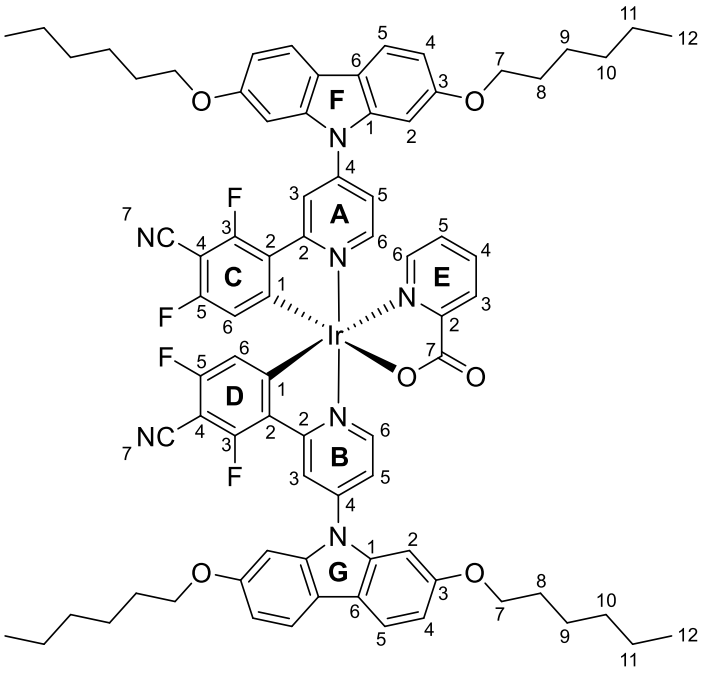

Ir complex 6

A mixture of **11** (300 mg, 0.52 mmol) and $IrCl_3 \bullet 3H_2O$ (87 mg, 0.25 mmol) in 2-ethoxyethanol (5 ml) was heated to 110 °C overnight under argon. Picolinic acid (106 mg, 0.86 mmol) and Na_2CO_3 (26 mg, 0.25 mmol) were added and the mixture was heated to 110 °C for 3 h. The reaction was cooled, the solvent removed *in vacuo* and water (20 ml) and CH_2Cl_2 (20 ml) were added. The layers were separated and the aqueous layer was extracted with further CH_2Cl_2 (2 x 20 ml). The organic phases were combined, dried over $MgSO_4$, filtered and the solvent removed. The residue was purified by column chromatography (4% EtOAc in CH_2Cl_2) to leave **6** as a yellow solid (196 mg, 54%); Anal. Calcd. for **6**•2(CH_2Cl_2) $C_{80}H_{80}Cl_4F_4IrN_7O_6$, C, 58.39; H, 4.90; N, 5.96. Found: C, 58.58; H, 4.86; N, 6.01; δ_H (600 MHz; $CDCl_3$; Me_4Si) 8.90 (1H, d, *J* 6.4, H_{A6}), 8.68 (1H, t, *J* 2.6, H_{B3}), 8.63 (1H, t, *J* 2.4, H_{A3}), 8.48 (1H, d, *J* 7.8, H_{E3}), 8.14 (1H, td, *J* 7.8, 1.6, H_{E4}), 7.91 (1H, d, *J* 5.5, H_{E6}), 7.87 (4H, dd, *J* 8.5, 3.9, H_{F5}+H_{G5}), 7.69 (1H, dd, *J*, H_{A5}), 7.67 (1H, dd, *J* 5.6, 1.4, H_{E5}), 7.55 (1H, d, *J* 6.2, H_{B6}), 7.48 (1H, dd, *J* 6.4, 2.4, H_{B5}), 7.17 (2H, d, *J* 2.1, H_{G2}), 7.15 (2H, d, *J* 2.1, H_{F2}), 6.97 (4H, dd, *J* 8.5, 2.1, H_{F5}+H_{G5}), 6.26 (1H, d, *J* 8.1, H_{C6}), 5.97 (1H, d, *J* 8.2, H_{D6}), 4.05 (8H, td, *J* 6.6, 2.4, H_{F7}+H_{G7}), 1.78-1.90 (8H, m, H_{F8}+H_{G8}), 1.48-1.56 (8H, m, H_{F9}+H_{G9}), 1.28-1.37 (16H, m, H_{F10}+H_{G10}+H_{F11}+H_{G11}), 0.80-0.98 (12H, m, H_{F12}+H_{G12}); δ_F (376 MHz; $CDCl_3$; Me_4Si) -101.18 (1F,

dd, *J* 8.2, 4.2), -101.91 (1F, dd, *J* 8.2, 3.9), -105 .62 (1F, d, *J* 4.3), -106.62 (1F, t, *J* 4.0); δ_C (151 MHz; $CDCl_3$; Me_4Si) 172.54 (C_{E7}), 165.36 (d, *J* 6.7, C_{B2}), 164.02 (d, *J* 6.5, C_{A2}), 163.09 (dd, *J* 266.0, 4.3, $C_{C3/5}$), 162.67 (dd, *J*, 269.9, 4.1, $C_{D3/5}$), 161.61 (d, *J* 7.3, C_{D1}), 161.11 (d, *J* 7.2, C_{C1}), 160.76 (dd, *J* 272.2, 5.2 $C_{C3/5}$), 160.56 (dd, *J* 272.2, 4.8, $C_{D3/5}$), 158.47 (C_{G3}), 158.42 (C_{F3}), 151.23 (C_{E2}), 150.03 (C_{A6}), 149.44 (C_{B6}), 148.93 (C_{A4}), 148.86 (C_{B4}), 148.53 (C_{E6}), 140.19 (C_{F1}), 140.17 (C_{G1}) , 139.79 (C_{E4}), 129.55 (C_{E3}+C_{E5}) , 129.49 (C_{D2}), 129.36 (C_{C2}), 120.75 ($C_{F/G5}$) , 120.68 ($C_{F/G5}$), 119.61 (d, *J* 20.0, C_{B3}), 119.54 (C_{B5}+C_{A5}), 119.05 (d, *J* 18.9, C_{A3}), 119.05 (C_{F6}/C_{G6}), 118.96 (C_{F6}/C_{G6}), 116.34 (d, *J* 14.7, C_{C6}), 115.87 (d, *J* 16.9, C_{D6}) , 110.55 (C_{F5}/C_{G5}), 110.34 ($C_{C7/D7}$), 110.29 ($C_{C7/D7}$), 110.13 (C_{F5}/C_{G5}), 96.58 (C_{F2}), 96.33 (C_{G2}), 86.67 (t, *J* 20.1, C_{D4}), 86.40 (t, *J* 20.2, C_{C4}), 69.03 (C_{F7}/C_{G7}) , 69.00 (C_{F7}/C_{G7}), 31.75 ($C_{F10/G10/F11/G11}$), 31.74 ($C_{F10/G10/F11/G11}$), 29.49 (C_{F8}/C_{G8}), 29.46 (C_{F8}/C_{G8}), 25.91 , 25.90 ($C_{F9/G9}$) , 23.97 ($C_{F9/G9}$), 22.74 ($C_{F10/G10/F11/G11}$+$C_{F10/G10/F11/G11}$), 14.18 (C_{F12}+C_{G12}); HRMS (FTMS+ESI): calcd for $[C_{78}H_{76}F_4{}^{191}IrN_7O_6]^+$: 1473.5399. Found: 1473.5367

Acknowledgements.

EPSRC grant EP/K0394/23/1 is acknowledged for funding equipment used in the Department of Chemistry, Durham University.

Author Contributions.

The synthesis and purification of ligands and complexes were performed by H.B, Y.Z., V.N.K., J.S.S. and L.J.O. with supervision from M.R.B.. Theoretical calculations were carried out by H.B.; electrochemical data were obtained by M.A.F. and H.B.; X-ray crystal structures were solved by A.S.B.; photophysical data were obtained by F.B.D., M.A.F. and H.B.; devices were fabricated by G.C.G. with supervision from A.P.M.. The writing of the manuscript was coordinated by H.B. with input from all coauthors.

1 V. W.-W. Yam and K. M.-C. Wong, *Chem. Commun.*, 2011, **47**, 11579–11592.

2 H. Xu, R. Chen, Q. Sun, W. Lai, Q. Su, W. Huang and X. Liu, *Chem. Soc. Rev.*, 2014, **43**, 3259–3302.

3 D. Magde, M. D. Magde and E. C. Glazer, *Coord. Chem. Rev.*, 2016, **306**, 447–467.

4 V. W. W. Yam, Ed., *Photofunctional Transition Metal Complexes*, Springer Berlin Heidelberg, Berlin, Heidelberg, 2007, vol. 123.

5 E. Longhi and L. De Cola, in *Iridium(III) in Optoelectronic and Photonics Applications*, John Wiley & Sons, Ltd, Chichester, UK, 2017, pp. 205–274.

6 W. Y. Wong, Z. He, S. K. So, K. L. Tong and Z. Lin, *Organometallics*, 2005, **24**, 4079–4082.

7 D. N. Kozhevnikov, V. N. Kozhevnikov, M. Z. Shafikov, A. M. Prokhorov, D. W. Bruce and J. A. G. Williams, *Inorg. Chem.*, 2011, **50**, 3804–3815.

8 M. Tavasli, S. Bettington, M. R. Bryce, H. A. Al Attar, F. B. Dias, S. King and A. P. Monkman, *J. Mater. Chem.*, 2005, **15**, 4963–4970.

9 Y. You, Y. Han, Y. M. Lee, S. Y. Park, W. Nam and S. J. Lippard, *J. Am. Chem. Soc.*, 2011, **133**, 11488–11491.

10 Y. You, S. Lee, T. Kim, K. Ohkubo, W. S. Chae, S. Fukuzumi, G. J. Jhon, W. Nam and S. J. Lippard, *J. Am. Chem. Soc.*, 2011, **133**, 18328–18342.

11 K. K. W. Lo, K. Y. Zhang, S. K. Leung and M. C. Tang, *Angew. Chemie - Int. Ed.*, 2008, **47**, 2213–2216.

12 C. H. Shin, J. O. Huh, M. H. Lee and Y. Do, *Dalton Trans.*, 2009, 6476–6479.

13 L. Xiao, Z. Chen, B. Qu, J. Luo, S. Kong, Q. Gong and J. Kido, *Adv. Mater.*, 2011, **23**, 926–952.

14 G. M. Farinola and R. Ragni, *Chem. Soc. Rev.*, 2011, **40**, 3467–3482.

15 Y. S. Yeh, Y. M. Cheng, P. T. Chou, G. H. Lee, C. H. Yang, Y. Chi, C. F. Shu and C. H. Wang, *ChemPhysChem*, 2006, **7**, 2294–2297.

16 S. Ladouceur, L. Donato, M. Romain, B. P. Mudraboyina, M. B. Johansen, J. A. Wisner and E. Zysman-Colman, *Dalton Trans.*, 2013, **42**, 8838–8847.

17 Y. Luo, W. Hu and W. Shen, *ChemPhysChem*, 2018, **19**, 2200–2207.

18 S. Kumar, Y. Hisamatsu, Y. Tamaki, O. Ishitani and S. Aoki, *Inorg. Chem.*, 2016, **55**, 3829–3843.

19 C. Climent, P. Alam, S. S. Pasha, G. Kaur, A. R. Choudhury, I. R. Laskar, P. Alemany and D. Casanova, *J. Mater. Chem. C*, 2017, **5**, 7784–7798.

20 E. Baranoff and B. F. E. Curchod, *Dalt. Trans.*, 2015, **44**, 8318–8329.

21 V. N. Kozhevnikov, Y. Zheng, M. Clough, H. A. Al-Attar, G. C. Griffiths, K. Abdullah, S. Raisys, V. Jankus, M. R. Bryce and A. P. Monkman, *Chem. Mater.*, 2013, **25**, 2352–2358.

22 X. Xu, X. Yang, J. Dang, G. Zhou, Y. Wu, H. Li and W.-Y. Wong, *Chem. Commun.*, 2014, **50**, 2473–2476.

23 B. A. Kamino, B. Mills, C. Reali, M. J. Gretton, M. A. Brook and T. P. Bender, *J. Org. Chem.*, 2012, **77**, 1663–1674.

24 G. R. Dick, E. M. Woerly and M. D. Burke, *Angew. Chemie - Int. Ed.*, 2012, **51**, 2667–2672.

25 D. M. Knapp, E. P. Gillis and M. D. Burke, *J. Am. Chem. Soc.*, 2009, **131**, 6961–6963.

26 M. Nonoyama, *Bull. Chem. Soc. Jpn.*, 1974, **47**, 767–768.

27 C. Lin, Y. Chiu, Y. Chi, Y. Tao, L. Liao, M. Tseng and G. Lee, *Organometallics*, 2012, **31**, 4349–4355.

28 H. Oh, K. M. Park, H. Hwang, S. Oh, J. H. Lee, J. S. Lu, S. Wang and Y. Kang, *Organometallics*, 2013, **32**, 6427–6436.

29 R. D. Sanner and V. G. Young, *Acta Crystallogr. Sect. E Crystallogr. Commun.*, 2018, **74**, 1467–1470.

30 M.-L. Xu, G.-B. Che, X.-Y. Li and Q. Xiao, *Acta Crystallogr. Sect. E Struct. Reports Online*, 2009, **65**, m28–m28.

31 T.-Y. Li, Y.-M. Jing, X. Liu, Y. Zhao, L. Shi, Z. Tang, Y.-X. Zheng and J.-L. Zuo, *Sci. Rep.*, 2015, **5**, 14912.

32 E. Baranoff, B. F. E. Curchod, F. Monti, F. Steimer, G. Accorsi, I. Tavernelli, U. Rothlisberger, R. Scopelliti, M. Grätzel and M. K. Nazeeruddin, *Inorg. Chem.*, 2012, **51**, 799–811.

33 Y. Zhao, J. Tang, H. Zhang and Y. Ma, *Eur. J. Inorg. Chem.*, 2014, **2014**, 4843–4851.

34 A. Maggiore, M. Pugliese, F. Di Maria, G. Accorsi, M. Gazzano, E. Fabiano, V. Tasco, M. Esposito, M. Cuscunà, L. Blasi, A. Capodilupo, G. Ciccarella, G. Gigli and V. Maiorano, *Inorg. Chem.*, 2016, **55**, 6532–6538.

35 Y. Kang, Y.-L. Chang, J.-S. Lu, S.-B. Ko, Y. Rao, M. Varlan, Z.-H. Lu and S. Wang, *J. Mater. Chem. C*, 2013, **1**, 441–

450.

36 P. J. Hay, *J. Phys. Chem. A*, 2002, **106**, 1634–1641.

37 J. U. Y. Shin, J. I. Y. Park, C. Liu, J. He and S. C. Kim, *Pure Appl. Chem.*, 2005, **77**, 801–814.

38 Z. Yang, Z. Mao, Z. Xie, Y. Zhang, S. Liu, J. Zhao, J. Xu, Z. Chi and M. P. Aldred, *Chem. Soc. Rev.*, 2017, 46, 915–1016.

39 M. J. Frisch, G. W. Trucks, H. B. Schlegel, G. E. Scuseria, M. A. Robb, J. R. Cheeseman, G. Scalmani, V. Barone, G. A. Petersson, H. Nakatsuji, X. Li, M. Caricato, A. Marenich, J. Bloino, B. G. Janesko, R. Gomperts, B. Mennucci, H. P. Hratchian, J. V. Ortiz, A. F. Izmaylov, J. L. Sonnenberg, D. Williams-Young, F. Ding, F. Lipparini, F. Egidi, J. Goings, B. Peng, A. Petrone, T. Henderson, D. Ranasinghe, V. G. Zakrzewski, J. Gao, N. Rega, G. Zheng, W. Liang, M. Hada, M. Ehara, K. Toyota, R. Fukuda, J. Hasegawa, M. Ishida, T. Nakajima, Y. Honda, O. Kitao, H. Nakai, T. Vreven, K. Throssell, J. A. J. Montgomery, J. E. Peralta, F. Ogliaro, M. Bearpark, J. J. Heyd, E. Brothers, K. N. Kudin, V. N. Staroverov, T. Keith, R. Kobayashi, J. Normand, K. Raghavachari, A. Rendell, J. C. Burant, S. S. Iyengar, J. Tomasi, M. Cossi, J. M. Millam, M. Klene, C. Adamo, R. Cammi, J. W. Ochterski, R. L. Martin, K. Morokuma, O. Farkas, J. B. Foresman and D. J. Fox, Gaussian 09, Revision A.02.

40 N. M. O'Boyle, A. L. Tenderholt and K. M. Langner, *J. Comput. Chem.*, 2008, **29**, 839–845.

41 A. D. Becke, *J. Chem. Phys.*, 1993, **98**, 5648–5652.

42 C. Lee, W. Yang and R. G. Parr, *Phys. Rev. B*, 1988, **37**, 785–789.

43 T. H. Dunning and P. J. Hay, in *Methods of Electronic Structure Theory*, ed. H. F. Schaefer, Springer US, Boston, MA, 1977, pp. 1–27.

44 P. J. Hay and W. R. Wadt, *J. Chem. Phys.*, 1985, **82**, 299–310.

45 W. R. Wadt and P. J. Hay, *J. Chem. Phys.*, 1985, **82**, 284–298.

46 P. J. Hay and W. R. Wadt, *J. Chem. Phys.*, 1985, **82**, 270–283.

47 G. A. Petersson and M. A. Al-Laham, *J. Chem. Phys.*, 1991, **94**, 6081–6090.

48 G. A. Petersson, A. Bennett, T. G. Tensfeldt, M. A. Al-Laham, W. A. Shirley and J. Mantzaris, *J. Chem. Phys.*, 1988, **89**, 2193–2218.

49 J. Tomasi and M. Persico, *Chem. Rev.*, 1994, **94**, 2027–2094.

50 J. Tomasi, B. Mennucci and R. Cammi, *Chem. Rev.*, 2005, 105, 2999–3093.

51 A. V. Marenich, C. J. Cramer and D. G. Truhlar, *J. Phys. Chem. B*, 2009, **113**, 6378–6396.

Supporting Information

Unusual Dual-Emissive Heteroleptic Iridium Complexes Incorporating TADF Cyclometalating Ligands

Helen Benjamin,[a] Yonghao Zheng,[a,b] Valery N. Kozhevnikov,[a,c] Jamie S. Siddle,[a] Luke J. O'Driscoll, [a] Mark A. Fox,[a] Andrei S. Batsanov,[a] Gareth C. Griffiths,[d] Fernando B. Dias,[d] Andrew P. Monkman,[d] and Martin R. Bryce*[,a]

[a] *Department of Chemistry, Durham University, Durham DH1 3LE, U.K.* m.r.bryce@durham.ac.uk

[b] *School of Optoelectronic Science and Engineering, University of Electronic Science and Technology of China (UESTC), Chengdu 610054, China*

[c] *Department of Applied Sciences, Northumbria University, Newcastle-Upon-Tyne, NE1 8ST, U.K.*

[d] *Department of Physics, Durham University, Durham DH1 3LE, U.K.*

Contents

Synthesis of MIDA boronic esters

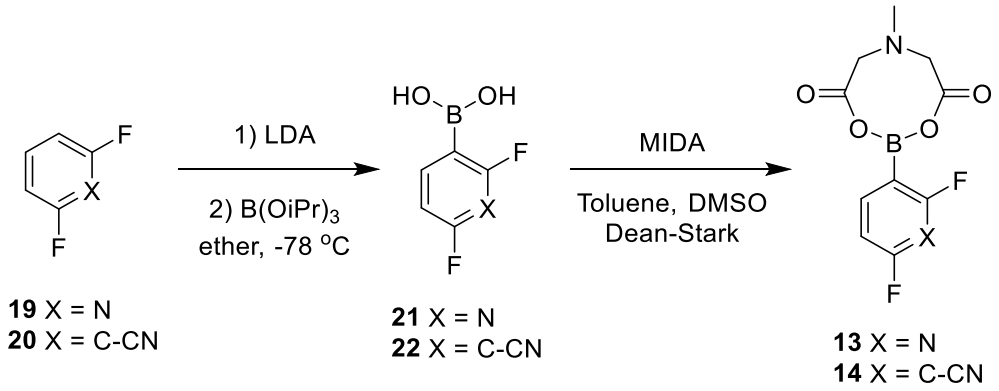

19 X = N
20 X = C-CN

21 X = N
22 X = C-CN

13 X = N
14 X = C-CN

Scheme S1: Synthesis of the required MIDA-boronic esters

2,6-Difluoro-3-pyridylboronic acid 21

^{n}BuLi (45 ml, 2.5 M in hexanes) was added dropwise to a stirred solution of DIPA (14.5 ml, 103.5 mmol) in diethyl ether (100 ml, dry) at 0 °C under argon. The solution was stirred at 0 °C for 30 min before the temperature was lowered to -78 °C. 2,6-difluoropyridine, **19** (8.5 ml, 93.7 mmol) was added dropwise and the mixture was stirred at -78 °C for 3 h. Triisopropyl borate (32.5 ml, 140.8 mmol) was slowly added, and the reaction mixture was stirred at -78 °C for 30 min before being quenched with water (100 ml) and left to warm to RT overnight. The reaction mixture was extracted with diethyl ether (3 x 50 ml) and the aqueous layer carefully acidified to pH 6 with 48% HBr. A second extraction was performed using ethyl acetate (3 x 50 ml) and the organic layers were combined and evaporated *in vacuo*. After recrystallisation from toluene, **21** was obtained as an off white powder (8.74 g, 59%); δ_H (400 MHz; d_6-acetone; Me_4Si) 8.40 (1H, q, *J* 4.5), 7.56 (2H, s), 7.04 (1H, d, *J* 8.0); δ_C (100 MHz; d_6-acetone; Me_4Si) 164.9 (dd, *J* 244.9, 14.2), 163.0 (dd, *J* 243.9, 15.2), 152.5 (t, *J* 7.9), 105.8 (dd, *J* 33.0, 5.4); δ_F (376 MHz; $CDCl_3$) -61.5 (1F, s), -68.4 (1F, s).

2,6-Difluoro-3-(6-methyl-4,8-dioxo-1,3,6,2-dioxazaborocan-2-yl)pyridine 13

A mixture of 2,6-difluoro-3-pyridylboronic acid, **21** (8.74 g, 55.0 mmol), *N*-methyliminodiacetic acid (MIDA) (8.18 g, 55.6 mmol), DMSO (45 ml), and toluene (95 ml) was heated under reflux with a Dean Stark trap overnight. After cooling to room temperature, the organic solvents were removed *in vacuo*. The product was washed with small amounts of dichloromethane, toluene and diethyl ether. **13** was obtained as a cream powder (13.33 g, 90%); δ_H (400 MHz; d_6-acetone; Me_4Si) 8.27 (1H, q, *J* 8.5), 7.08 (1H, ddd, *J*

7.6, 2.4, 1.8), 4.37 (4H, dd, *J* 97.2, 17.2), 2.98 (3H, s); δ_C (100 MHz; d_6-acetone; Me_4Si) 167.7, 164.0 (dd, *J* 240.2, 14.0), 162.9 (dd, *J* 243.1, 15.5), 151.5 (t, *J* 8.0), 106.0 (dd, *J* 32.9, 5.2), 62.7, 47.3; δ_B (128 MHz; d_6-acetone) 10.7 (br s).

2,4-Difluoro-3-cyanophenylboronic acid 22

^{n}BuLi (13.8 ml, 2.5 M in hexanes) was added dropwise to a stirred solution of DIPA (5.24 ml, 37.3 mmol) in THF (40 ml, dry) at 0 ˚C under argon. The solution was stirred at 0 ˚C for 30 min before the temperature was lowered to -78 ˚C. A solution of 2,6-difluorobenzonitrile **20** (4.00 g, 28.8 mmol) in THF (15 ml, dry) was added dropwise via cannula and the mixture was stirred at -78 ˚C for 1 h. Triisopropyl borate (9.95 ml, 43.1 mmol) was slowly added, and the reaction mixture was stirred at -78 ˚C for 1 h before being left to warm to RT overnight. Dilute HCl was added and the solution was extracted with EtOAc. The solvent was removed *in vacuo* to leave a sticky brown solid. The solid was redissolved in EtOAc and extracted with aqueous KOH (150 ml). The aqueous layer was acidified to pH 5 with dilute HCl and extracted with EtOAc. The solvent was removed *in vacuo* to give a beige solid, 2,4-difluoro-3-cyanophenylboronic acid **22** (4.39 g, 84%); δ_H (400 MHz; acetone-d_6; Me_4Si) 8.13 (1H, dt, *J* 8.6 7.1), 7.71 (2H, s), 7.32 (1H, td, *J* 8.6 0.9); δ_F (376 MHz; acetone-d_6; Me_4Si) -98.62 (1F, d, *J* 6.6), -105.73 (1F, t, *J* 7.6); δ_B (400 MHz; acetone-d_6; Me_4Si) 27.22 (1B, s); NMR data are consistent with the literature data.[S1]

2,6-Difluoro-3-(6-methyl-4,8-dioxo-1,3,6,2-dioxazaborocan-2-yl)benzonitrile 14

A mixture of **22** (4.39 g, 24.0 mmol), *N*-methyliminodiacetic acid (MIDA) (4.24 g, 28.8 mmol), DMSO (40 ml), and toluene (80 ml) was heated under reflux with a Dean Stark trap overnight. The mixture was cooled to room temperature, and water (50 ml) was added. The precipitate was filtered off, washed with water and dried under vacuum to give **14** as an off-white solid (5.10 g, 72%); δ_H (400 MHz; $CDCl_3$; Me_4Si) 7.82 (1H, q, *J* 7.5), 7.39 (1H, t, *J* 8.7), 4.40 (2H, d, *J* 17.3), 4.08 (2H, d, *J* 17.3), 2.62 (3H, s); δ_F (376 MHz; DMSO-d_6; Me_4Si) -97.74 (d, *J* 7.6), -104.91 (ddt, *J* 11.1, 6.6, 3.1); NMR data are consistent with the literature data.[S1]

Mass spectrometry of complexation reactions

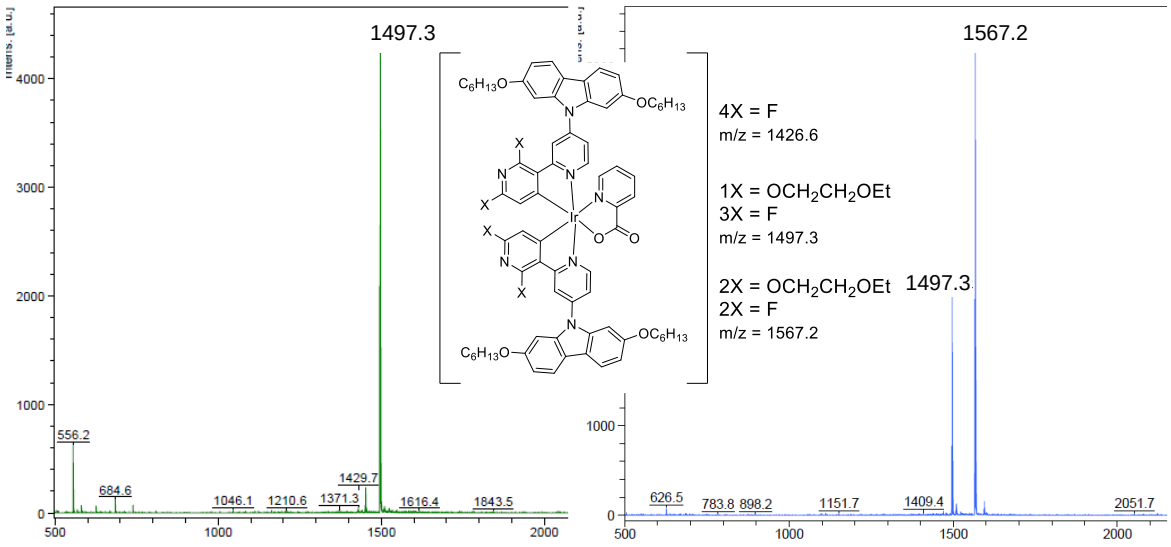

Figure S1: Mass spectra (MALDI-TOF) of two products isolated from the reaction of **10** with $IrCl_3.3H_2O$ and picolinic acid in ethoxyethanol at 130 ^oC.

X-ray crystallography

Table S1: Crystal data

Compound	**2**	**3**
CCDC	1962578	1962579
Formula	$C_{44}H_{34}F_4IrN_5O_2 \cdot 1.5\ C_6H_{14}$	$C_{48}H_{34}F_4IrN_5O_2 \cdot 4\ CDCl_3$
$D_{calc.}$/ g cm^{-3}	1.480	1.693
μ/mm^{-1}	2.86	2.94
Formula Weight	1062.22	1462.50
Size/mm^3	0.08×0.13×0.23	0.06×0.08×0.10
T/K	120	120
Crystal System	triclinic	triclinic
Space Group	$P\bar{1}$ (no. 2)	$P\bar{1}$ (no. 2)
a/Å	12.7261(3)	10.0759(5)
b/Å	14.9853(4)	16.3073(8)
c/Å	15.3107(4)	17.9412(8)
α/°	60.976(1)	89.3872(15)
β/°	80.336(1)	76.7980(14)
γ/°	69.010(1)	89.1792(15)
V/Å^3	2383.7(1)	2869.64
Z	2	2
Wavelength/Å	0.71073	0.71073
Θ_{max}/°	60	58.3
Reflections measured	43050	59027
unique	13914	15449
with I>2σ(I)	12256	12529
R_{int}	0.035	0.059
Parameters/restraints	517/0	701/52
wR_2 (all data)	0.065	0.077
R_1 [I>2σ(I)]	0.026	0.036

X-ray diffraction experiments were carried out on Bruker 3-circle diffractometers SMART 6000 with a CCD area detector, using graphite-monochromated sealed-tube Mo-$K\alpha$ radiation (**2**) and D8 Venture with a PHOTON 100 CMOS area detector, using Mo-$K\alpha$ radiation from an Incoatec IμS microsource with focusing mirrors (**3**). The crystals were cooled using a Cryostream 700 (Oxford Cryosystems) open-flow N2 gas cryostat. The data were corrected for absorption by numerical integration based on the crystal face-indexing. Structure **2** was solved by direct methods using SHELXS 2013/1 program[S2], structure **3** by dual-space intrinsic phasing method using SHELXT 2018/2 program[S3], both were refined by full-matrix least squares using SHELXS 2018/3 program[S4] on Olex2 platform[S5]. Structure **2** contains infinite channels parallel to the [1 1 0] direction, comprising 28% of the crystal space (705 Å^3 per unit cell) and occupied by disordered solvent (observe integral electron density 151 e per unit cell, presumably ca. 3 molecules of hexane) which was masked using SMTBX program in OLEX2[S6].

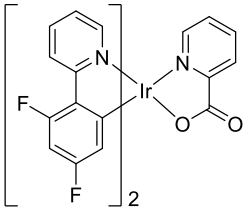

FIrpic

Figure S2: Structure of **FIrpic**.

Table S2: Selected bond distances (Å)

	FIrpic[a,b]	**1**[b,c]	**2**	**3**
Ir-N(1)	2.048[11]	2.040(2)	2.040(2)	2.046(2)
Ir-N(2)	2.041[8]	2.037(2)	2.032(2)	2.033(2)
Ir-N(3)	2.140[8]	2.143(2)	2.123(2)	2.123(3)
Ir-O(1)	2.154[7]	2.163(2)	2.110(2)	2.147(2)
Ir-C(1)	2.000[8]	2.001(2)	1.989(3)	1.996(3)
Ir-C(21)	1.991[9]	1.988(3)	1.982(2)	1.987(3)

[a] Weighted average from six X-ray structure determinations[S7–S11]; [b] Atom numbering in Table S2 is consistent with Figure 1 in the manuscript; [c] ref.[S12]

Cyclic voltammetry

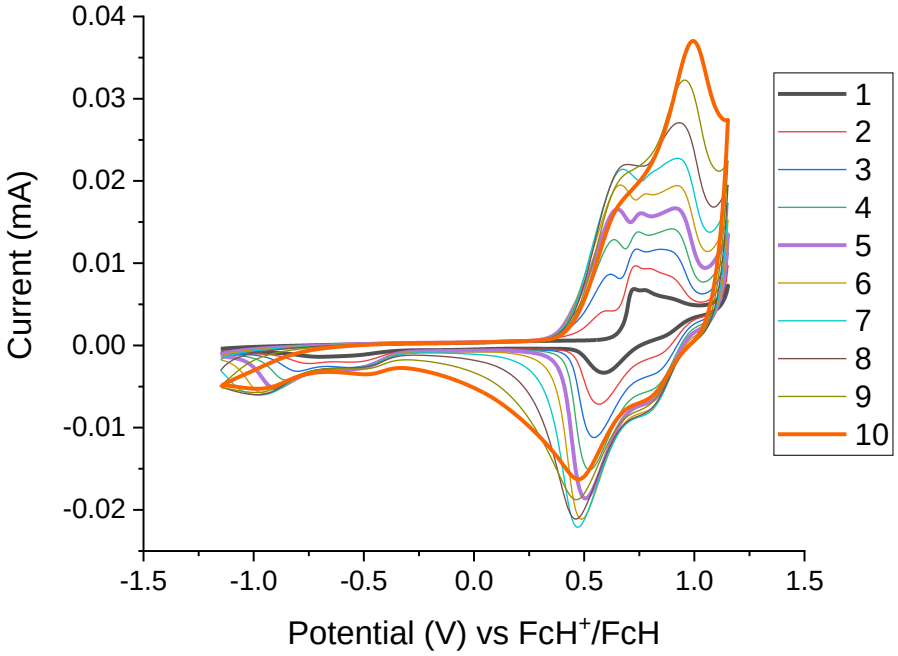

Figure S3: Cyclic voltammogram of 10 successive scans of complex **4** at 100 mV/s.

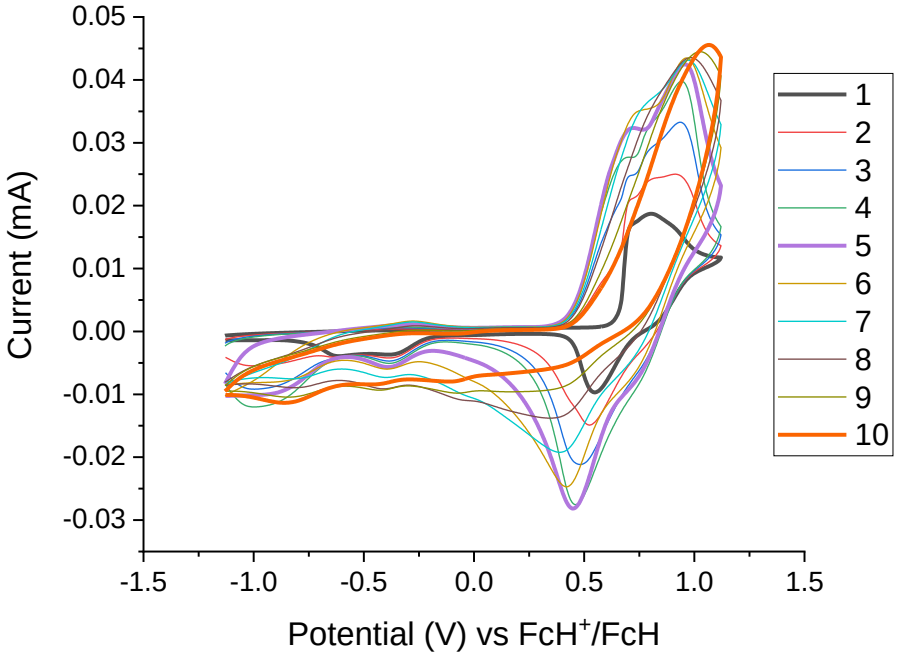

Figure S4: Cyclic voltammogram of 10 successive scans of complex **5** at 100 mV/s.

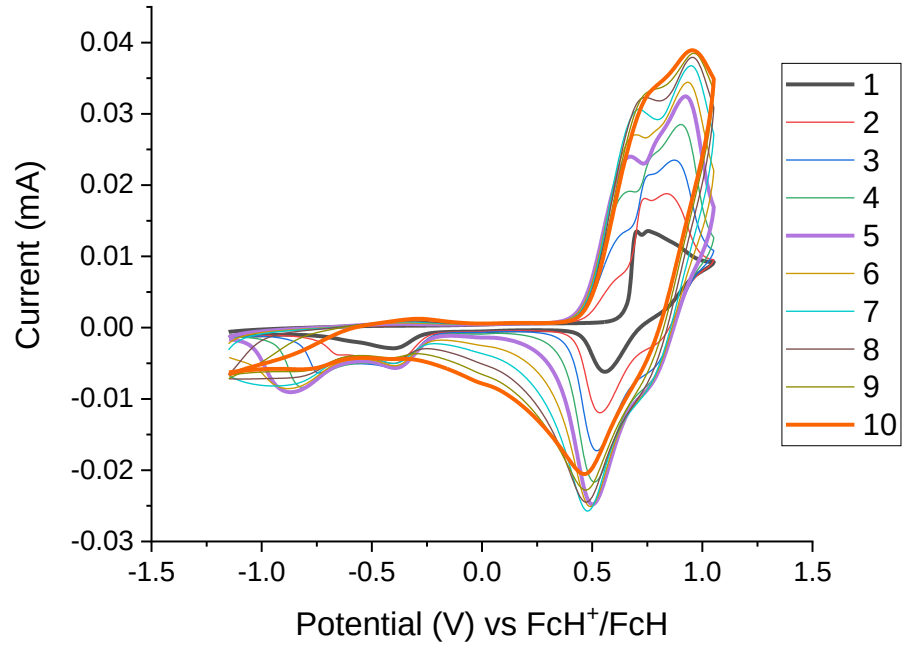

Figure S5: Cyclic voltammogram of 10 successive scans of complex **6** at 100 mV/s.

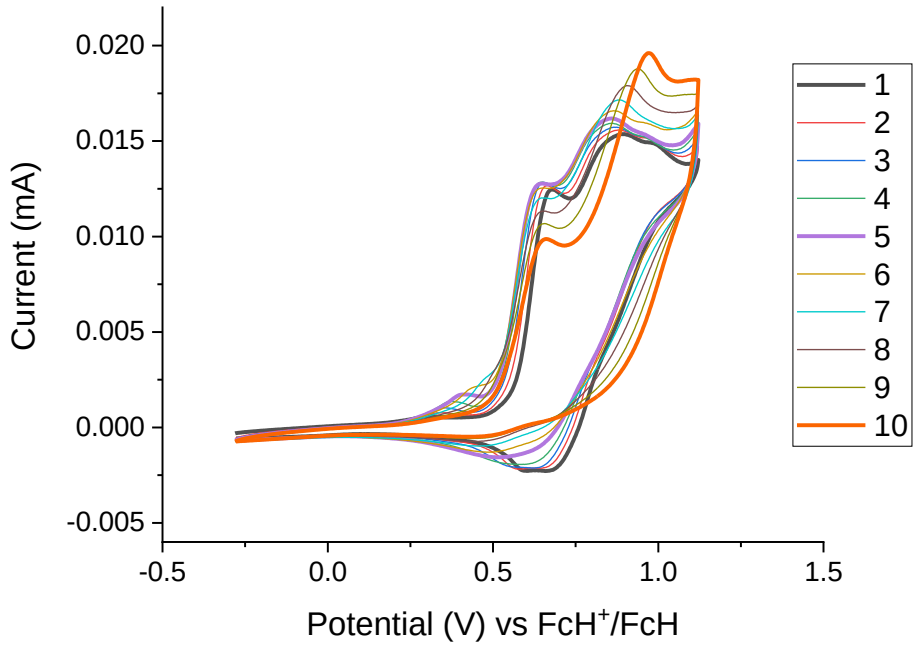

Figure S6: Cyclic voltammogram of 10 successive scans of ligand **9** at 100 mV/s.

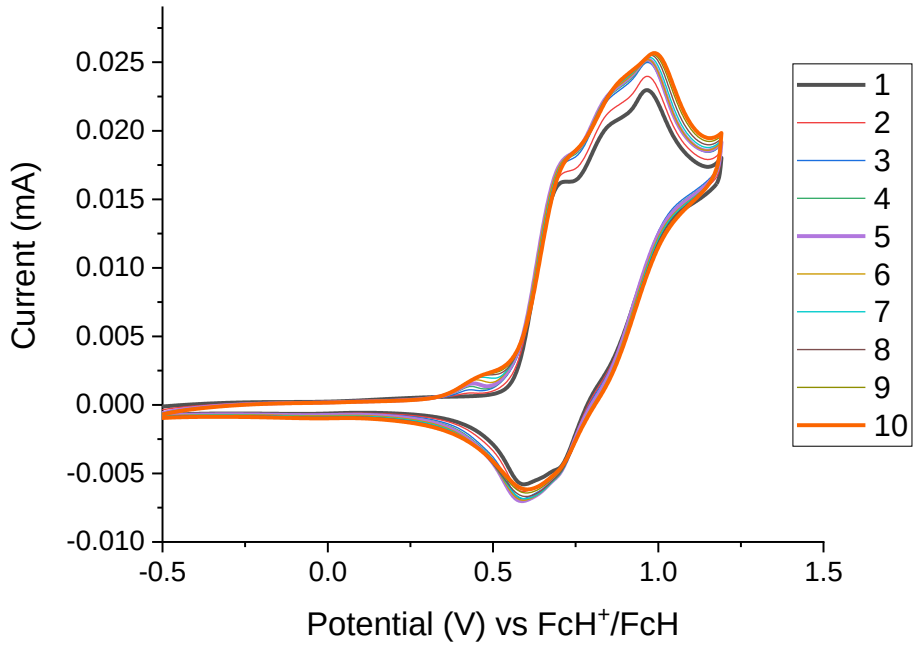

Figure S7: Cyclic voltammogram of 10 successive scans of ligand **10** at 100 mV/s.

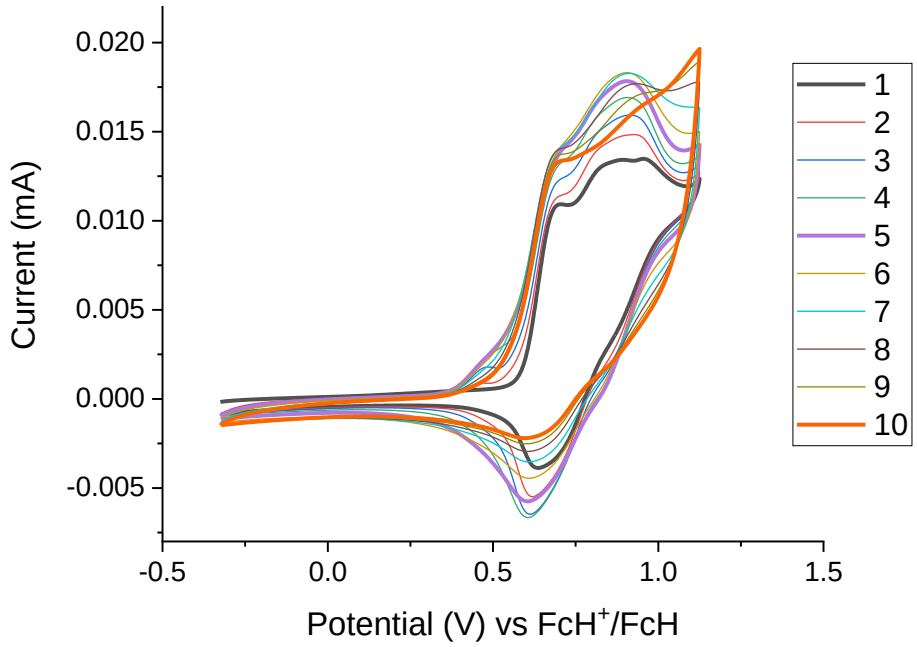

Figure S8: Cyclic voltammogram of 10 successive scans of ligand **11** at 100 mV/s.

Photophysics

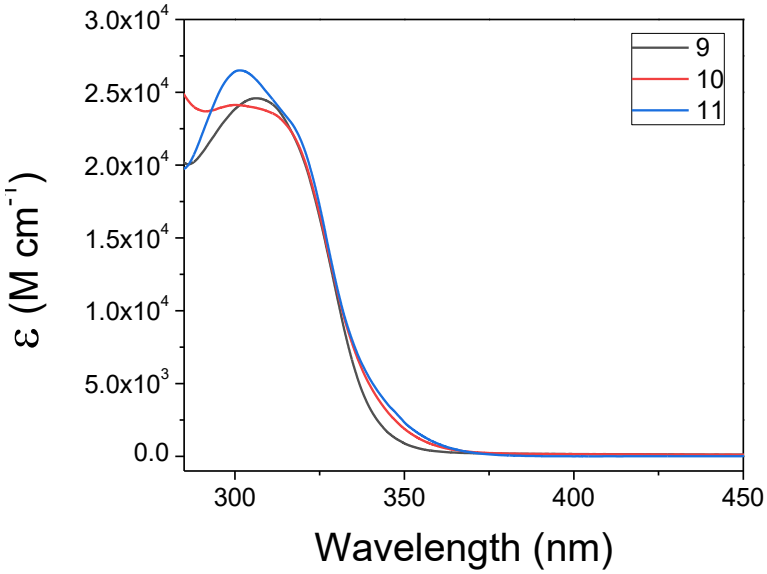

Figure S9: Absorption spectra of ligands **9-11** in toluene (< 5 x 10^{-5} M).

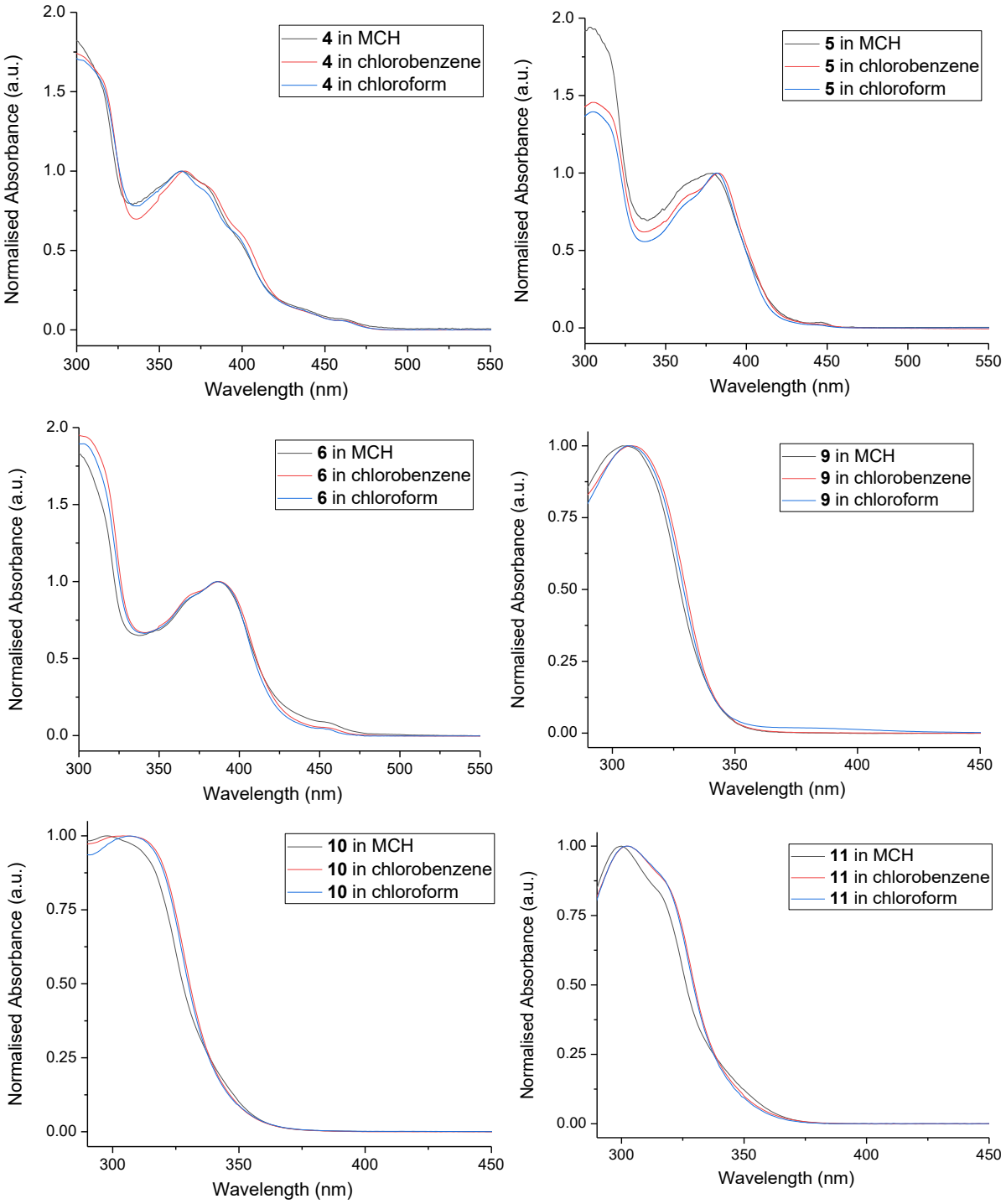

Figure S10: Absorption spectra of dual emissive complexes **4**-**6**, and ligands **9**-**11** in different solvents [< 10^{-5} M]. MCH = methylcyclohexane.

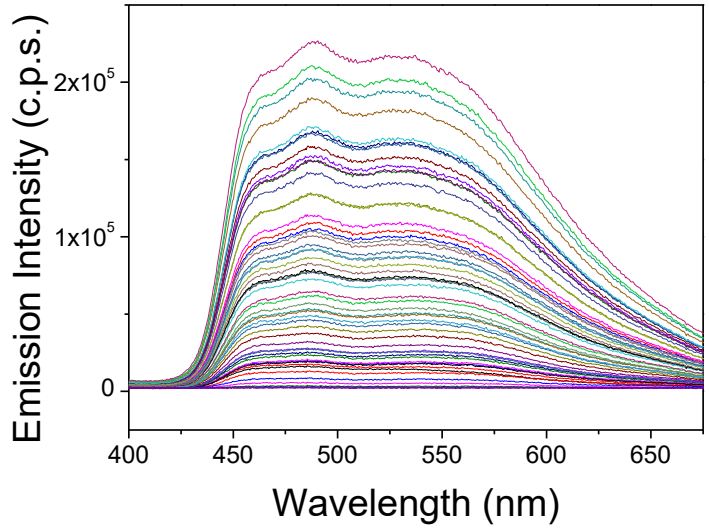

Figure S11: The decay profile of complex **5** in chlorobenzene (λ_{ex} = 355 nm) (< 5 x 10^{-5} M).

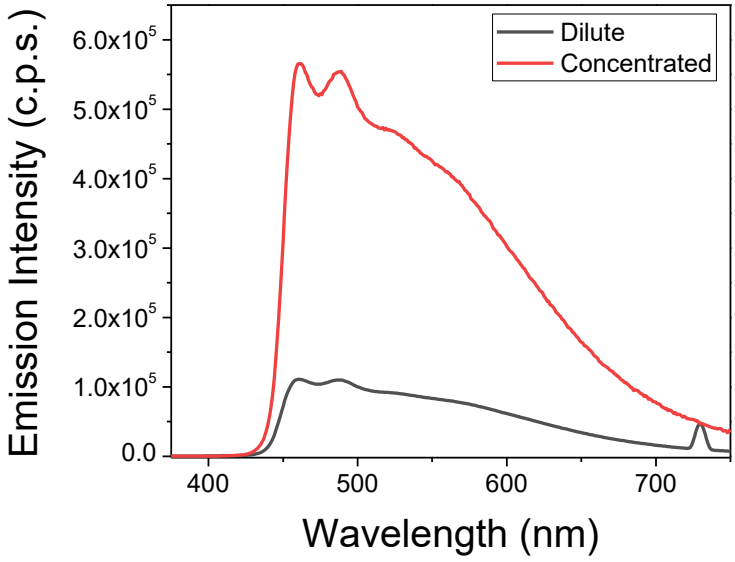

Figure S12: Emission spectra of concentrated (10^{-4} M) and dilute (10^{-5} M) solutions of **5** in chlorobenzene (λ_{ex} = 365 nm).

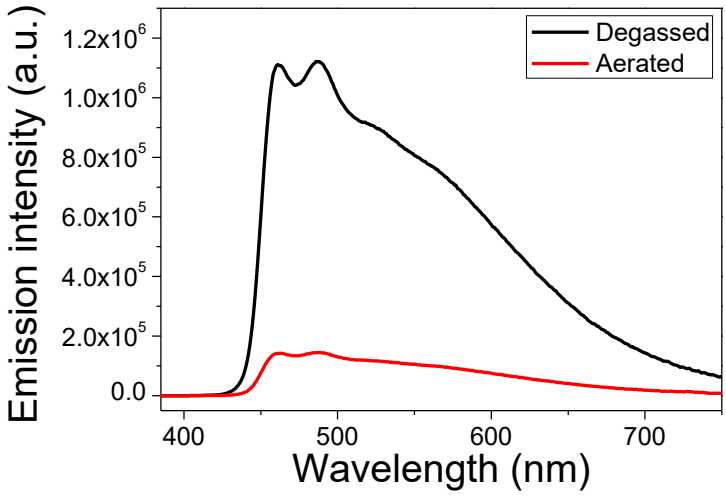

Figure S13: Emission of **5** in degassed and aerated chlorobenzene (λ_{ex} = 365 nm).

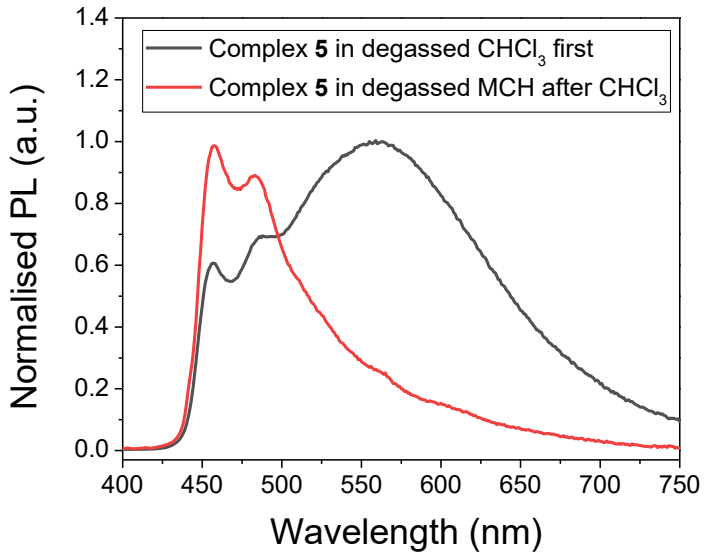

Figure S14: Degradation test: Emission of **5** in degassed $CHCl_3$. The solvent was the removed and the residue was then re-dissolved in MCH (degassed). λ_{ex} = 365 nm.

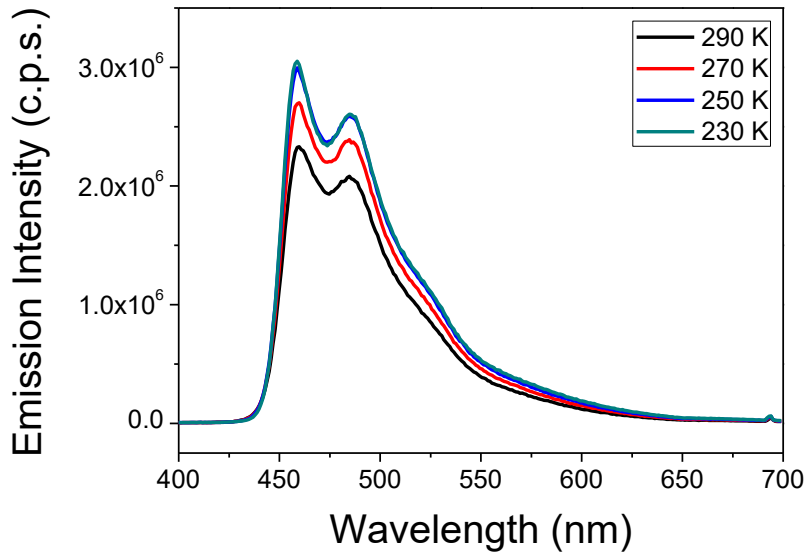

Figure S15: Emission of **5** in zeonex films.

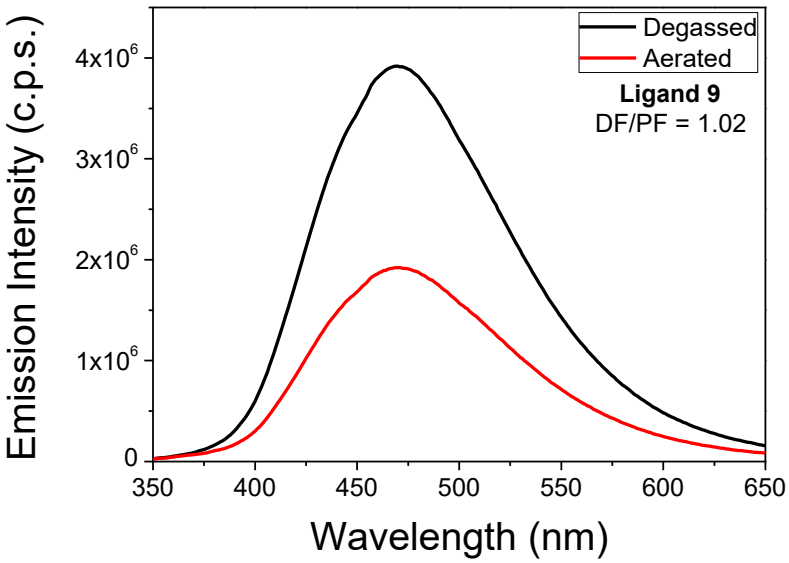

Figure S16: Emission of ligand **9** in degassed and aerated chlorobenzene (λ_{ex} = 340 nm). DF/PF = the ratio between delayed and prompt emission, calculated from the following:

$$\frac{\int I_{DF}^{deg}(\lambda)d\lambda}{\int I_{PF}^{O2}(\lambda)d\lambda} = \frac{\Phi_{PF}+\Phi_{DF}}{\Phi_{PF}} = 1 + \frac{\Phi_{DF}}{\Phi_{PF}}.$$

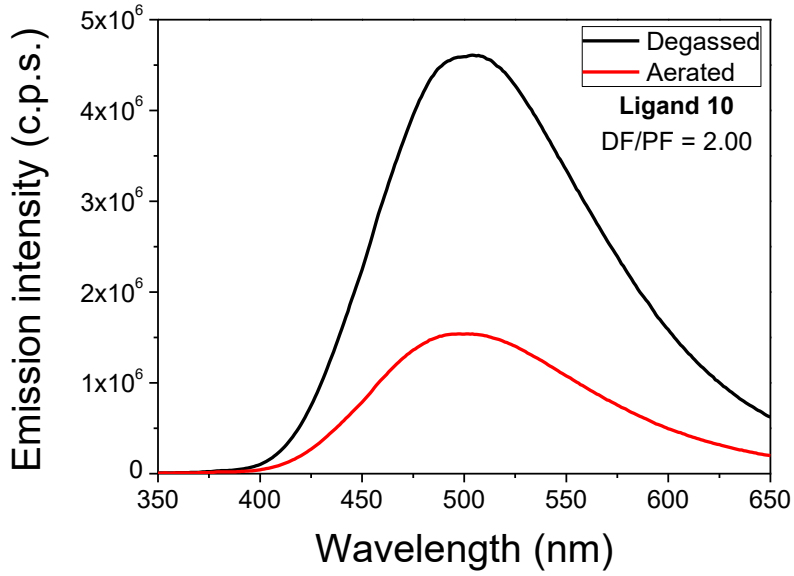

Figure S17: Emission of ligand **10** in degassed and aerated chlorobenzene (λ_{ex} = 340 nm). DF/PF = the ratio between delayed and prompt emission, calculated from the following:

$$\frac{\int I_{DF}^{deg}(\lambda)d\lambda}{\int I_{PF}^{O2}(\lambda)d\lambda} = \frac{\Phi_{PF}+\Phi_{DF}}{\Phi_{PF}} = 1 + \frac{\Phi_{DF}}{\Phi_{PF}}.$$

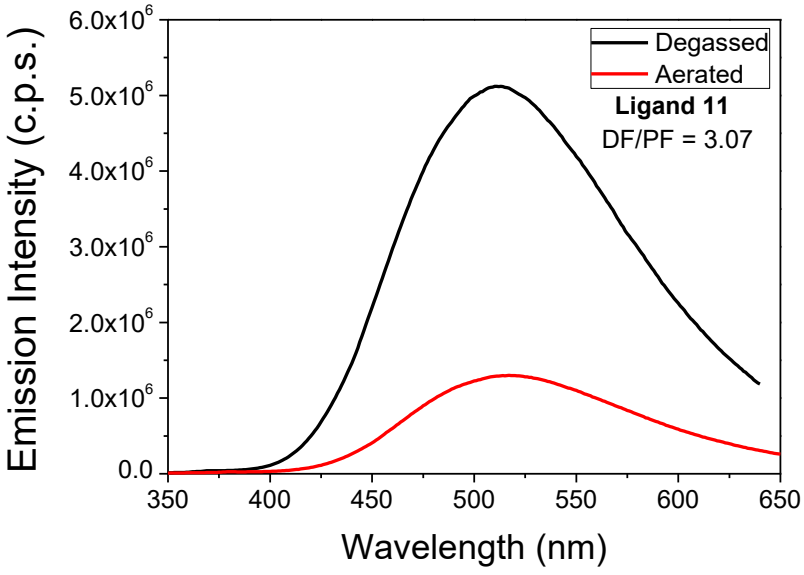

Figure S18: Emission of ligand **11** in degassed and aerated chlorobenzene (λ_{ex} = 340 nm). DF/PF = the ratio between delayed and prompt emission, calculated from the following:

$$\frac{\int I_{DF}^{deg}(\lambda)d\lambda}{\int I_{PF}^{O2}(\lambda)d\lambda} = \frac{\Phi_{PF}+\Phi_{DF}}{\Phi_{PF}} = 1 + \frac{\Phi_{DF}}{\Phi_{PF}}.$$

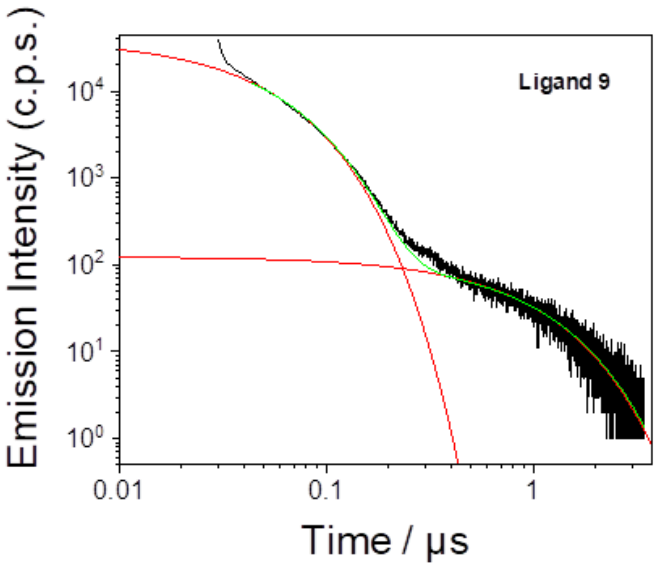

Equation	y = A1*exp(-x/t1) + A2*exp(-x/t2) + y0
Plot	E
y0	0 ± 0
A1	37662.37912 ± 24.48561
t1	0.039 ± 0
A2	119.52 ± 0
t2	0.76762 ± 0
Reduced Chi-Sqr	1536.586
R-Square (COD)	0.9983
Adj. R-Square	0.9983

Figure S19: Emission lifetime of ligand **9** in degassed chlorobenzene (λ_{ex} = 340 nm). Fittings of individual decay components shown in red, fitting of the total decay shown in green.

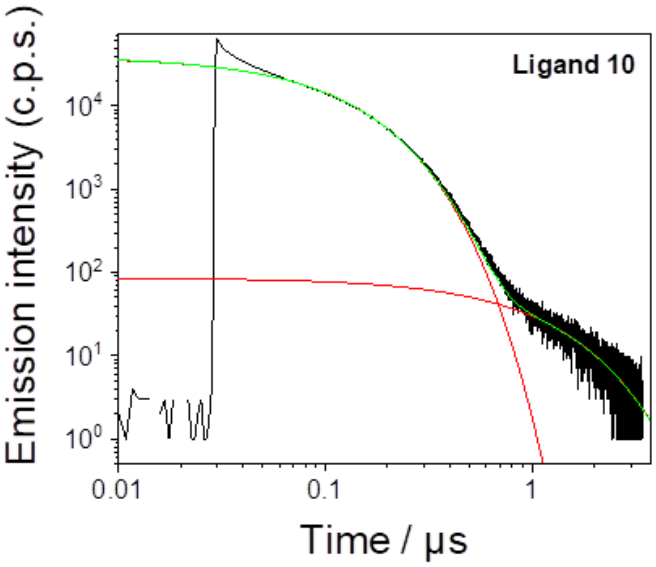

Equation	y = A1*exp(-x/t1) + A2*exp(-x/t2) + y0
Plot	Decay
y0	0 ± 0
A1	39245.73951 ± 36.27786
t1	0.09947 ± 7.6519E-5
A2	85 ± 0
t2	0.946 ± 0
Reduced Chi-Sqr	4143.207
R-Square (COD)	0.99937
Adj. R-Square	0.99937

Figure S20: Emission lifetime of ligand **10** in degassed chlorobenzene (λ_{ex} = 340 nm). Fittings of individual decay components shown in red, fitting of the total decay shown in green.

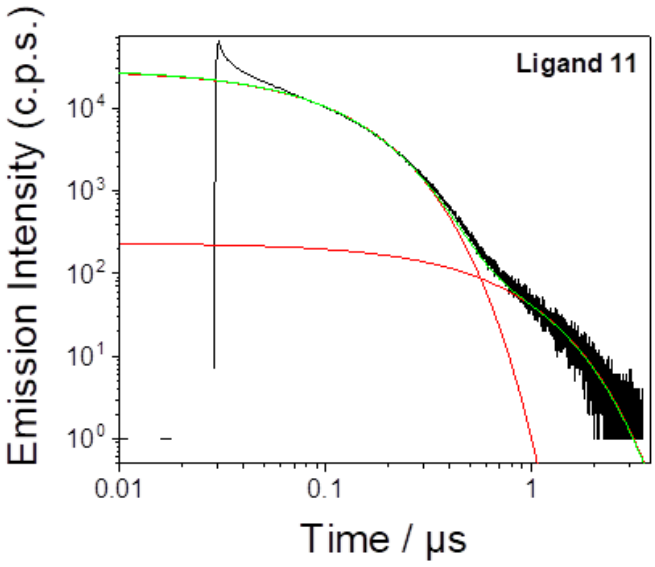

Equation	y = A1*exp(-x/t1) + A2*exp(-x/t2) + y0
Plot	Decay
y0	0 ± 0
A1	29434.19468 ± 35.66585
t1	0.09408 ± 8.78317E-5
A2	233 ± 0
t2	0.57 ± 0
Reduced Chi-Sqr	2631.265
R-Square (COD)	0.99915
Adj. R-Square	0.99915

Figure S21: Emission lifetime of ligand **11** in degassed chlorobenzene (λ_{ex} = 340 nm). Fittings of individual decay components shown in red, fitting of the total decay shown in green.

DFT calculations

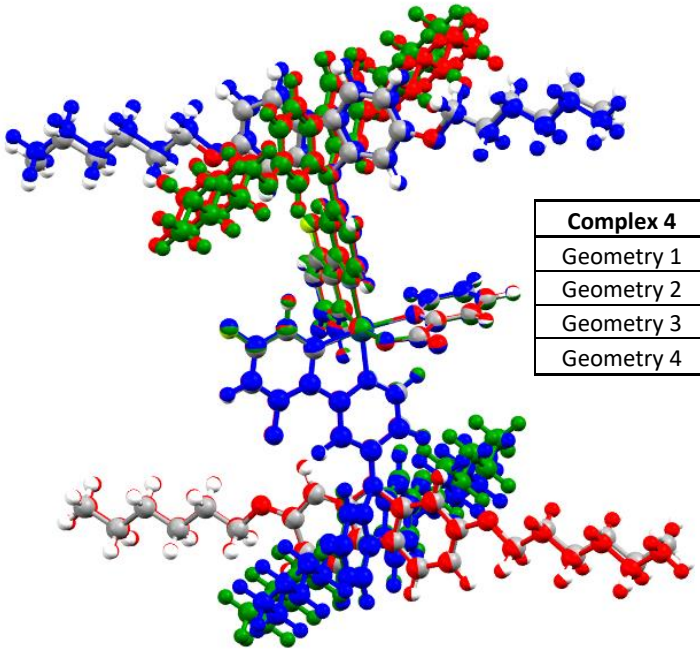

	Energy of S_0	
Complex 4	kJ/mol	Difference in kJ/mol
Geometry 1	-10841593.55	0.00
Geometry 2	-10841593.64	-0.09
Geometry 3	-10841593.31	0.33
Geometry 4	-10841593.36	0.19

Figure S22: Geometries of the three ground states found for complex **4**. Geometry 1 is coloured by element, Geometry 2 is coloured red, Geometry 3 is coloured in blue, Geometry 4 is coloured in green.

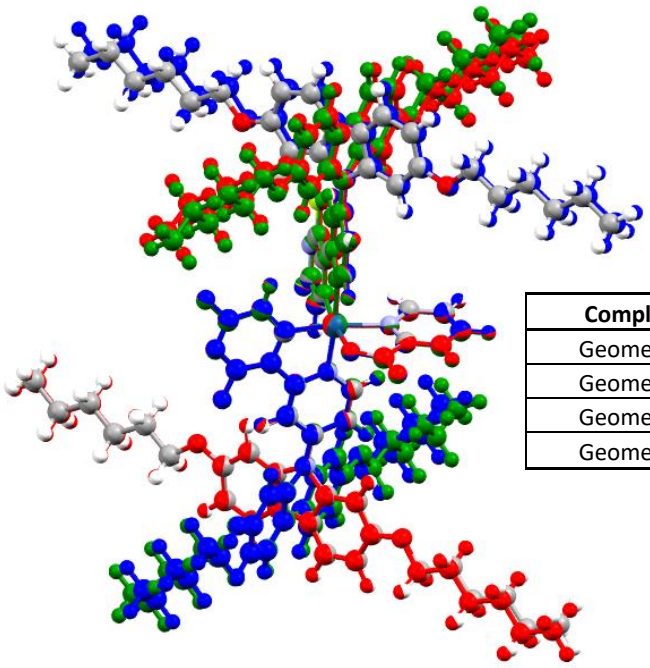

	Energy of S_0	
Complex 5	kJ/mol	Difference in kJ/mol
Geometry 1	-10924950.79	0.00
Geometry 2	-10924950.85	-0.07
Geometry 3	-10924950.92	-0.13
Geometry 4	-10924950.65	0.20

Figure S23: Geometries of the three ground states found for complex **5**. Geometry 1 is coloured by element, Geometry 2 is coloured red, Geometry 3 is coloured in blue, Geometry 4 is coloured in green.

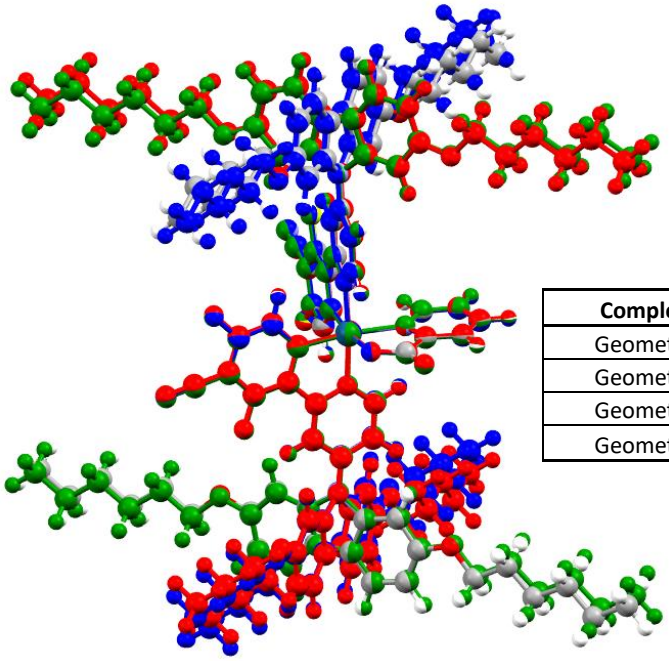

	Energy of S_0	
Complex 6	kJ/mol	Difference in kJ/mol
Geometry 1	-11320866.67	0.00
Geometry 2	-11320866.83	-0.16
Geometry 3	-11320866.72	-0.05
Geometry 4	-11320866.50	0.33

Figure S24: Geometries of the three ground states found for complex **6**. Geometry 1 is coloured by element, Geometry 2 is coloured red, Geometry 3 is coloured in blue, Geometry 4 is coloured in green.

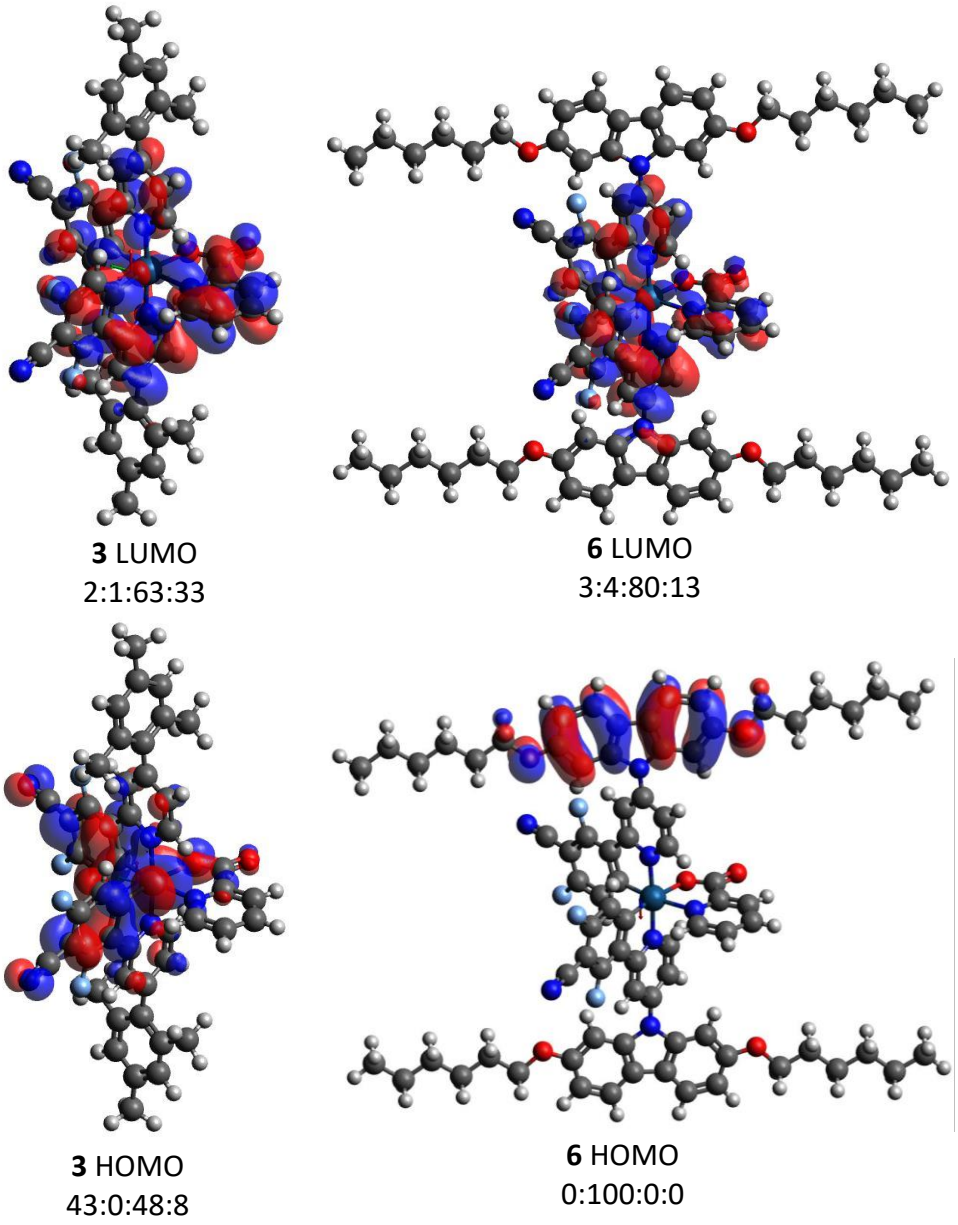

Figure S25: Frontier molecular orbitals for **3** and **6**. Isocontours set to ±0.02 e/bohr^3. Ir:mesityl/carbazolyl:phenylpyridyl:picolyl % orbital contribution ratio listed for each orbital.

Table S3: *Energy and Distribution of Complex **2** Frontier Orbitals*

MO	eV	Ir	mesityl1	pyridine1	phenyl1	mesityl2	pyridine2	phenyl2	pic
L+5	-1.16	2	1	45	7	0	10	2	33
L+4	-1.19	2	1	27	3	1	55	7	4
L+3	-1.42	1	0	12	2	0	19	3	62
L+2	-1.85	4	1	53	21	0	12	5	2
L+1	-1.91	5	0	5	3	1	36	18	32
LUMO	-1.99	1	0	8	4	0	15	7	64
HOMO	-6.13	52	0	5	14	0	4	14	12
H-1	-6.19	50	0	7	4	0	2	6	30
H-2	-6.61	45	6	2	4	14	13	11	5
H-3	-6.61	3	91	3	0	2	1	1	0
H-4	-6.63	9	0	0	1	82	4	2	1
H-5	-6.67	1	94	2	3	0	0	0	1

Table S4*: Energy and Distribution of Complex **3** Frontier orbitals*

MO	eV	Ir	mesityl1	pyridine1	phenyl1	mesityl2	pyridine2	phenyl2	pic
L+5	-1.27	2	1	28	6	1	47	8	8
L+4	-1.29	2	0	5	14	0	7	57	15
L+3	-1.5	1	0	14	5	1	21	10	48
L+2	-1.94	5	1	50	22	0	12	5	5
L+1	-1.99	5	0	1	0	1	22	12	60
LUMO	-2.07	2	0	13	7	1	28	15	33
HOMO	-6.04	43	0	3	21	0	3	21	8
H-1	-6.26	52	0	8	2	0	2	3	33
H-2	-6.65	0	97	3	0	0	0	0	0
H-3	-6.66	1	0	0	0	96	3	0	0
H-4	-6.7	31	36	2	5	5	9	7	4
H-5	-6.7	21	62	0	1	4	5	4	2

Table S5: *Complex **4**, Geometry 1 - Frontier orbital energies and distributions*

MO	eV	Ir	carbazole1	pyridine1	phenyl1	carbazole2	pyridine2	phenyl2	pic
L+5	-1.05	1	2	28	5	1	13	2	46
L+4	-1.1	2	2	38	6	3	42	6	2
L+3	-1.29	1	1	15	3	2	25	4	50
L+2	-1.7	5	6	53	16	1	13	4	2
L+1	-1.74	5	1	5	2	3	36	14	33
LUMO	-1.83	1	1	8	3	2	17	6	63
HOMO	-5.36	0	100	0	0	0	0	0	0
H-1	-5.37	0	0	0	0	100	0	0	0
H-2	-5.6	43	4	3	20	1	3	19	7
H-3	-5.7	28	48	11	1	1	1	2	8
H-4	-5.79	10	1	0	1	76	11	0	1
H-5	-6.07	28	36	6	6	0	1	2	20

Table S6: *Complex **4**, Geometry 2 - Frontier orbital energies and distributions*

MO	eV	Ir	carbazole1	pyridine1	phenyl1	carbazole2	pyridine2	phenyl2	pic
L+5	-1.04	1	2	26	5	1	14	3	47
L+4	-1.1	2	2	40	6	2	40	6	2
L+3	-1.29	1	1	14	2	2	26	5	49
L+2	-1.7	5	6	55	17	1	10	3	3
L+1	-1.74	5	0	4	1	4	39	14	32
LUMO	-1.82	1	1	8	3	2	17	6	63
HOMO	-5.36	0	100	0	0	0	0	0	0
H-1	-5.37	0	0	0	0	100	0	0	0
H-2	-5.6	44	3	3	20	1	3	19	7
H-3	-5.7	27	48	11	1	2	1	2	9
H-4	-5.79	11	2	1	1	74	11	0	1
H-5	-6.07	28	35	6	6	1	1	2	20

Table S7: *Complex **4**, Geometry 3 - Frontier orbital energies and distributions*

MO	eV	Ir	carbazole1	pyridine1	phenyl1	carbazole2	pyridine2	phenyl2	pic
L+5	-1.04	1	2	26	5	1	15	3	48
L+4	-1.1	2	2	40	6	2	39	6	2
L+3	-1.29	1	1	14	3	2	26	5	49
L+2	-1.7	4	6	57	17	1	7	2	5
L+1	-1.74	5	0	2	1	4	43	16	29
LUMO	-1.82	1	1	8	3	1	15	6	64
HOMO	-5.36	0	100	0	0	0	0	0	0
H-1	-5.37	0	0	0	0	100	0	0	0
H-2	-5.6	44	3	3	20	1	3	19	7
H-3	-5.7	26	51	11	1	0	1	2	9
H-4	-5.79	10	0	0	1	76	12	0	1
H-5	-6.07	29	35	6	6	0	1	2	20

Table S8: *Complex **4**, Geometry 4 - Frontier orbital energies and distributions*

MO	eV	Ir	carbazole1	pyridine1	phenyl1	carbazole2	pyridine2	phenyl2	pic
L+5	-1.04	1	1	14	2	2	27	5	46
L+4	-1.09	2	3	42	6	2	38	6	2
L+3	-1.29	1	2	24	4	1	15	3	51
L+2	-1.7	5	1	12	4	6	54	17	2
L+1	-1.73	5	4	38	14	1	5	2	30
LUMO	-1.83	1	1	15	6	1	7	3	66
HOMO	-5.36	0	0	0	0	100	0	0	0
H-1	-5.38	0	100	0	0	0	0	0	0
H-2	-5.6	43	1	3	19	3	3	20	7
H-3	-5.69	27	3	1	2	46	10	1	9
H-4	-5.79	11	72	11	0	3	1	1	1
H-5	-6.07	28	1	1	2	36	6	7	20

Table S9: *Complex **5**, Geometry 1 - Frontier orbital energies and distributions*

MO	eV	Ir	carbazole1	pyridine1	phenyl1	carbazole2	pyridine2	phenyl2	pic
L+5	-1.19	1	2	19	4	1	13	2	58
L+4	-1.27	2	3	43	6	2	37	5	1
L+3	-1.44	1	1	18	3	2	30	5	40
L+2	-1.9	4	5	48	17	1	6	2	17
L+1	-1.92	4	0	2	1	2	23	10	57
LUMO	-2.01	2	1	14	7	3	34	15	24
HOMO	-5.4	0	100	0	0	0	0	0	0
H-1	-5.4	0	0	0	0	100	0	0	0
H-2	-5.82	14	65	10	0	4	1	1	5
H-3	-5.88	6	4	1	0	78	11	0	1
H-4	-6.13	51	0	4	15	0	4	15	11
H-5	-6.27	37	20	5	4	0	2	3	29

Table S10: *Complex **5**, Geometry 2 - Frontier orbital energies and distributions*

MO	eV	Ir	carbazole1	pyridine1	phenyl1	carbazole2	pyridine2	phenyl2	pic
L+5	-1.19	1	1	18	4	1	14	2	58
L+4	-1.27	2	3	45	7	2	35	5	1
L+3	-1.44	1	1	17	3	2	31	5	40
L+2	-1.9	4	4	41	15	0	1	0	34
L+1	-1.92	4	1	9	3	3	27	11	41
LUMO	-2	2	1	14	6	3	34	15	24
HOMO	-5.4	0	100	0	0	0	0	0	0
H-1	-5.41	0	0	0	0	100	0	0	0
H-2	-5.82	14	67	11	0	1	1	1	5
H-3	-5.87	6	2	0	0	80	11	0	1
H-4	-6.12	51	0	4	15	0	4	15	11
H-5	-6.27	37	20	5	4	1	1	3	29

Table S11: *Complex **5**, Geometry 3 - Frontier orbital energies and distributions*

MO	eV	Ir	carbazole1	pyridine1	phenyl1	carbazole2	pyridine2	phenyl2	pic
L+5	-1.19	1	1	17	4	1	14	2	59
L+4	-1.27	2	3	46	7	2	35	5	1
L+3	-1.44	1	1	17	3	2	31	5	39
L+2	-1.89	4	4	39	14	0	1	0	38
L+1	-1.92	4	1	12	4	3	27	11	38
LUMO	-2.00	2	1	14	7	3	35	16	22
HOMO	-5.39	0	100	0	0	0	0	0	0
H-1	-5.41	0	0	0	0	100	0	0	0
H-2	-5.82	13	69	11	0	0	0	1	5
H-3	-5.88	6	0	0	0	81	11	0	1
H-4	-6.12	51	0	4	15	0	3	15	11
H-5	-6.27	37	19	5	4	0	2	3	29

Table S12: *Complex **5**, Geometry 4 - Frontier orbital energies and distributions*

MO	eV	Ir	carbazole1	pyridine1	phenyl1	carbazole2	pyridine2	phenyl2	pic
L+5	-1.19	1	2	19	4	1	14	2	57
L+4	-1.27	2	3	43	6	3	37	6	1
L+3	-1.44	1	1	18	3	2	29	5	41
L+2	-1.90	4	5	46	17	0	2	1	25
L+1	-1.91	5	1	5	2	3	29	12	45
LUMO	-2.00	2	1	13	6	3	32	14	29
HOMO	-5.40	0	100	0	0	0	0	0	0
H-1	-5.41	0	0	0	0	100	0	0	0
H-2	-5.82	15	64	10	0	3	1	1	5
H-3	-5.88	6	4	1	0	77	11	0	1
H-4	-6.12	51	0	4	15	0	4	15	11
H-5	-6.27	36	21	5	4	0	1	3	28

Table S13: *Complex **6**, Geometry 1 - Frontier orbital energies and distributions*

MO	eV	Ir	carbazole1	pyridine1	phenyl1	carbazole2	pyridine2	phenyl2	pic
L+5	-1.27	2	0	3	16	0	3	67	8
L+4	-1.35	2	2	42	6	3	36	8	0
L+3	-1.52	1	1	19	5	2	31	9	32
L+2	-1.96	4	2	21	8	0	0	0	65
L+1	-1.99	4	3	27	11	2	23	10	21
LUMO	-2.08	3	1	15	8	3	38	19	13
HOMO	-5.42	0	100	0	0	0	0	0	0
H-1	-5.43	0	0	0	0	100	0	0	0
H-2	-5.86	13	66	10	1	5	1	1	4
H-3	-5.91	6	5	1	0	78	10	0	1
H-4	-6.03	44	1	3	20	1	3	20	8
H-5	-6.33	38	18	6	3	0	1	2	31

Table S14: Complex **6**, Geometry 2 - *Frontier orbital energies and distributions*

MO	eV	Ir	carbazole1	pyridine1	phenyl1	carbazole2	pyridine2	phenyl2	pic
L+5	-1.27	2	0	3	16	0	3	68	8
L+4	-1.35	2	3	43	7	3	36	8	0
L+3	-1.52	1	1	19	5	2	31	9	32
L+2	-1.96	4	2	14	5	0	0	0	74
L+1	-1.99	4	3	33	13	2	23	10	11
LUMO	-2.08	3	1	15	8	3	37	19	13
HOMO	-5.42	0	100	0	0	0	0	0	0
H-1	-5.43	0	0	0	0	100	0	0	0
H-2	-5.86	13	70	10	1	1	0	1	5
H-3	-5.91	6	1	0	1	80	10	1	1
H-4	-6.03	43	1	3	20	2	3	20	8
H-5	-6.33	38	18	6	3	1	1	3	31

Table S15: Complex **6**, Geometry 3 - *Frontier orbital energies and distributions*

MO	eV	Ir	carbazole1	pyridine1	phenyl1	carbazole2	pyridine2	phenyl2	pic
L+5	-1.27	2	0	4	15	0	3	67	7
L+4	-1.34	2	3	43	7	3	35	8	0
L+3	-1.52	1	1	18	5	2	32	9	31
L+2	-1.95	4	2	19	7	0	0	0	68
L+1	-1.99	4	3	30	12	2	21	9	19
LUMO	-2.08	3	1	13	7	4	40	20	12
HOMO	-5.42	0	100	0	0	0	0	0	0
H-1	-5.43	0	0	0	0	100	0	0	0
H-2	-5.86	12	70	10	1	1	0	1	4
H-3	-5.92	6	1	0	1	80	11	0	1
H-4	-6.02	44	1	3	20	1	3	20	8
H-5	-6.33	38	18	5	3	0	1	3	31

Table S16: Complex **6**, Geometry 4 - *Frontier orbital energies and distributions*

MO	eV	Ir	carbazole1	pyridine1	phenyl1	carbazole2	pyridine2	phenyl2	pic
L+5	-1.27	2	0	4	16	0	3	68	7
L+4	-1.35	2	2	42	6	3	37	8	0
L+3	-1.52	1	1	20	5	2	30	9	32
L+2	-1.96	4	2	17	6	0	0	0	70
L+1	-1.99	4	3	30	12	2	24	10	13
LUMO	-2.08	2	1	15	8	3	36	18	15
HOMO	-5.42	0	100	0	0	0	0	0	0
H-1	-5.43	0	0	0	0	100	0	0	0
H-2	-5.86	13	67	10	1	3	1	1	5
H-3	-5.92	7	3	0	1	77	10	1	1
H-4	-6.03	43	1	3	20	2	4	20	7
H-5	-6.33	38	19	6	3	0	1	3	30

TD-DFT calculations

Table S17: TD-DFT calculations showing the energy and composition of excited states T_1-T_5 for complex **2**. Calculations were conducted at the optimised S_0 geometry. Electron density transfer to/from key groups is shown (%).

No.	wavelength (nm)	major contributions	Ir	mesityl1	pyridine1	phenyl1	mesityl2	pyridine2	phenyl2	picolinate
1	413.3771	H-7->L+2 (13%), H-1->L+2 (17%), HOMO->LUMO (12%), HOMO->L+2 (25%)	42-->4 (-38)	1-->1 (0)	9-->39 (30)	19-->16 (-3)	0-->0 (0)	3-->15 (12)	9-->7 (-2)	17-->18 (1)
2	406.9191	H-2->L+1 (14%), HOMO->L+1 (16%), HOMO->L+2 (11%)	42-->4 (-38)	2-->0 (-2)	4-->15 (11)	8-->6 (-2)	7-->1 (-6)	10-->29 (19)	17-->13 (-4)	10-->33 (23)
3	406.5855	H-1->LUMO (45%), H-1->L+1 (21%)	49-->3 (-46)	0-->0 (0)	6-->7 (1)	6-->3 (-3)	0-->1 (1)	2-->22 (20)	8-->11 (3)	28-->53 (25)
4	378.9132	H-1->LUMO (11%), HOMO->LUMO (41%), HOMO->L+1 (23%)	45-->3 (-42)	0-->0 (0)	5-->7 (2)	12-->3 (-9)	0-->1 (1)	3-->22 (19)	11-->11 (0)	23-->54 (31)
5	375.4253	H-1->L+2 (46%), HOMO->L+2 (24%)	49-->4 (-45)	0-->1 (1)	7-->44 (37)	8-->18 (10)	0-->0 (0)	3-->15 (12)	8-->6 (-2)	25-->11 (-14)

Table S18: TD-DFT calculations showing the energy and composition of excited states T_1-T_5 for complex **3**. Calculations were conducted at the optimised S_0 geometry. Electron density transfer to/from key groups is shown (%).

No.	wavelength (nm)	major contributions	Ir	mesityl1	pyridine1	phenyl1	mesityl2	pyridine2	phenyl2	picolinate
1	423.5011	HOMO->LUMO (41%), HOMO->L+1 (13%)	39-->3 (-36)	0-->1 (1)	5-->20 (15)	20-->10 (-10)	0-->1 (1)	4-->23 (19)	19-->12 (-7)	13-->31 (18)
2	418.0464	HOMO->L+2 (33%)	40-->4 (-36)	2-->1 (-1)	5-->35 (30)	18-->18 (0)	0-->0 (0)	4-->16 (12)	16-->8 (-8)	15-->18 (3)
3	403.8047	H-1->LUMO (25%), H-1->L+1 (52%)	52-->4 (-48)	0-->0 (0)	8-->7 (-1)	2-->4 (2)	0-->1 (1)	2-->23 (21)	3-->13 (10)	33-->49 (16)
4	389.4587	H-1->LUMO (17%), H-1->L+2 (34%), HOMO->L+2 (31%)	48-->4 (-44)	0-->1 (1)	6-->40 (34)	11-->19 (8)	0-->0 (0)	2-->16 (14)	11-->8 (-3)	22-->13 (-9)
5	385.6549	HOMO->LUMO (23%), HOMO->L+1 (56%)	42-->4 (-38)	0-->0 (0)	4-->7 (3)	21-->4 (-17)	0-->1 (1)	3-->23 (20)	20-->12 (-8)	10-->49 (39)

Table S19: TD-DFT calculations showing the energy and composition of excited states T_1-T_5 for complex **4**, geometry 1. Calculations were conducted at the optimised S_0 geometry. Electron density transfer to/from key groups is shown (%).

No.	wavelength (nm)	major contributions	Ir	carbazole1	pyridine1	phenyl1	carbazole2	pyridine2	phenyl2	picolinate
1	442.1533	H-3->L+2 (28%), H-2->LUMO (12%), H-2->L+1 (12%)	32-->4 (-28)	29-->3 (-26)	8-->30 (22)	11-->9 (-2)	1-->2 (1)	2-->19 (17)	9-->7 (-2)	8-->26 (18)
2	437.2106	H-4->L+1 (10%), H-3->L+2 (19%), H-2->L+1 (18%), H-2->L+2 (10%)	32-->4 (-28)	14-->2 (-12)	5-->23 (18)	11-->7 (-4)	16-->2 (-14)	5-->24 (19)	13-->9 (-4)	6-->28 (22)
3	419.2621	H-5->LUMO (17%), H-5->L+1 (11%), H-3->LUMO (24%), H-3->L+1 (21%)	29-->3 (-26)	40-->1 (-39)	9-->13 (4)	5-->5 (0)	1-->2 (1)	1-->23 (22)	4-->9 (5)	12-->44 (32)
4	417.399	H-3->LUMO (10%), H-2->LUMO (20%), H-2->L+2 (46%)	39-->3 (-36)	14-->4 (-10)	5-->36 (31)	16-->11 (-5)	1-->1 (0)	2-->14 (12)	15-->5 (-10)	8-->25 (17)
5	413.0466	H-2->LUMO (44%), H-2->L+1 (41%)	43-->3 (-40)	4-->1 (-3)	3-->10 (7)	20-->4 (-16)	1-->2 (1)	3-->25 (22)	19-->9 (-10)	7-->45 (38)

Table S20: TD-DFT calculations showing the energy and composition of excited states T_1-T_5 for complex **4**, geometry 2. Calculations were conducted at the optimised S_0 geometry. Electron density transfer to/from key groups is shown (%).

No.	Wavelength (nm)	Major contributions	Ir	carbazole1	pyridine1	phenyl1	carbazole2	pyridine2	phenyl2	picolinate
1	442.106	H-3->L+2 (34%), H-2->LUMO (12%), H-2->L+1 (10%)	31-->4 (-27)	28-->4 (-24)	8-->35 (27)	10-->11 (1)	4-->2 (-2)	2-->17 (15)	8-->6 (-2)	9-->22 (13)
2	437.2723	H-4->L+1 (11%), H-3->L+2 (10%), H-2->L+1 (22%)	32-->4 (-28)	8-->2 (-6)	4-->20 (16)	12-->6 (-6)	19-->3 (-16)	6-->26 (20)	14-->9 (-5)	6-->30 (24)
3	419.7163	H-5->LUMO (16%), H-5->L+1 (10%), H-3->LUMO (24%), H-3->L+1 (21%)	29-->3 (-26)	39-->1 (-38)	8-->13 (5)	5-->5 (0)	2-->2 (0)	1-->24 (23)	4-->9 (5)	12-->43 (31)
4	417.399	H-3->LUMO (11%), H-3->L+2 (11%), H-2->LUMO (14%), H-2->L+2 (49%)	39-->3 (-36)	16-->4 (-12)	5-->40 (35)	15-->13 (-2)	1-->1 (0)	2-->12 (10)	14-->4 (-10)	8-->22 (14)
5	412.8953	H-2->LUMO (42%), H-2->L+1 (43%)	44-->3 (-41)	3-->1 (-2)	3-->9 (6)	20-->3 (-17)	1-->3 (2)	3-->27 (24)	19-->10 (-9)	7-->45 (38)

Table S21: TD-DFT calculations showing the energy and composition of excited states T_1-T_5 for complex **4**, geometry 3. Calculations were conducted at the optimised S_0 geometry. Electron density transfer to/from key groups is shown (%).

No.	wavelength (nm)	major contributions	Ir	carbazole1	pyridine1	phenyl1	carbazole2	pyridine2	phenyl2	picolinate
1	441.8066	H-3->L+2 (31%), H-2->LUMO (13%), H-2->L+1 (11%)	31-->4 (-27)	28-->4 (-24)	8-->34 (26)	11-->11 (0)	3-->2 (-1)	2-->16 (14)	9-->6 (-3)	8-->24 (16)
2	437.3032	H-4->L+1 (11%), H-3->L+2 (15%), H-2->L+1 (25%)	32-->4 (-28)	11-->2 (-9)	4-->19 (15)	12-->6 (-6)	15-->3 (-12)	5-->28 (23)	14-->10 (-4)	6-->28 (22)
3	418.8797	H-5->LUMO (15%), H-3->LUMO (20%), H-3->L+1 (18%)	30-->3 (-27)	39-->2 (-37)	8-->17 (9)	6-->6 (0)	0-->2 (2)	1-->22 (21)	5-->8 (3)	12-->40 (28)
4	416.9919	H-3->LUMO (15%), H-2->LUMO (17%), H-2->L+2 (42%)	38-->3 (-35)	18-->4 (-14)	5-->36 (31)	14-->11 (-3)	0-->1 (1)	2-->11 (9)	14-->4 (-10)	8-->30 (22)
5	412.8265	H-2->LUMO (40%), H-2->L+1 (37%), H-2->L+2 (13%)	44-->3 (-41)	3-->1 (-2)	3-->13 (10)	20-->4 (-16)	1-->3 (2)	3-->25 (22)	19-->9 (-10)	7-->41 (34)

Table S22: TD-DFT calculations showing the energy and composition of excited states T_1-T_5 for complex **4**, geometry 4. Calculations were conducted at the optimised S_0 geometry. Electron density transfer to/from key groups is shown (%).

No.	wavelength (nm)	major contributions	Ir	carbazole1	pyridine1	phenyl1	carbazole2	pyridine2	phenyl2	picolinate
1	441.7437	H-3->L+2 (36%)	30-->4 (-26)	5-->2 (-3)	2-->18 (16)	8-->6 (-2)	29-->4 (-25)	8-->35 (27)	9-->11 (2)	9-->20 (11)
2	436.9025	H-4->L+1 (11%), H-2->L+1 (23%)	32-->4 (-28)	20-->3 (-17)	6-->26 (20)	14-->10 (-4)	7-->2 (-5)	3-->19 (16)	12-->6 (-6)	5-->30 (25)
3	420.2427	H-5->LUMO (18%), H-5->L+1 (10%), H-3->LUMO (30%), H-3->L+1 (20%)	28-->3 (-25)	2-->2 (0)	1-->23 (22)	3-->8 (5)	40-->1 (-39)	9-->11 (2)	4-->4 (0)	12-->48 (36)
4	417.4552	H-3->L+2 (11%), H-2->LUMO (18%), H-2->L+2 (53%)	40-->4 (-36)	1-->1 (0)	2-->13 (11)	16-->4 (-12)	12-->4 (-8)	4-->41 (37)	17-->13 (-4)	8-->20 (12)
5	413.0879	H-2->LUMO (49%), H-2->L+1 (35%)	43-->3 (-40)	1-->2 (1)	3-->24 (21)	19-->9 (-10)	3-->1 (-2)	3-->10 (7)	20-->4 (-16)	7-->47 (40)

Table S23: TD-DFT calculations showing the energy and composition of excited states T_1-T_5 for complex **5**, geometry 1. Calculations were conducted at the optimised S_0 geometry. Electron density transfer to/from key groups is shown (%).

No.	wavelength (nm)	major contributions	Ir	carbazole1	pyridine1	phenyl1	carbazole2	pyridine2	phenyl2	picolinate
1	436.6102	H-2->LUMO (19%), H-2->L+2 (47%)	18-->4 (-14)	55-->4 (-51)	10-->39 (29)	4-->14 (10)	3-->1 (-2)	1-->13 (12)	2-->5 (3)	7-->19 (12)
2	430.2019	H-1->LUMO (62%), H-1->L+1 (22%)	0-->3 (3)	0-->1 (1)	0-->13 (13)	0-->6 (6)	100-->8 (-92)	0-->28 (28)	0-->12 (12)	0-->30 (30)
3	429.1595	H-3->LUMO (35%), H-3->L+1 (20%)	16-->3 (-13)	3-->1 (-2)	1-->12 (11)	2-->5 (3)	61-->3 (-58)	10-->28 (18)	4-->12 (8)	3-->35 (32)
4	427.4285	HOMO->LUMO (34%), HOMO->L+2 (52%)	0-->3 (3)	100-->10 (-90)	0-->31 (31)	0-->12 (12)	0-->1 (1)	0-->16 (16)	0-->7 (7)	0-->19 (19)
5	409.7703	H-5->LUMO (10%), H-5->L+1 (27%), H-2->L+1 (21%)	28-->4 (-24)	38-->1 (-37)	7-->12 (5)	3-->5 (2)	2-->2 (0)	1-->23 (22)	3-->10 (7)	18-->43 (25)

Table S24: TD-DFT calculations showing the energy and composition of excited states T_1-T_5 for complex **5**, geometry 2. Calculations were conducted at the optimised S_0 geometry. Electron density transfer to/from key groups is shown (%).

No.	wavelength (nm)	major contributions	Ir	carbazole1	pyridine1	phenyl1	carbazole2	pyridine2	phenyl2	picolinate
1	436.6102	H-2->LUMO (17%), H-2->L+2 (43%)	17-->4 (-13)	58-->3 (-55)	10-->31 (21)	3-->12 (9)	1-->1 (0)	1-->12 (11)	2-->5 (3)	7-->32 (25)
2	429.8738	H-1->LUMO (57%), H-1->L+1 (25%)	0-->3 (3)	0-->1 (1)	0-->12 (12)	0-->5 (5)	99-->8 (-91)	0-->30 (30)	0-->13 (13)	0-->27 (27)
3	428.9368	H-3->LUMO (32%), H-3->L+1 (22%)	15-->3 (-12)	1-->1 (0)	1-->12 (11)	2-->5 (3)	65-->3 (-62)	9-->31 (22)	4-->14 (10)	2-->31 (29)
4	427.1929	HOMO->LUMO (31%), HOMO->L+1 (11%), HOMO->L+2 (47%)	0-->3 (3)	100-->10 (-90)	0-->26 (26)	0-->10 (10)	0-->1 (1)	0-->15 (15)	0-->6 (6)	0-->29 (29)
5	410.1634	H-5->LUMO (10%), H-5->L+1 (19%), H-5->L+2 (15%), H-2->L+1 (16%), H-2->L+2 (12%)	27-->4 (-23)	41-->2 (-39)	8-->21 (13)	3-->8 (5)	1-->2 (1)	1-->21 (20)	3-->9 (6)	18-->35 (17)

Table S25: TD-DFT calculations showing the energy and composition of excited states T_1-T_5 for complex **5**, geometry 3. Calculations were conducted at the optimised S_0 geometry. Electron density transfer to/from key groups is shown (%).

No.	wavelength (nm)	major contributions	Ir	carbazole1	pyridine1	phenyl1	carbazole2	pyridine2	phenyl2	picolinate
1	436.3643	H-2->LUMO (18%), H-2->L+1 (10%), H-2->L+2 (40%)	17-->4 (-13)	60-->3 (-57)	10-->29 (19)	3-->11 (8)	0-->1 (1)	1-->13 (12)	2-->6 (4)	7-->34 (27)
2	429.6205	H-1->LUMO (62%), H-1->L+1 (27%)	0-->3 (3)	0-->1 (1)	0-->13 (13)	0-->6 (6)	100-->9 (-91)	0-->30 (30)	0-->13 (13)	0-->25 (25)
3	428.6995	H-3->LUMO (37%), H-3->L+1 (25%)	16-->3 (-13)	1-->1 (0)	1-->13 (12)	2-->6 (4)	63-->3 (-60)	10-->32 (22)	4-->14 (10)	2-->29 (27)
4	427.812	HOMO->LUMO (32%), HOMO->L+1 (15%), HOMO->L+2 (42%)	0-->3 (3)	100-->9 (-91)	0-->24 (24)	0-->9 (9)	0-->2 (2)	0-->16 (16)	0-->7 (7)	0-->30 (30)
5	409.432	H-5->L+1 (18%), H-5->L+2 (17%), H-2->L+1 (14%), H-2->L+2 (14%)	28-->4 (-24)	40-->2 (-38)	7-->22 (15)	3-->8 (5)	0-->2 (2)	1-->19 (18)	3-->8 (5)	18-->35 (17)

Table S26: TD-DFT calculations showing the energy and composition of excited states T_1-T_5 for complex **5**, geometry 4. Calculations were conducted at the optimised S_0 geometry. Electron density transfer to/from key groups is shown (%).

No.	wavelength (nm)	major contributions	Ir	carbazole1	pyridine1	phenyl1	carbazole2	pyridine2	phenyl2	picolinate
1	436.7178	H-2->LUMO (17%), H-2->L+2 (48%)	18-->4 (-14)	55-->4 (-51)	10-->36 (26)	4-->14 (10)	3-->1 (-2)	1-->10 (9)	2-->4 (2)	8-->27 (19)
2	428.9814	H-3->LUMO (17%), H-3->L+1 (13%), H-1->LUMO (26%), H-1->L+1 (13%)	9-->3 (-6)	1-->1 (0)	1-->10 (9)	1-->4 (3)	78-->6 (-72)	5-->30 (25)	2-->13 (11)	1-->34 (33)
3	428.3737	H-3->LUMO (14%), H-3->L+1 (11%), H-1->LUMO (32%), H-1->L+1 (15%)	6-->3 (-3)	1-->1 (0)	0-->10 (10)	1-->4 (3)	85-->7 (-78)	4-->29 (25)	2-->13 (11)	1-->33 (32)
4	426.7518	HOMO->LUMO (30%), HOMO->L+2 (52%)	0-->3 (3)	100-->11 (-89)	0-->30 (30)	0-->11 (11)	0-->1 (1)	0-->13 (13)	0-->6 (6)	0-->26 (26)
5	410.9519	H-5->LUMO (12%), H-5->L+1 (20%), H-5->L+2 (10%), H-2->LUMO (12%), H-2->L+1 (19%), H-2->L+2 (10%)	26-->4 (-22)	42-->2 (-40)	8-->17 (9)	2-->7 (5)	2-->2 (0)	1-->23 (22)	2-->10 (8)	17-->35 (18)

Table S27: TD-DFT calculations showing the energy and composition of excited states T_1-T_5 for complex **6**, geometry 1. Calculations were conducted at the optimised S_0 geometry. Electron density transfer to/from key groups is shown (%).

No.	wavelength (nm)	major contributions	Ir	carbazole1	pyridine1	phenyl1	carbazole2	pyridine2	phenyl2	picolinate
1	439.8474	H-2->LUMO (17%), H-2->L+1 (21%), H-2->L+2 (18%)	19-->4 (-15)	51-->2 (-49)	8-->21 (13)	5-->9 (4)	6-->2 (-4)	2-->21 (19)	5-->10 (5)	5-->31 (26)
2	438.3855	H-1->LUMO (71%), H-1->L+1 (22%)	0-->3 (3)	0-->2 (2)	0-->17 (17)	0-->8 (8)	100-->6 (-94)	0-->33 (33)	0-->16 (16)	0-->14 (14)
3	435.0017	HOMO->LUMO (37%), HOMO->L+1 (32%), HOMO->L+2 (22%)	0-->3 (3)	100-->6 (-94)	0-->20 (20)	0-->9 (9)	0-->2 (2)	0-->23 (23)	0-->11 (11)	0-->27 (27)
4	434.3769	H-4->LUMO (15%), H-3->LUMO (32%), H-3->L+1 (14%)	18-->3 (-15)	5-->2 (-3)	2-->19 (17)	7-->9 (2)	50-->3 (-47)	7-->33 (26)	7-->16 (9)	3-->15 (12)
5	413.4598	H-4->LUMO (43%), H-3->LUMO (16%), H-2->LUMO (13%)	28-->3 (-25)	11-->1 (-10)	4-->16 (12)	12-->9 (-3)	23-->3 (-20)	5-->34 (29)	12-->19 (7)	5-->15 (10)

Table S28: TD-DFT calculations showing the energy and composition of excited states T_1-T_5 for complex **6**, geometry 2. Calculations were conducted at the optimised S_0 geometry. Electron density transfer to/from key groups is shown (%).

No.	wavelength (nm)	major contributions	Ir	carbazole1	pyridine1	phenyl1	carbazole2	pyridine2	phenyl2	picolinate
1	440.2222	H-2->LUMO (17%), H-2->L+1 (30%), H-2->L+2 (14%)	19-->4 (-15)	56-->2 (-54)	9-->24 (15)	4-->10 (6)	1-->2 (1)	1-->23 (22)	4-->10 (6)	6-->25 (19)
2	437.72	H-1->LUMO (69%), H-1->L+1 (23%)	0-->3 (3)	0-->2 (2)	0-->19 (19)	0-->9 (9)	100-->6 (-94)	0-->33 (33)	0-->16 (16)	0-->12 (12)
3	435.0781	HOMO->LUMO (36%), HOMO->L+1 (41%), HOMO->L+2 (15%)	0-->3 (3)	100-->6 (-94)	0-->22 (22)	0-->9 (9)	0-->2 (2)	0-->24 (24)	0-->11 (11)	0-->21 (21)
4	434.0423	H-4->LUMO (18%), H-3->LUMO (28%), H-3->L+1 (15%)	19-->3 (-16)	4-->2 (-2)	2-->20 (18)	7-->9 (2)	49-->3 (-46)	7-->33 (26)	7-->16 (9)	3-->13 (10)
5	413.2669	H-4->LUMO (41%), H-3->LUMO (26%)	27-->3 (-24)	5-->2 (-3)	3-->17 (14)	11-->9 (-2)	32-->3 (-29)	6-->33 (27)	11-->19 (8)	5-->15 (10)

Table S29: TD-DFT calculations showing the energy and composition of excited states T_1-T_5 for complex **6**, geometry 3. Calculations were conducted at the optimised S_0 geometry. Electron density transfer to/from key groups is shown (%).

No.	wavelength (nm)	major contributions	Ir	carbazole1	pyridine1	phenyl1	carbazole2	pyridine2	phenyl2	picolinate
1	438.9909	H-2->LUMO (15%), H-2->L+1 (26%), H-2->L+2 (17%)	20-->4 (-16)	54-->2 (-52)	9-->22 (13)	5-->9 (4)	1-->2 (1)	1-->21 (20)	5-->10 (5)	6-->30 (24)
2	437.2723	H-1->LUMO (72%), H-1->L+1 (20%)	0-->3 (3)	0-->2 (2)	0-->16 (16)	0-->8 (8)	100-->7 (-93)	0-->34 (34)	0-->17 (17)	0-->13 (13)
3	434.2856	H-3->LUMO (13%), HOMO->LUMO (19%), HOMO->L+1 (23%), HOMO->L+2 (11%)	7-->3 (-4)	65-->5 (-60)	1-->20 (19)	3-->9 (6)	18-->2 (-16)	3-->26 (23)	3-->13 (10)	1-->21 (20)
4	434.0879	H-3->LUMO (19%), HOMO->LUMO (13%), HOMO->L+1 (16%)	10-->3 (-7)	49-->2 (-47)	1-->20 (19)	4-->9 (5)	27-->3 (-24)	4-->29 (25)	4-->14 (10)	2-->20 (18)
5	412.9228	H-4->LUMO (41%), H-3->LUMO (23%)	27-->3 (-24)	6-->1 (-5)	3-->15 (12)	11-->8 (-3)	30-->3 (-27)	6-->35 (29)	11-->20 (9)	5-->14 (9)

Table S30: TD-DFT calculations showing the energy and composition of excited states T_1-T_5 for complex **6**, geometry 4. Calculations were conducted at the optimised S_0 geometry. Electron density transfer to/from key groups is shown (%).

No.	wavelength (nm)	major contributions	Ir	carbazole1	pyridine1	phenyl1	carbazole2	pyridine2	phenyl2	picolinate
1	440.1441	H-2->LUMO (17%), H-2->L+1 (27%), H-2->L+2 (16%)	19-->4 (-15)	54-->2 (-52)	9-->22 (13)	4-->9 (5)	2-->2 (0)	1-->22 (21)	4-->10 (6)	6-->28 (22)
2	436.5026	H-1->LUMO (66%), H-1->L+1 (24%)	0-->3 (3)	0-->2 (2)	0-->19 (19)	0-->9 (9)	100-->7 (-93)	0-->31 (31)	0-->15 (15)	0-->14 (14)
3	434.7577	HOMO->LUMO (36%), HOMO->L+1 (38%), HOMO->L+2 (17%)	0-->3 (3)	100-->6 (-94)	0-->21 (21)	0-->9 (9)	0-->2 (2)	0-->23 (23)	0-->11 (11)	0-->24 (24)
4	433.6021	H-4->LUMO (17%), H-3->LUMO (24%), H-3->L+1 (15%)	20-->3 (-17)	8-->2 (-6)	2-->20 (18)	8-->9 (1)	44-->3 (-41)	7-->32 (25)	8-->16 (8)	4-->15 (11)
5	412.6067	H-4->LUMO (39%), H-3->LUMO (27%)	27-->3 (-24)	5-->2 (-3)	3-->17 (14)	11-->9 (-2)	32-->3 (-29)	6-->31 (25)	11-->18 (7)	5-->17 (12)

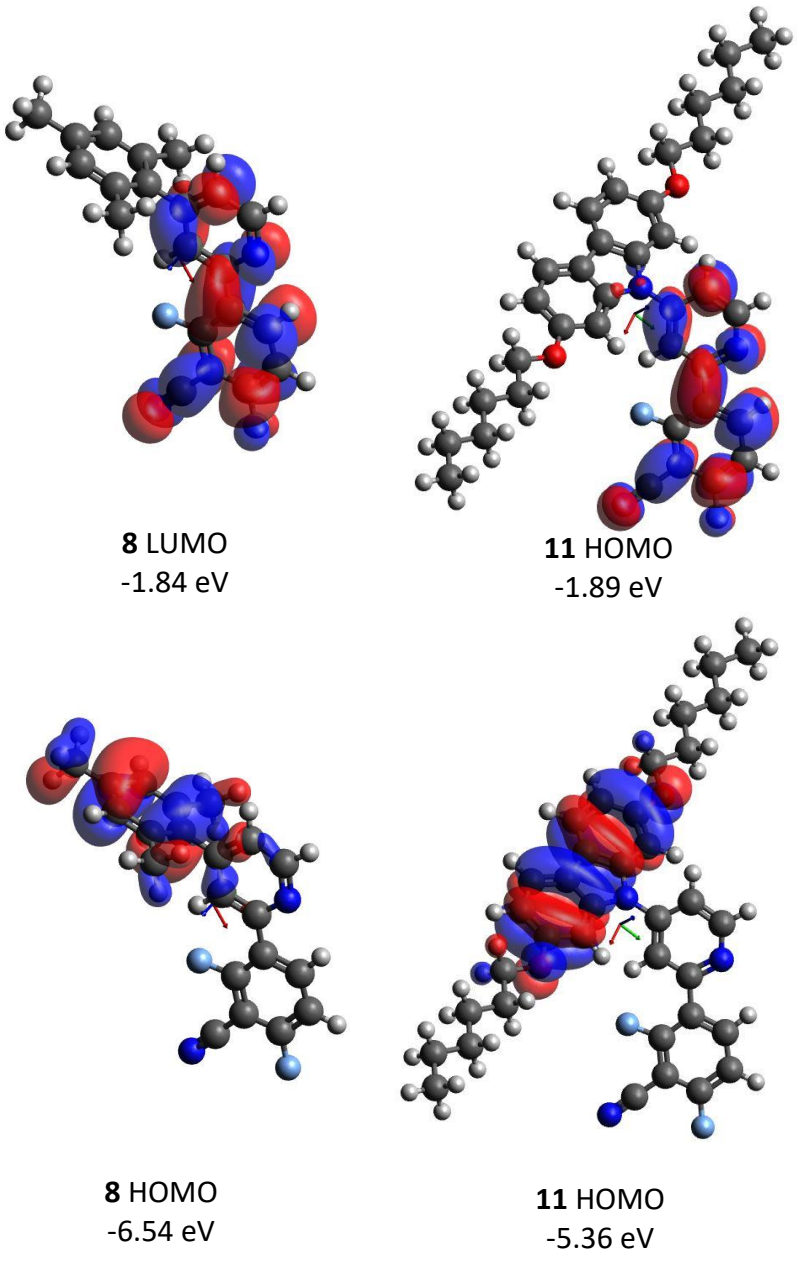

Figure S26: Frontier molecular orbitals for **8** and **11**. Isocontour set to 0.02000.

Table S31: TD-DFT calculations showing the energy and composition of excited states S_1-S_{10} for ligand **9**. Calculations were conducted at the optimised S_0 geometry. Electron density transfer to/from key groups is shown (%).

No.	Wavelength (nm)	Osc. Strength	Major contributions	carbazole	pyridine	phenyl
1	368.0257	0.0009	HOMO->LUMO (99%)	100-->3 (-97)	0-->57 (57)	0-->40 (40)
2	336.4382	0.0958	H-1->LUMO (98%)	89-->3 (-86)	11-->57 (46)	0-->40 (40)
3	315.3049	0.0001	HOMO->L+1 (99%)	100-->9 (-91)	0-->80 (80)	0-->12 (12)
4	294.8354	0.1585	H-1->L+1 (95%)	89-->9 (-80)	11-->80 (69)	0-->12 (12)
5	288.2549	0.6374	HOMO->L+2 (92%)	99-->99 (0)	1-->1 (0)	0-->0 (0)
6	286.1988	0.0014	H-1->L+2 (70%), HOMO->L+4 (24%)	92-->97 (5)	8-->2 (-6)	0-->0 (0)
7	278.0476	0.0026	H-5->LUMO (11%), H-4->LUMO (87%)	26-->3 (-23)	71-->57 (-14)	3-->40 (37)
8	267.7787	0.0031	HOMO->L+3 (99%)	100-->2 (-98)	0-->7 (7)	0-->91 (91)
9	266.5295	0.5571	H-2->LUMO (82%)	3-->4 (1)	36-->58 (22)	61-->38 (-23)
10	262.7674	0.0055	H-3->LUMO (95%)	100-->6 (-94)	0-->55 (55)	0-->39 (39)

Table S32: TD-DFT calculations showing the energy and composition of excited states S_1-S_{10} for ligand **10**. Calculations were conducted at the optimised S_0 geometry. Electron density transfer to/from key groups is shown (%).

No.	Wavelength (nm)	Osc. Strength	major contributions	carbazole	pyridine	phenyl
1	392.0945	0.0007	HOMO->LUMO (99%)	100-->3 (-97)	0-->49 (49)	0-->48 (48)
2	353.4629	0.0754	H-1->LUMO (98%)	89-->3 (-86)	11-->49 (38)	0-->48 (48)
3	325.1277	0.0005	HOMO->L+1 (90%)	100-->4 (-96)	0-->49 (49)	0-->47 (47)
4	301.0933	0.1438	H-1->L+1 (85%), H-1->L+2 (12%)	89-->5 (-84)	11-->48 (37)	0-->47 (47)
5	300.2766	0.0042	HOMO->L+1 (10%), HOMO->L+2 (88%)	100-->7 (-93)	0-->40 (40)	0-->53 (53)
6	288.1544	0.6462	HOMO->L+3 (92%)	99-->99 (0)	1-->1 (0)	0-->0 (0)
7	285.6581	0.0033	H-1->L+3 (69%), HOMO->L+4 (25%)	92-->97 (5)	8-->2 (-6)	0-->1 (1)
8	282.4306	0.0019	H-5->LUMO (39%), H-4->LUMO (58%)	50-->3 (-47)	47-->49 (2)	2-->48 (46)
9	276.9359	0.0687	H-1->L+1 (12%), H-1->L+2 (83%)	87-->6 (-81)	12-->41 (29)	2-->53 (51)
10	274.8181	0.0098	H-2->LUMO (96%)	100-->3 (-97)	0-->49 (49)	0-->48 (48)

Table S33: TD-DFT calculations showing the energy and composition of excited states S_1-S_{10} for ligand **11**. Calculations were conducted at the optimised S_0 geometry. Electron density transfer to/from key groups is shown (%).

No.	Wavelength (nm)	Osc. Strength	Major contributions	carbazole	pyridine	phenyl
1	405.7074	0.0006	HOMO->LUMO (98%)	100-->2 (-98)	0-->30 (30)	0-->68 (68)
2	362.2938	0.0631	H-1->LUMO (96%)	89-->2 (-87)	11-->30 (19)	0-->68 (68)
3	353.4629	0.0002	HOMO->L+1 (98%)	100-->1 (-99)	0-->25 (25)	0-->74 (74)
4	323.0269	0.0008	HOMO->L+2 (99%)	100-->11 (-89)	0-->83 (83)	0-->6 (6)
5	320.9614	0.0013	H-1->L+1 (95%)	89-->1 (-88)	11-->25 (14)	0-->74 (74)
6	298.2612	0.2113	H-1->L+2 (95%)	89-->11 (-78)	11-->83 (72)	0-->6 (6)
7	288.2683	0.6514	HOMO->L+3 (92%)	99-->99 (0)	1-->1 (0)	0-->0 (0)
8	285.5594	0.0004	H-2->LUMO (11%), H-1->L+3 (62%), HOMO->L+4 (22%)	93-->88 (-5)	7-->4 (-3)	0-->8 (8)
9	284.511	0.0009	H-5->LUMO (43%), H-4->LUMO (45%)	50-->2 (-48)	47-->30 (-17)	3-->69 (66)
10	281.3219	0.0057	H-2->LUMO (86%)	99-->13 (-86)	1-->27 (26)	0-->60 (60)

Device Fabrication

Devices were fabricated on glass substrates coated with a 125 nm layer of indium tin oxide (ITO) with a sheet resistance of 15 Ω/□ (VisionTek). Substrates were cleaned thoroughly in acetone and isopropyl alcohol (IPA) before undergoing ozone treatment for 5 min. A ca. 75 nm layer of poly(3,4-ethylenedioxythiophene):poly(styrenesulfonate) (PEDOT:PSS, Heraeus Clevios HIL 1.5) was spin coated at 2500 rpm for 1 min and then annealed at 200 °C for 3 min to remove water. The host material poly(vinylcarbazole) (PVK) was doped with 1,3-bis[(4-*tert*-butylphenyl)-1,3,4-oxadiazolyl]phenylene (OXD-7) and with the emissive iridium complex, blended in the ratio 100:50:8 (PVK:OXD-7:Ir) by weight in chlorobenzene solution at a concentration of 20 mg/mL PVK. The emissive layer was spin coated at 2500 rpm for 1 min and annealed at 120 °C for 10 min resulting in a film thickness of 76 ± 1 nm. TPBi and LiF/Al layers were thermally evaporated using the Kurt J. Lesker Spectros II deposition system operating at 1 x 10^{-6} mbar. Devices were encapsulated using UV curable epoxy (DELO KATIOBOND) and a glass cover slide, exposing to UV light for 3 min. Patterning of the ITO substrate combined with masking of the cathode produced four identical pixels of 5 mm x 4 mm for each device. The resulting structure of each device was ITO / PEDOT:PSS (50 nm) / PVK:OXD-7:Ir (75 nm) TPBi (25 nm)/LiF (1 nm)/Al. Current-voltage data, device efficiency, brightness and electroluminescence spectra were measured in a calibrated Labsphere LMS-100 integrating sphere. A home-written NI LabVIEW programme was used to control an Agilent 6632B DC power supply, and the emission properties of the device were measured using an Ocean Optics USB4000 CCD fibre optic spectrometer. Thicknesses of PVK:OXD-7:Ir layers were measured with a J A Woolam VASE Ellipsometer using thin films which had been spin coated on Si/SiO_2 substrates under the same conditions as the device films.

Thin Film measurements (zeonex)

Films of complex **5** doped in zeonex were fabricated as follows:
1) A solution of 100 mg/ml of zeonex in toluene was made
2) A solution of **5** in toluene was made at a concentration of 1 mg/5 ml.
3) The two solutions were mixed in a 1:1 v/v ratio and the resultant solution was spin-coated onto quartz substrates.

For decay measurements the substrates were mounted in a displex cryostat and evacuated with a turbomolecular pump. Samples were excited with a 450 nm dye laser pumped by a pulsed YAG laser emitting at 355 nm (from EKSPLA) at 45° angle to the substrate plane; the energy of each pulse was ca. 40 μJ per pulse. Emission was focused onto a spectrograph and detected on a sensitive gated iCCD camera (Stanford Computer Optics) with sub nanosecond resolution.

Copies of NMR spectra:

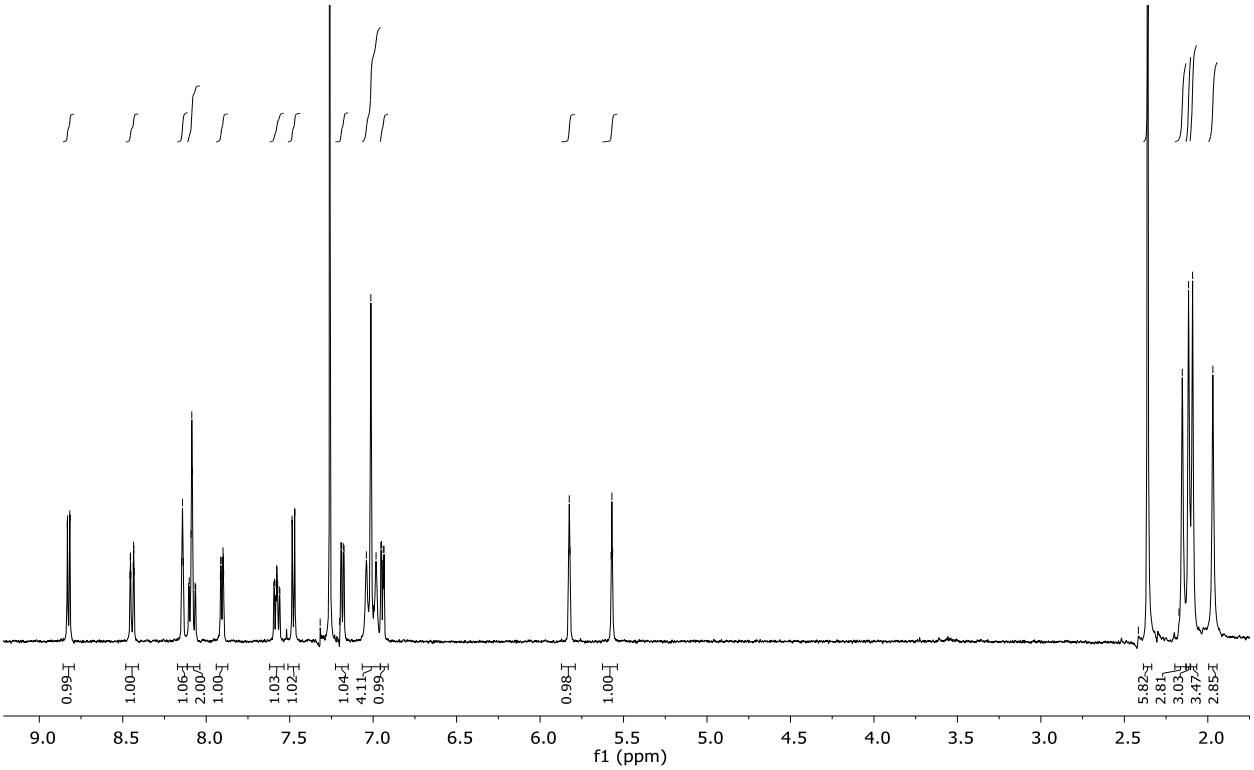

Figure S27: ^{1}H NMR spectrum of **2** in $CDCl_3$.

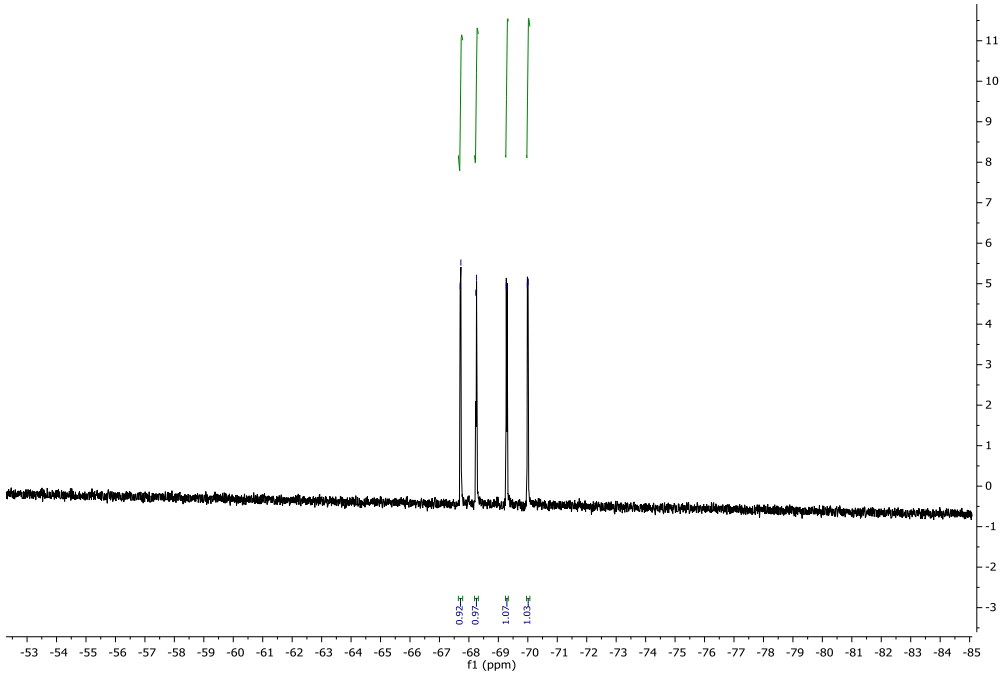

Figure S28: ^{19}F NMR spectrum of **2** in $CDCl_3$.

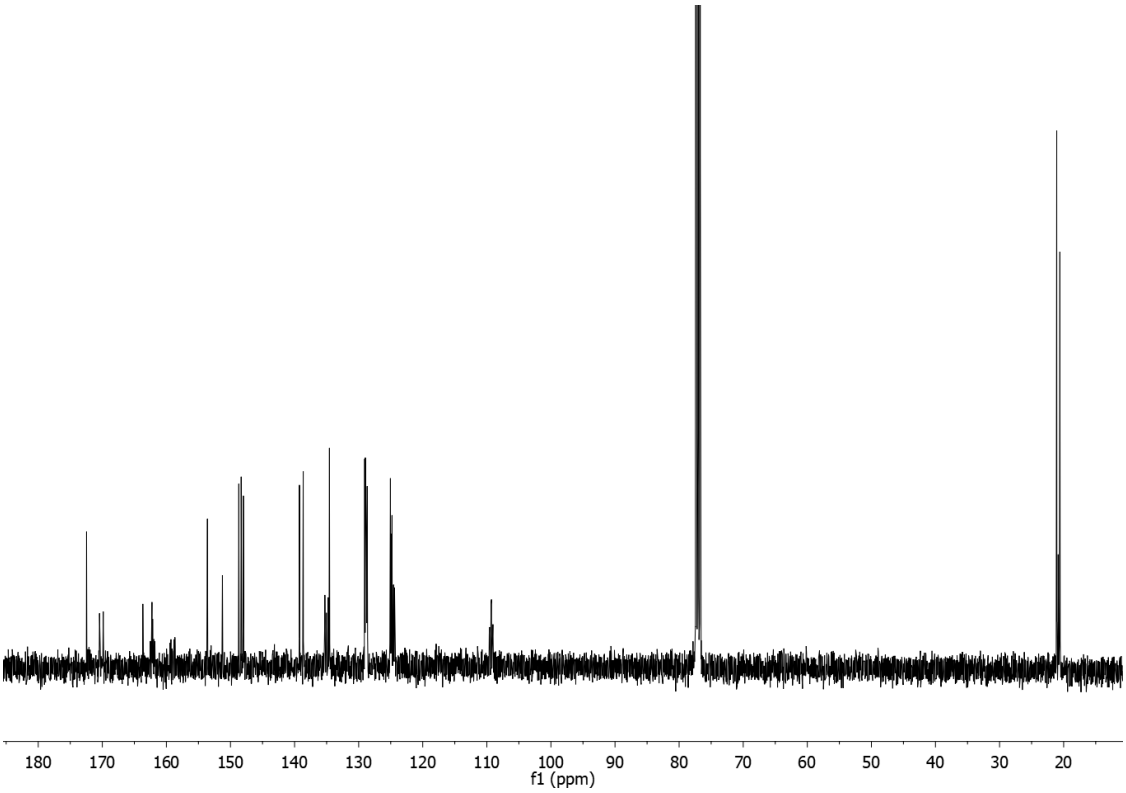

Figure S29: ^{13}C NMR spectrum of **2** in $CDCl_3$.

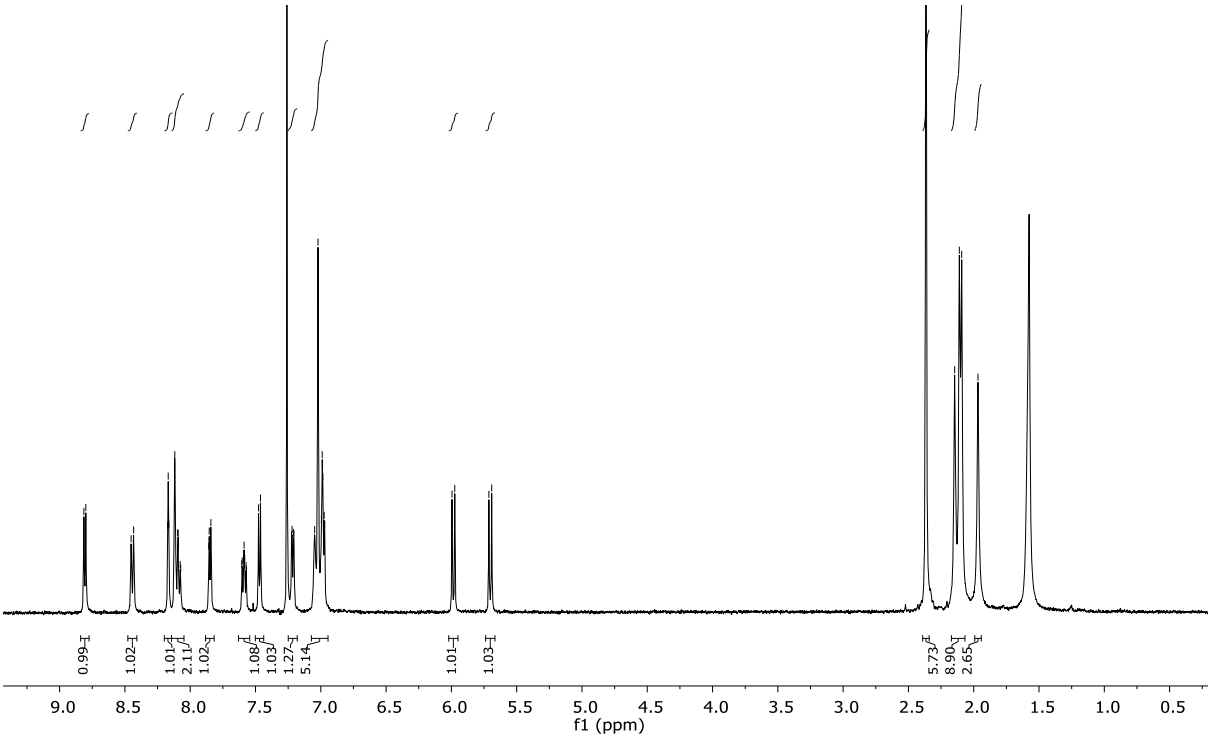

Figure S30: ^{1}H NMR spectrum of **3** in $CDCl_3$.

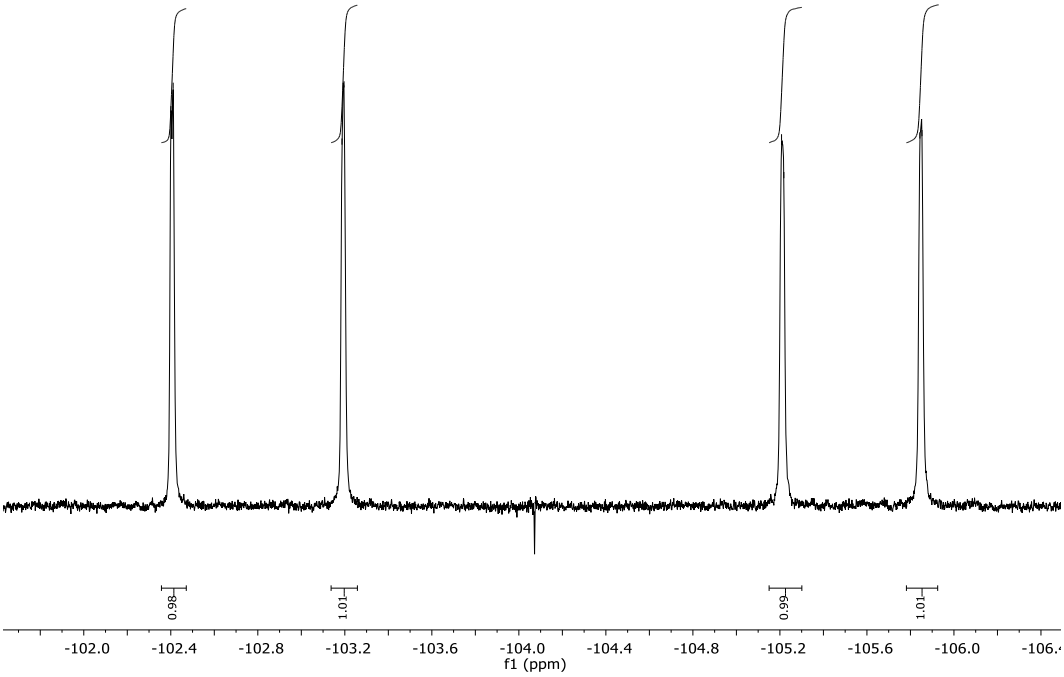

Figure S31: ^{19}F NMR spectrum of **3** in $CDCl_3$.

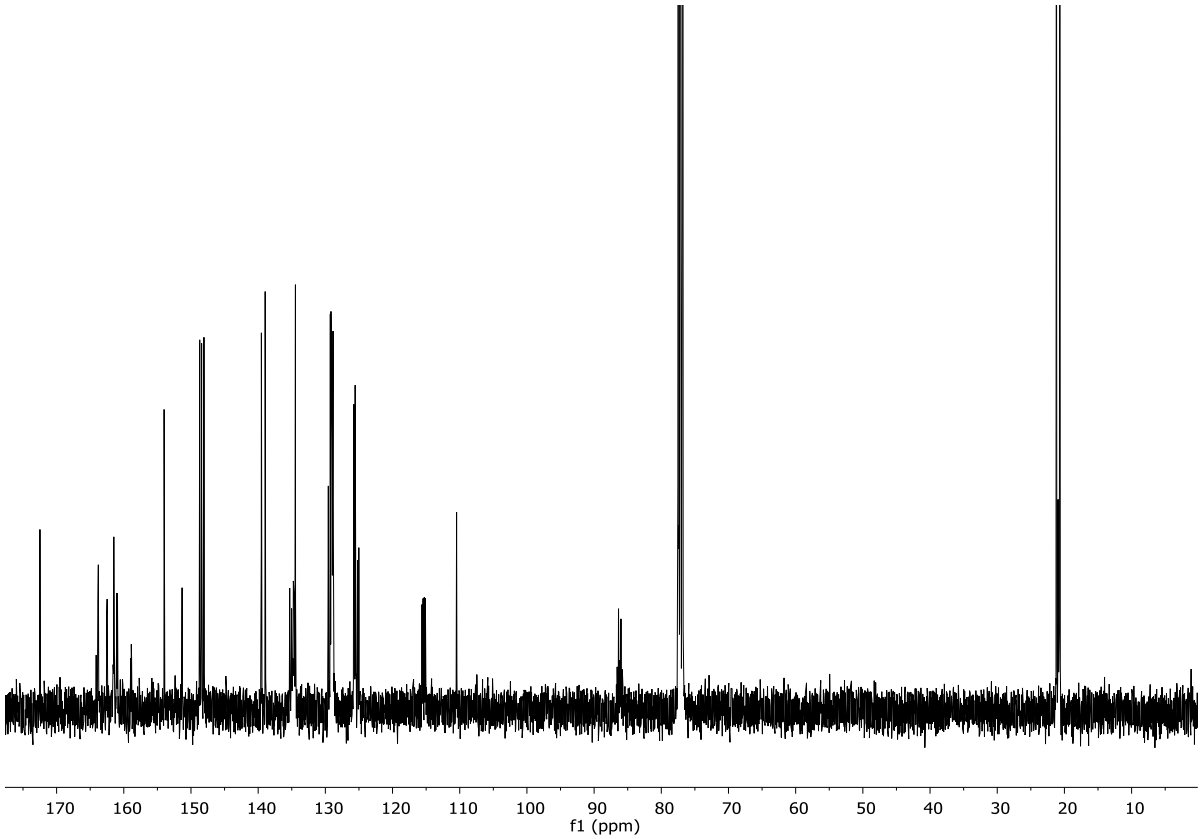

Figure S32: ^{13}C NMR spectrum of **3** in $CDCl_3$.

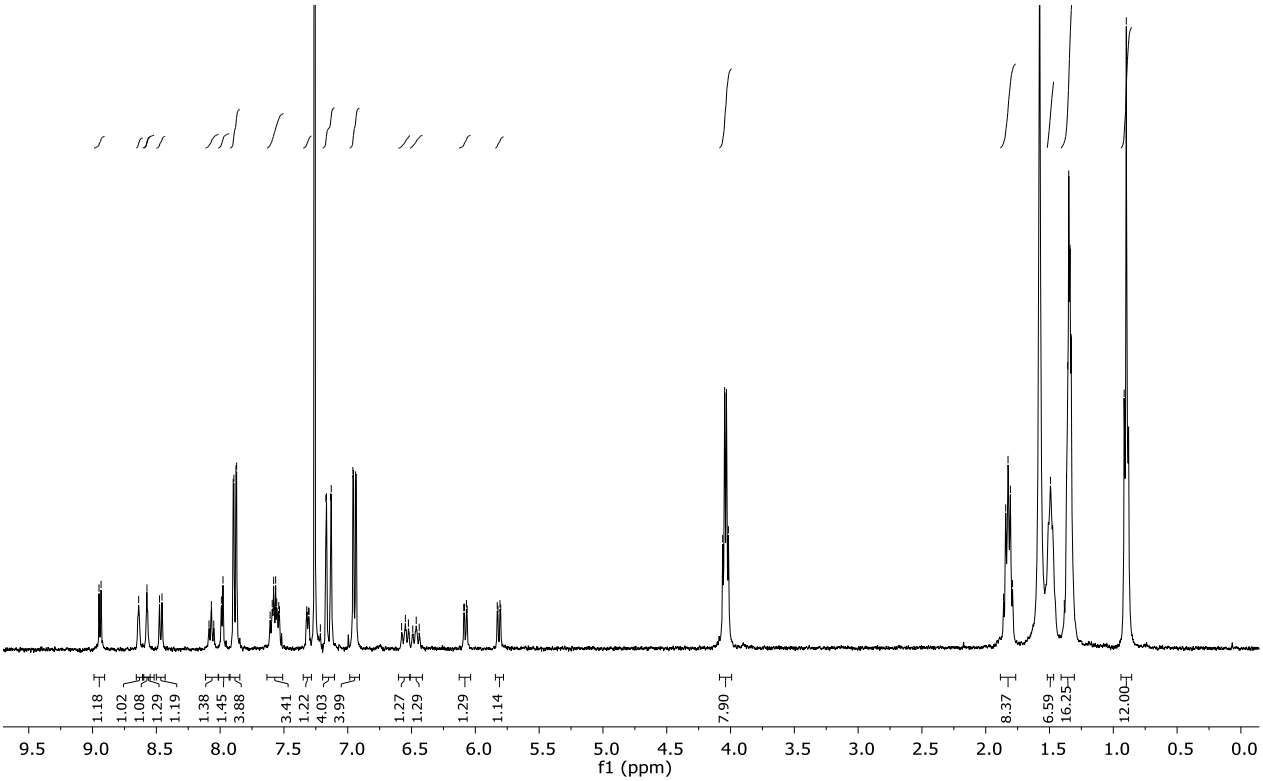

Figure S33: ^{1}H NMR spectrum of **4** in $CDCl_3$.

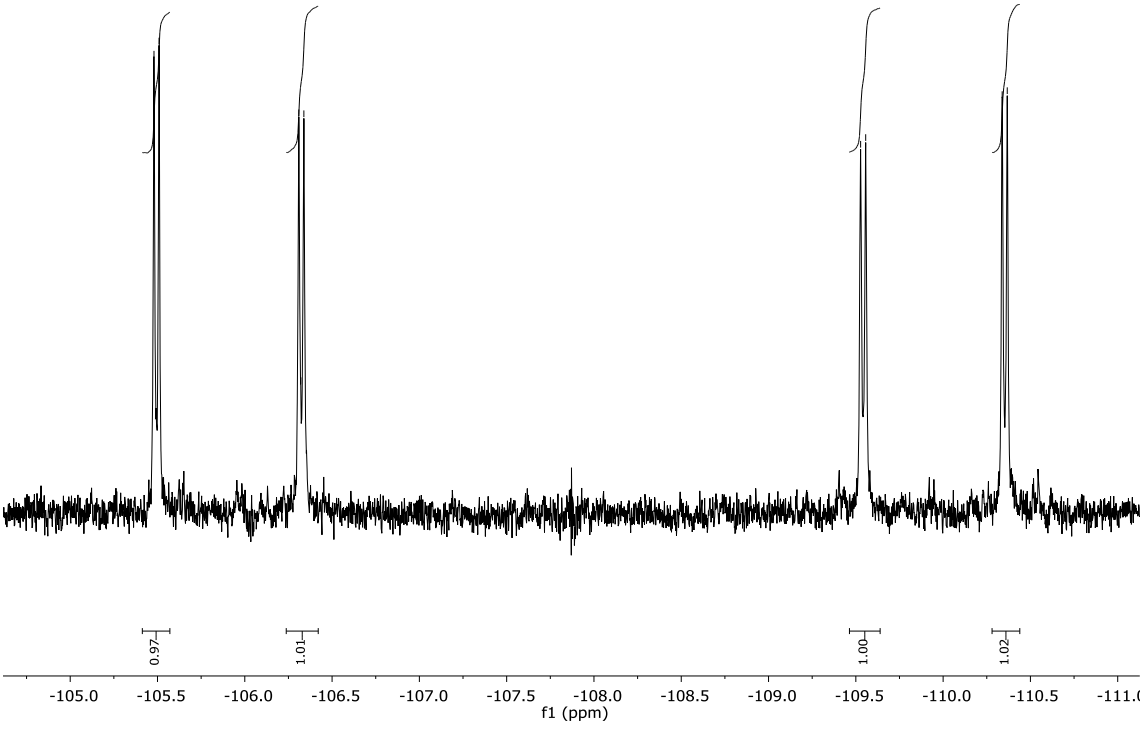

Figure S34 : ^{19}F NMR spectrum of **4** in $CDCl_3$.

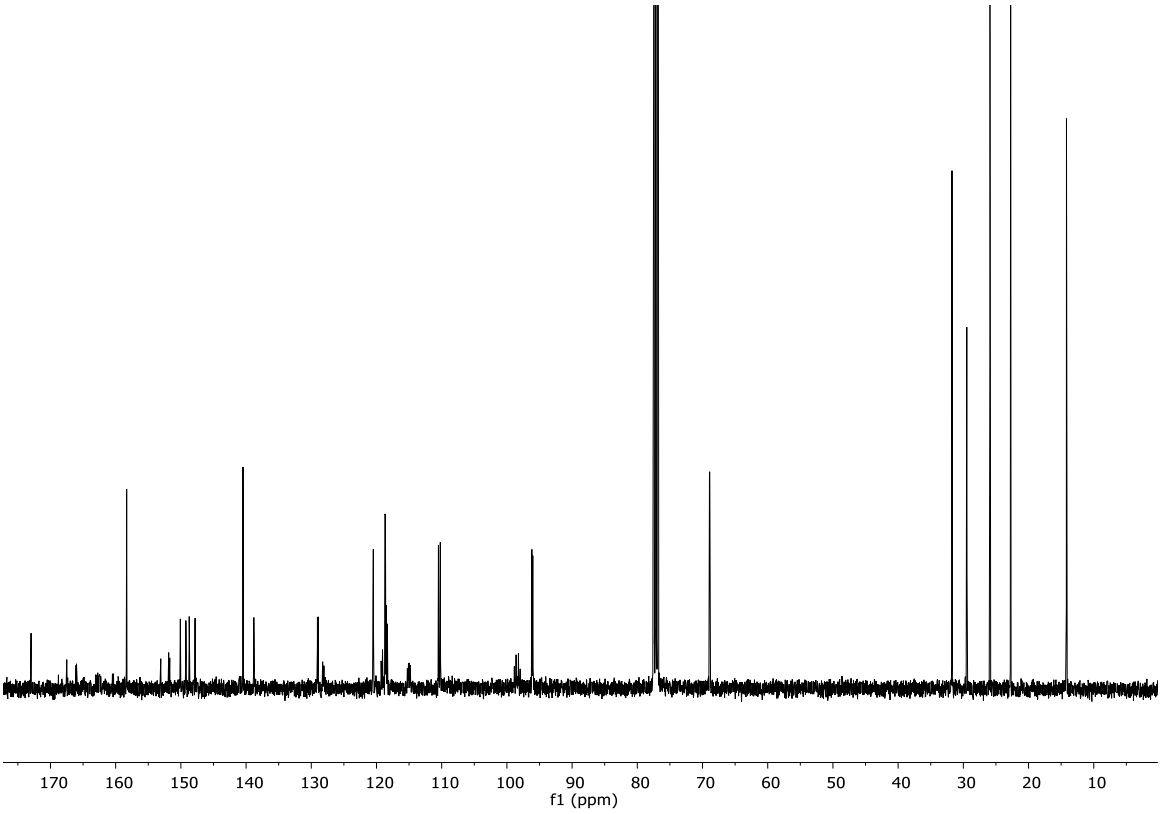

Figure S35: ^{13}C NMR spectrum of **4** in $CDCl_3$.

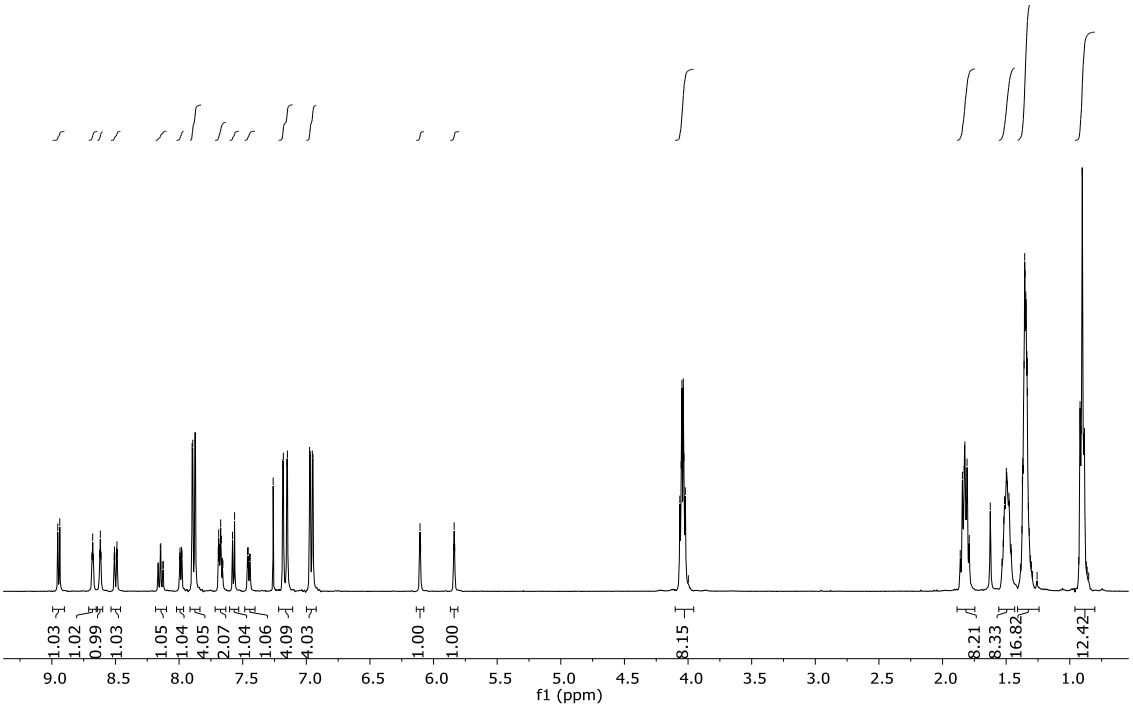

Figure S36: ^{1}H NMR spectrum of **5** in $CDCl_3$.

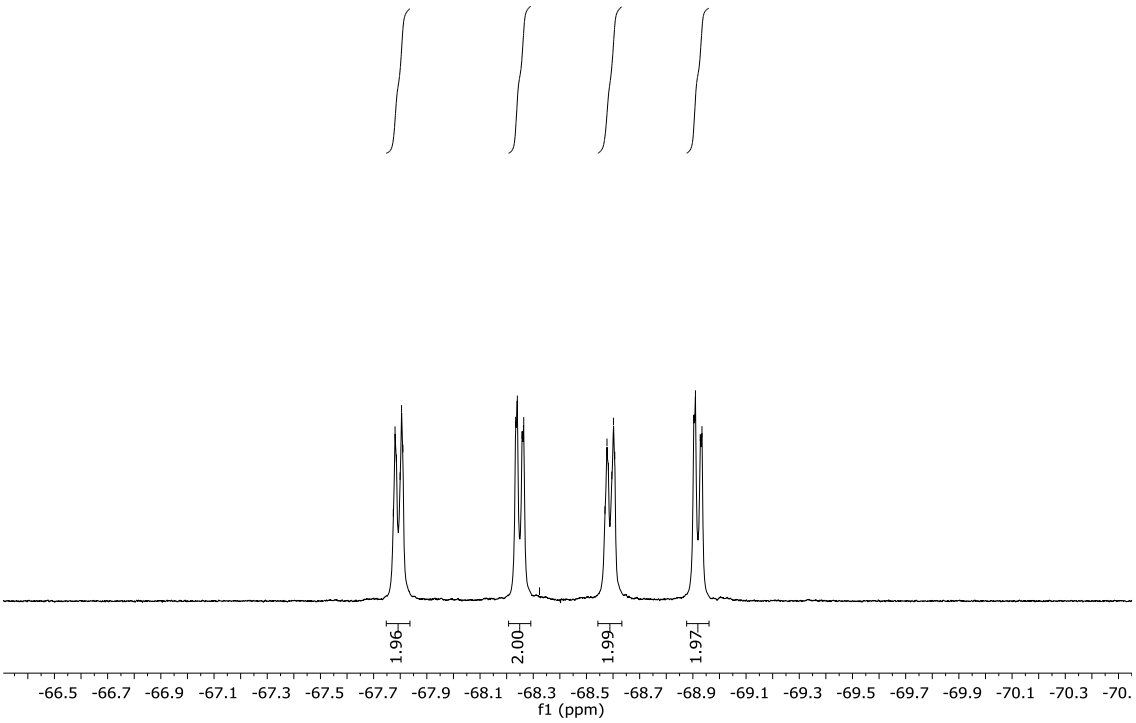

Figure S37: ^{19}F NMR spectrum of **5** in $CDCl_3$.

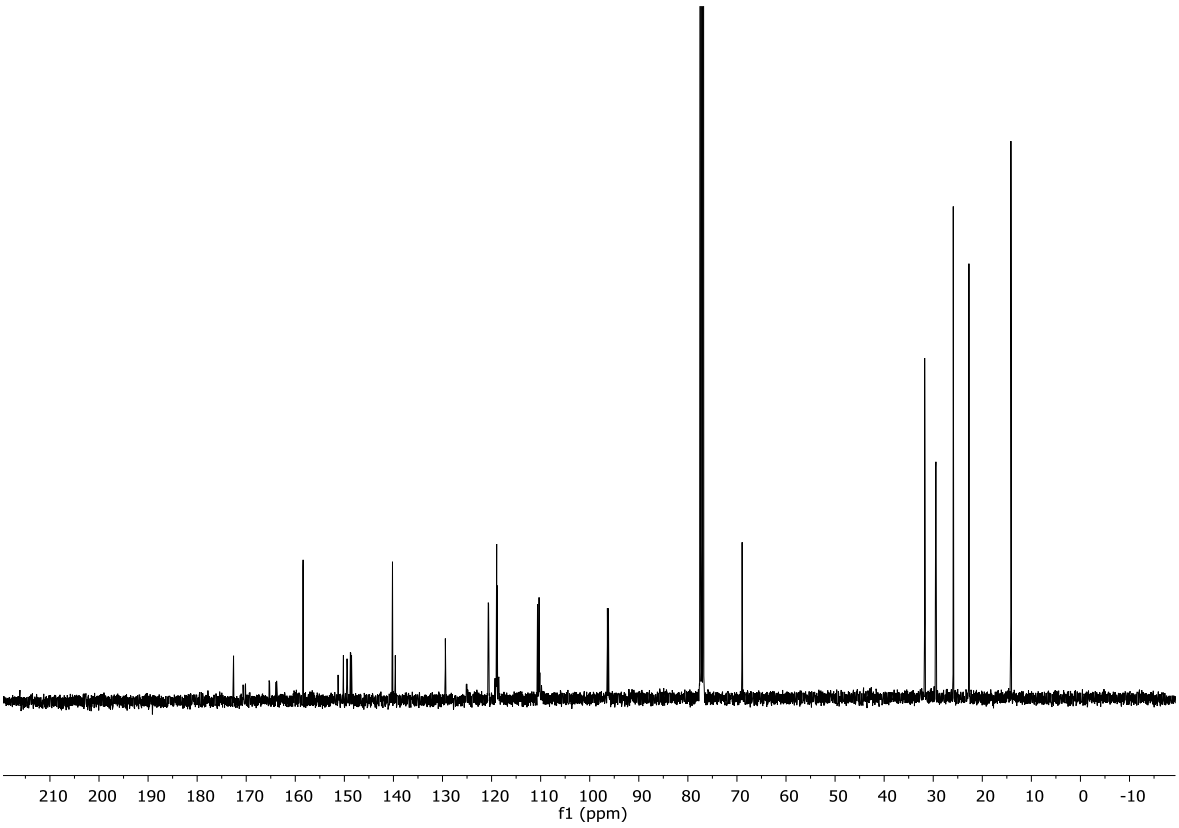

Figure S38: ^{13}C NMR spectrum of **5** in $CDCl_3$.

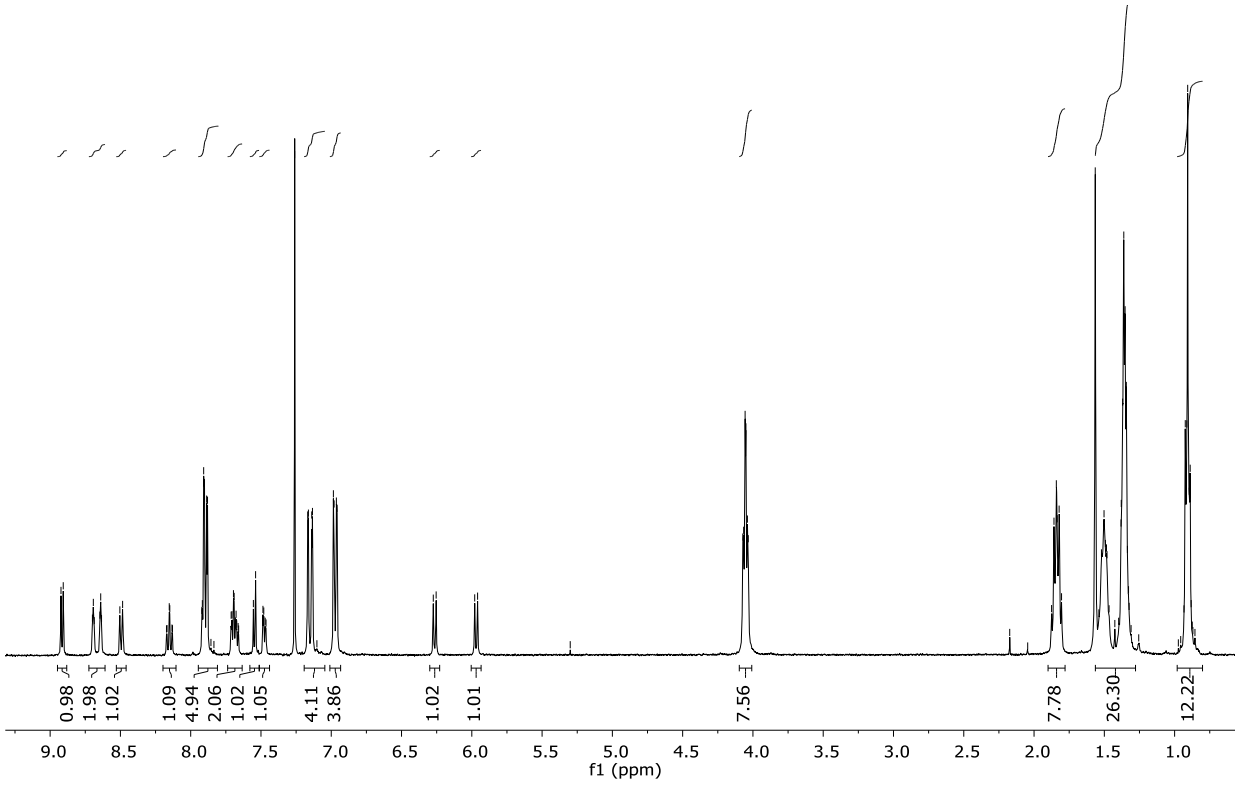

Figure S39: ^{1}H NMR spectrum of **6** in $CDCl_3$.

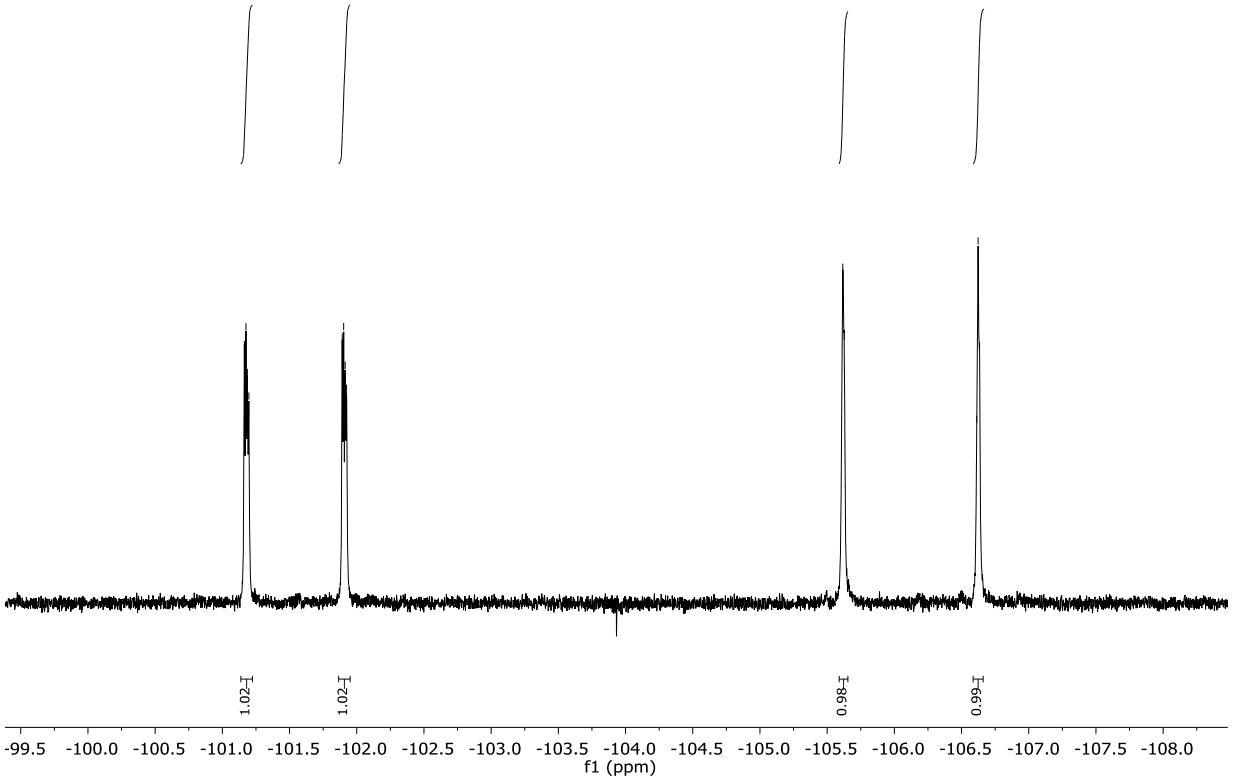

Figure S40: ^{19}F NMR spectrum of **6** in $CDCl_3$.

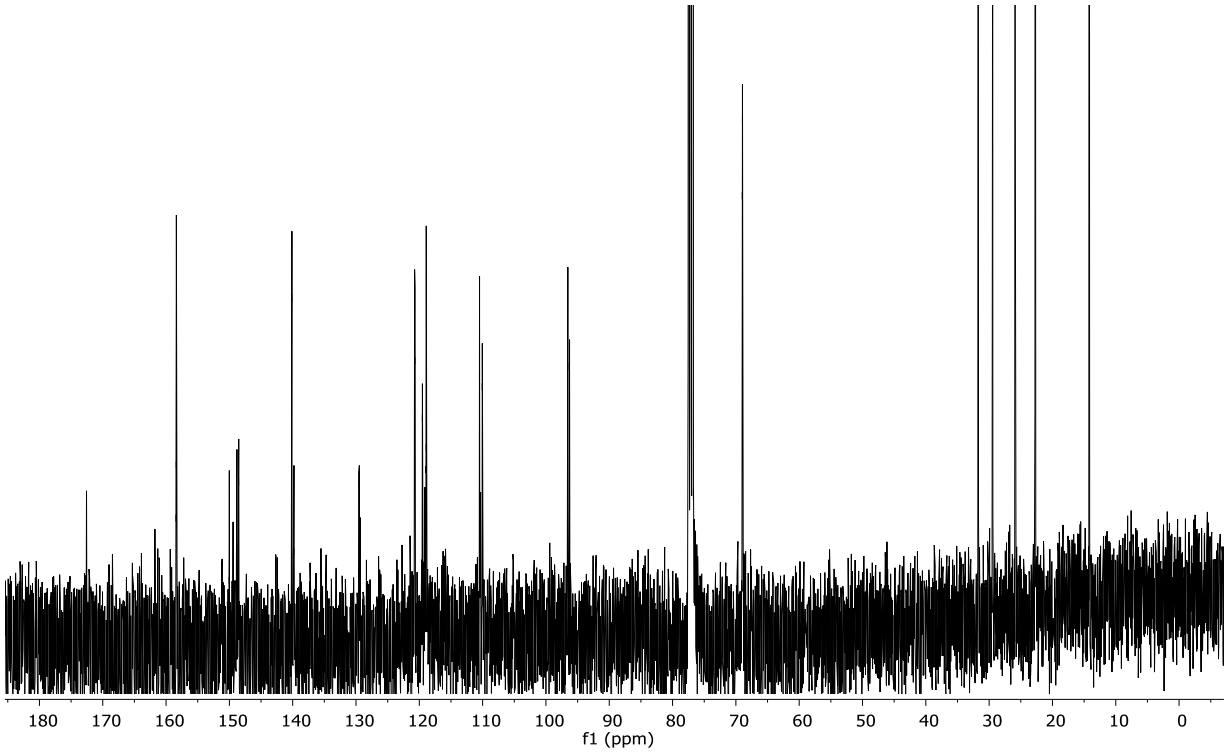

Figure S41: ^{13}C NMR spectrum of **6** in $CDCl_3$.

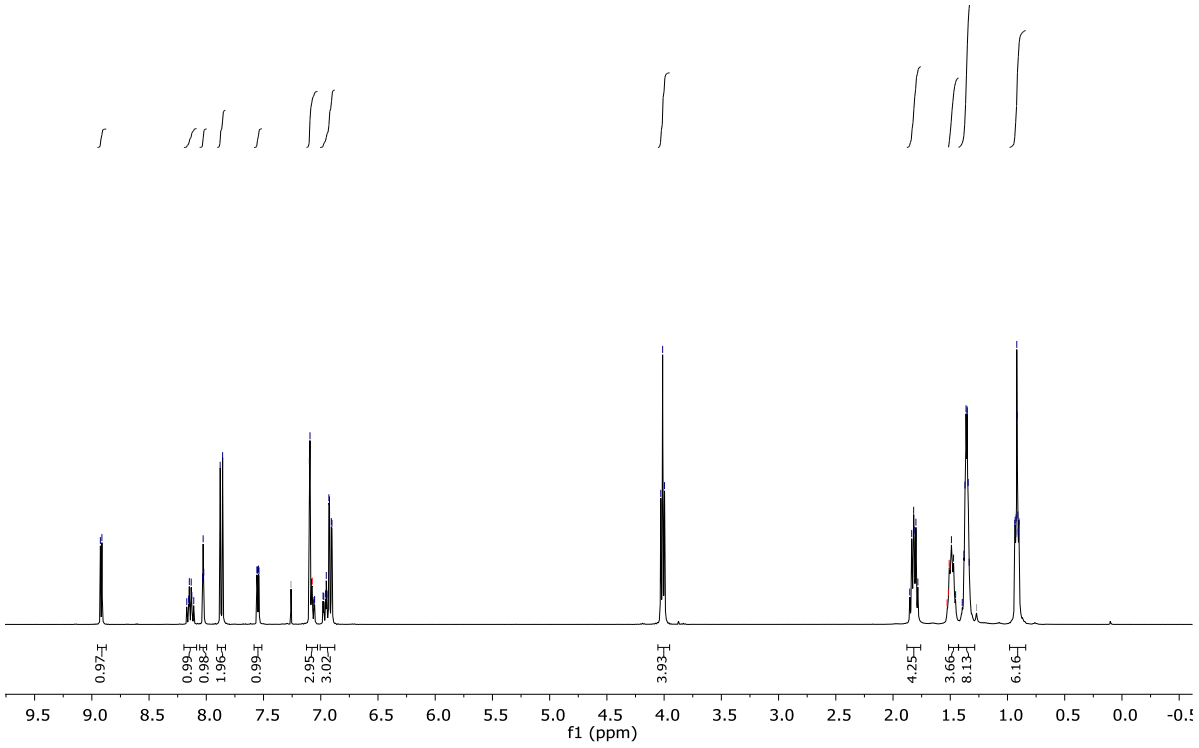

Figure S42: ^{1}H NMR spectrum of **9** in $CDCl_3$.

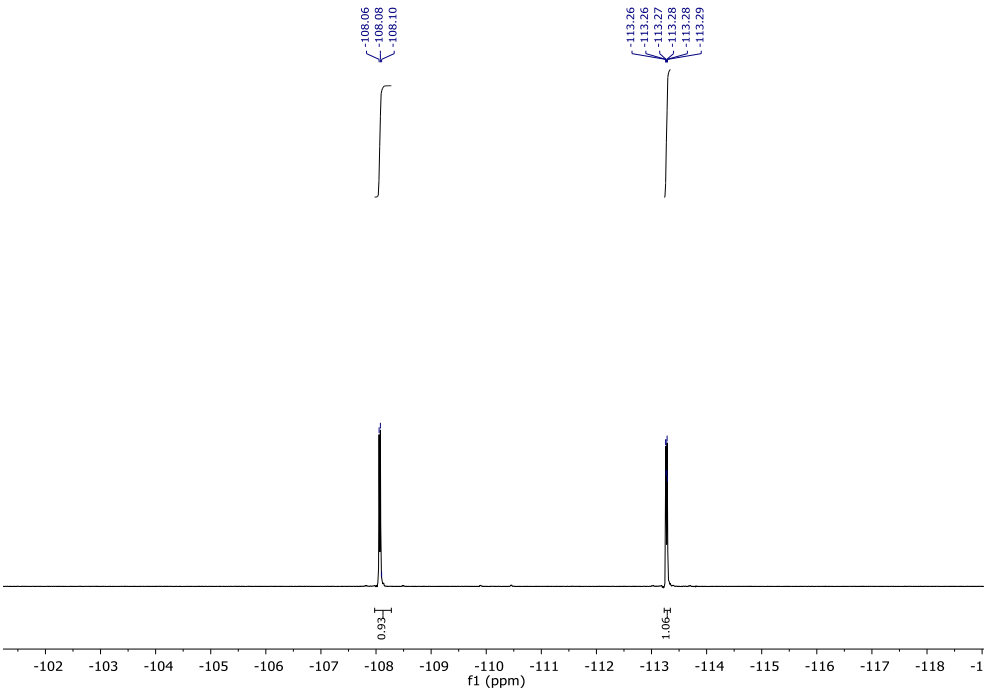

Figure S43: ^{19}F NMR spectrum of **9** in $CDCl_3$.

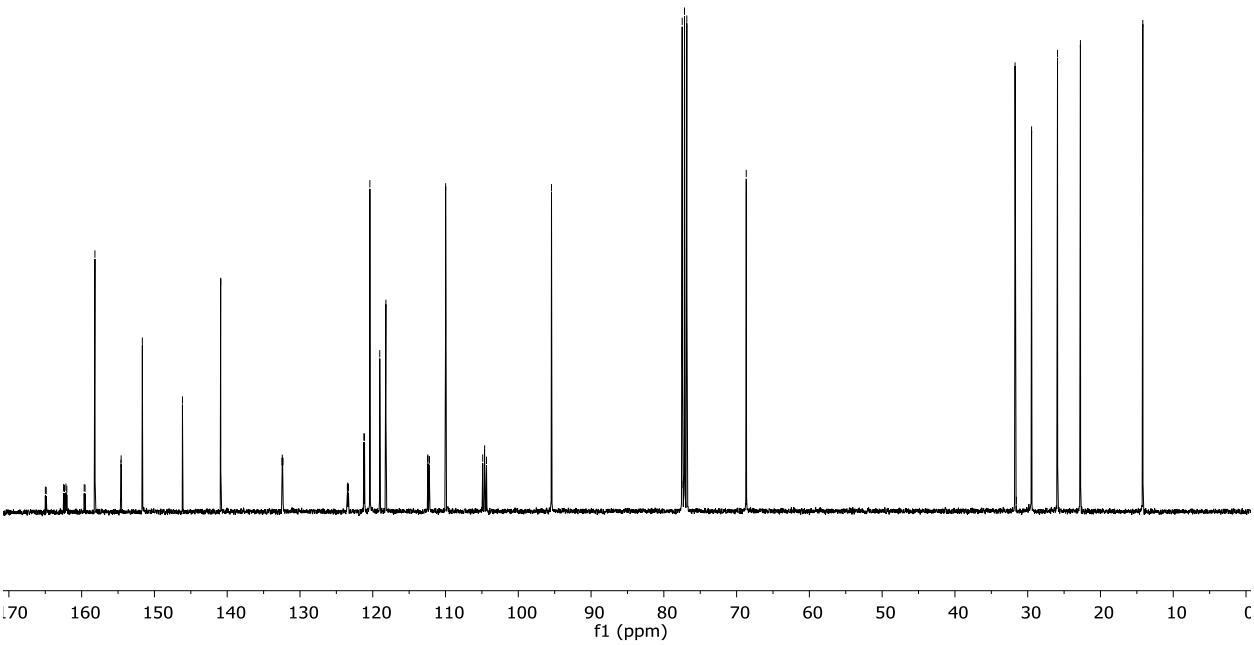

Figure S44: ^{13}C NMR spectrum of **9** in $CDCl_3$.

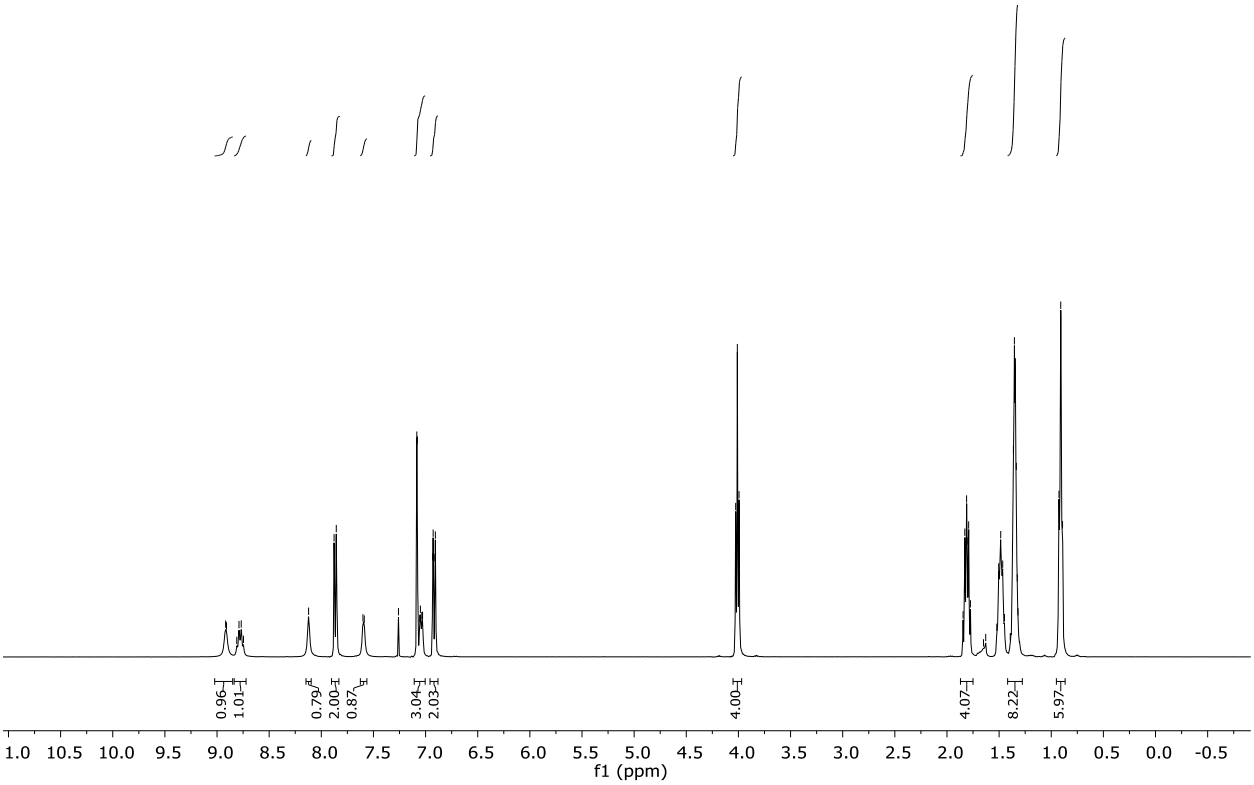

Figure S45: ^{1}H NMR spectrum of **10** in $CDCl_3$.

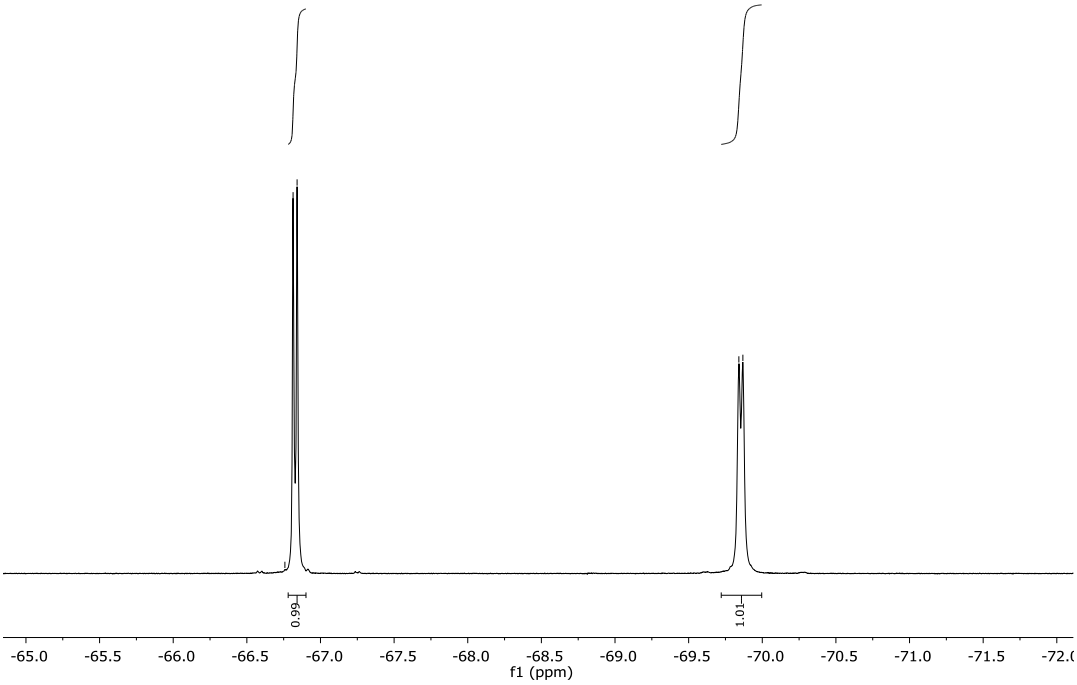

Figure S46: ^{19}F NMR spectrum of **10** in $CDCl_3$.

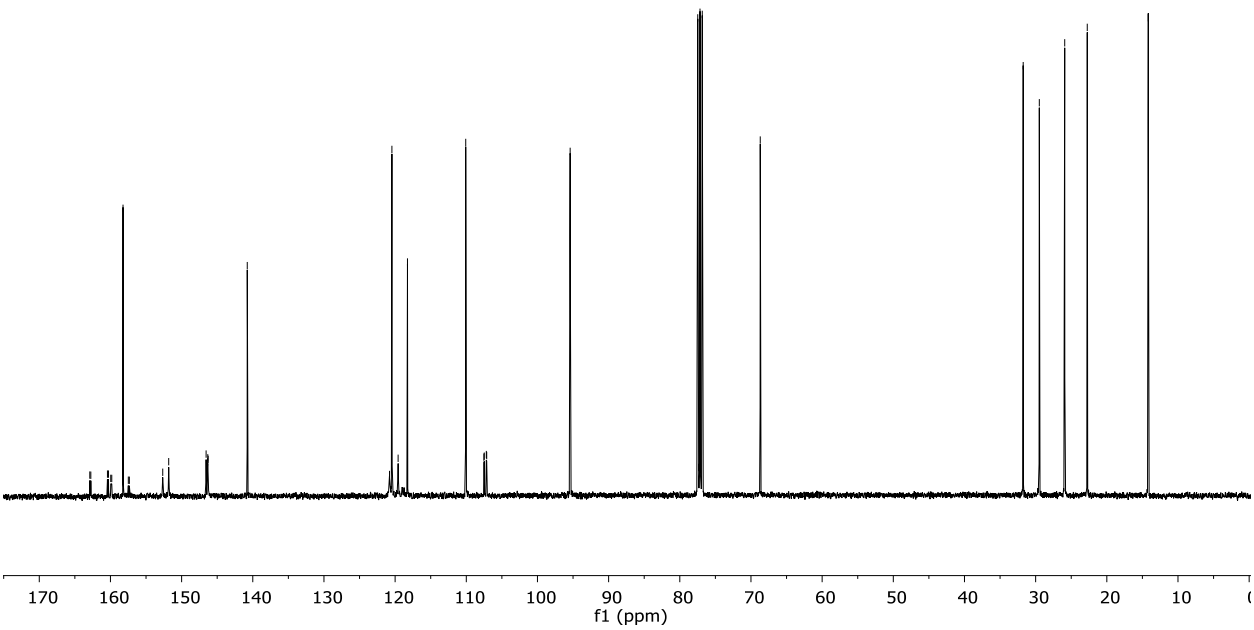

Figure S47: ^{13}C NMR spectrum of **10** in $CDCl_3$.

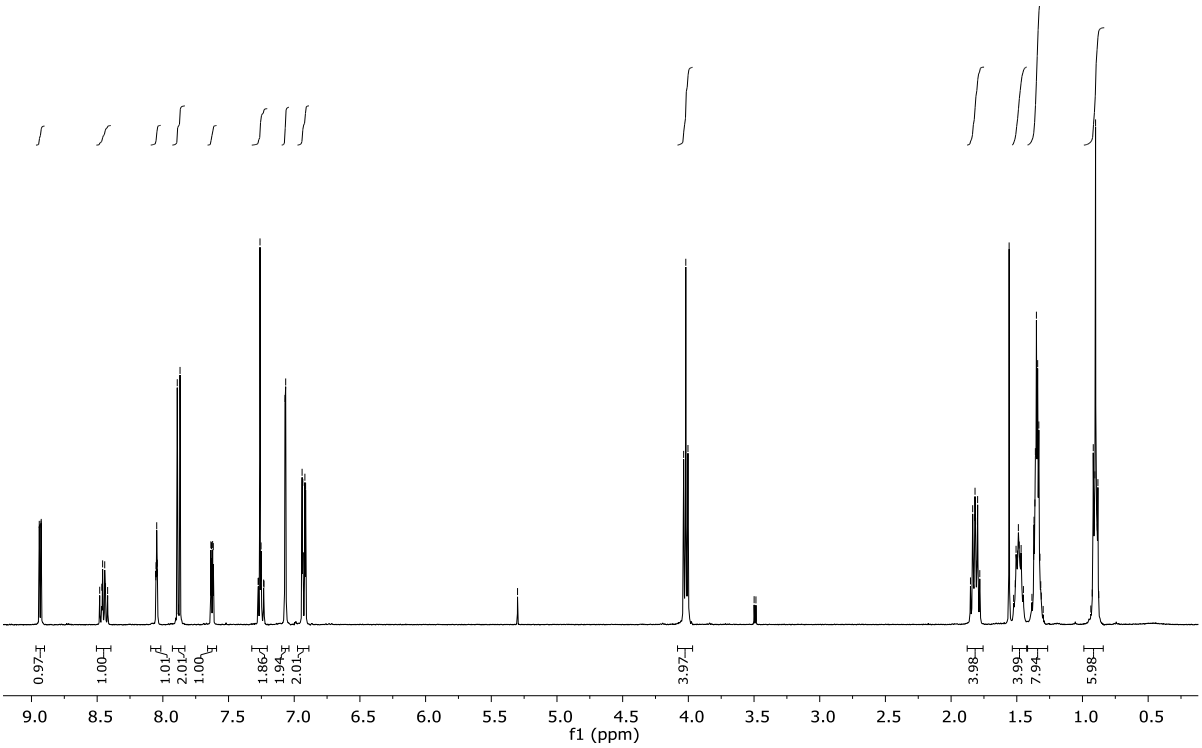

Figure S48: ^{1}H NMR spectrum of **11** in $CDCl_3$.

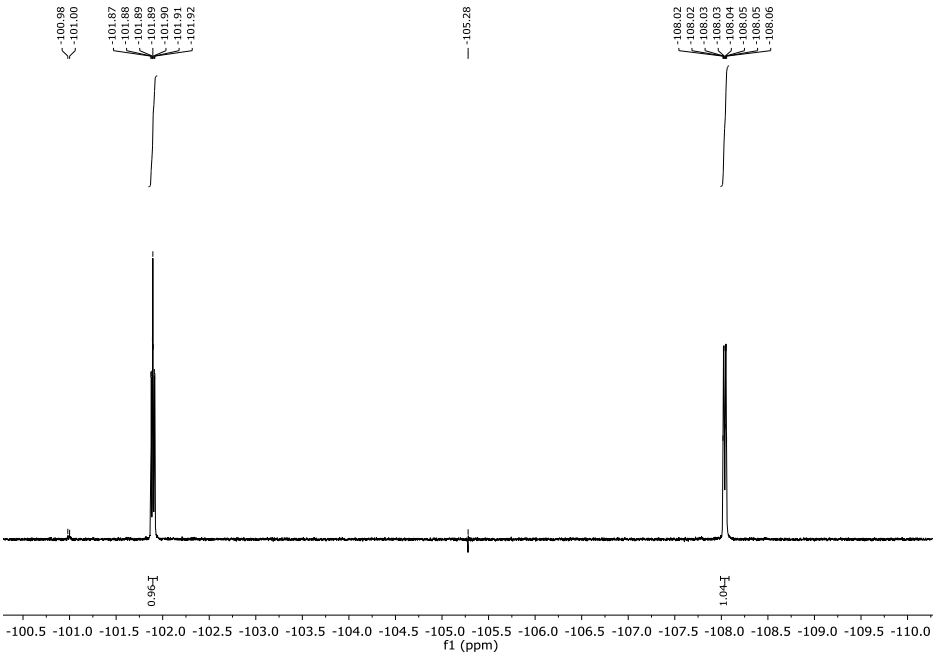

Figure S49: ^{19}F NMR spectrum of **11** in $CDCl_3$.

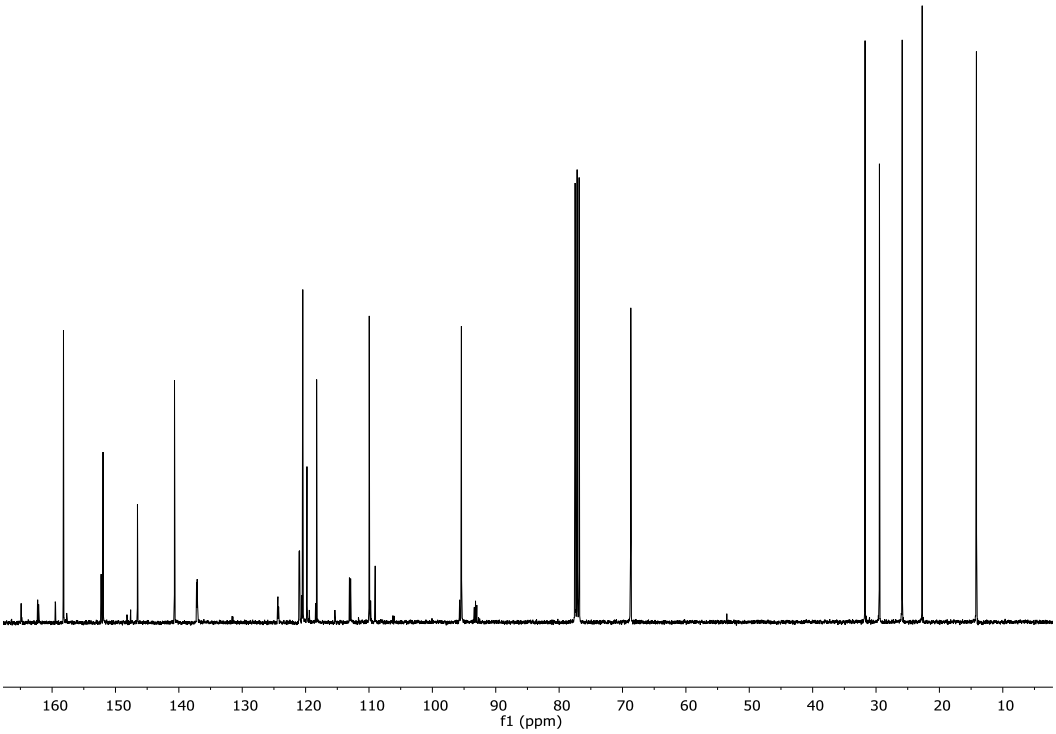

Figure S50: ^{13}C NMR spectrum of **11** in $CDCl_3$

References for the Supporting Information

1 V. N. Kozhevnikov, K. Dahms and M. R. Bryce, *J. Org. Chem.*, 2011, **76**, 5143–5148.

2 G. M. Sheldrick, *Acta Crystallogr. Sect. A Found. Crystallogr.*, 2008, 64, 112–122.

3 G. M. Sheldrick, *Acta Crystallogr. Sect. A Found. Adv.*, 2015, **71**, 3–8.

4 G. M. Sheldrick, *Acta Crystallogr. Sect. C Struct. Chem.*, 2015, **71**, 3–8.

5 O. V. Dolomanov, L. J. Bourhis, R. J. Gildea, J. A. K. Howard and H. Puschmann, *J. Appl. Crystallogr.*, 2009, **42**, 339–341.

6 B. Rees, L. Jenner and M. Yusupov, *Acta Crystallogr. Sect. D Biol. Crystallogr.*, 2005, **61**, 1299–1301.

7 M.-L. Xu, G.-B. Che, X.-Y. Li and Q. Xiao, *Acta Crystallogr. Sect. E Struct. Reports Online*, 2009, **65**, m28–m28.

8 T.-Y. Li, Y.-M. Jing, X. Liu, Y. Zhao, L. Shi, Z. Tang, Y.-X. Zheng and J.-L. Zuo, *Sci. Rep.*, 2015, **5**, 14912.

9 E. Baranoff, B. F. E. Curchod, F. Monti, F. Steimer, G. Accorsi, I. Tavernelli, U. Rothlisberger, R. Scopelliti, M. Grätzel and M. K. Nazeeruddin, *Inorg. Chem.*, 2012, **51**, 799–811.

10 Y. Zhao, J. Tang, H. Zhang and Y. Ma, *Eur. J. Inorg. Chem.*, 2014, **2014**, 4843–4851.

11 A. Maggiore, M. Pugliese, F. Di Maria, G. Accorsi, M. Gazzano, E. Fabiano, V. Tasco, M. Esposito, M. Cuscunà, L. Blasi, A. Capodilupo, G. Ciccarella, G. Gigli and V. Maiorano, *Inorg. Chem.*, 2016, **55**, 6532–6538.

12 R. D. Sanner and V. G. Young, *Acta Crystallogr. Sect. E Crystallogr. Commun.*, 2018, **74**, 1467–1470.